Evaluating the impact of snow fencing on snow conditions and ground temperatures in Hurricane Alley, Dempster Highway, Yukon, Canada.

by

Jennifer Kayley Humphries

A thesis submitted to the Faculty of Graduate and Postdoctoral Affairs in partial fulfillment of the requirements for the degree of

Master of Science

in

Geography

Carleton University
Ottawa, Ontario

Abstract

Snow fences were installed at two sites near the Dempster Highway, Yukon, ~ 10 km south of the territorial border, to examine their impact on snow accumulation and ground temperatures and evaluate their potential for snow management. Temperature sensors were installed in August 2018 and snow surveys were conducted throughout winter 2018–19. Natural snow accumulation ranged from a shallow snowpack in wind-scoured upland, to deep snow in the lee of a large hill. The snow fences accumulated wind-blown snow in large drifts of high density, which neared capacity by December. There were no zones of snow protection further downwind. Topographic factors were not found to significantly alter drift characteristics at the fences. Annual ground temperature was estimated to be higher beneath fence drifts than tundra by 1.3 °C at 10 cm depth and 1.0 °C at 50 cm depth.

Acknowledgements

This thesis is based on field research conducted along a highway in Northern Yukon between 2018 to the present. It would not have been possible to complete this thesis without help and support of the many kind people around me, only some of whom it is possible to give mention here.

Financial support for this thesis was provided by the Northern Transportation Adaptation Initiative, Transport Canada, Government of Yukon, and the Natural Sciences and Engineering Research Council of Canada. Support in conducting the fieldwork was provided by the Yukon Government Transportation Maintenance Branch (TMB), and Transportation Engineering Branch (TEB). Special thanks go to Cathy Brais whose insight and enthusiasm helped steer this project.

I am immensely grateful to all who helped in the field. Many thanks go out to Emma Stockton, Trevor Andersen, Peter Morse, and Alice Wilson for their time, effort and perspectives in the field, as well as Michael Scarizzi from the TEB, and Evan McLeod and Charles Nevado from the TMB for their assistance during set up of the project.

I would like to thank my supervisors – Dr. Chris Burn, for his continued personal and professional support over the years, as well as Dr. Elyn Hymphreys and Dr. Peter Morse who provided much needed feedback and helped turn preliminary drafts into a true thesis.

Thank you to all the new friends in the geography department, for helping make my graduate experience so positive. I owe many thanks to my friends and family for their

encouragement and patience throughout the project. Alice Wilson for her kindness, advice, and assistance with just about everything in my first year. Marlo Collier helped untangle my thoughts when I couldn't think straight and always encouraged me to move in the right direction. Emma Stockton's organizational skills and work ethic were a source of inspiration, and her humour, pool abilities and company brightened many of my days. Special thanks to my sisters, Brittany and Carley Humphries, and mother, Carmen Walker, for their emergency emotional support, as well as their endless patience.

Table of Contents

List of Tables

List of Figures

List of Appendices

Chapter 1: OVERVIEW AND OBJECTIVES

1.1 Introduction

This thesis examines the impact of structural snow fences on snow conditions and near-surface ground temperatures at sites along the Dempster Highway in Richardson Mountains, YT. Field investigations were carried out ~10 km south of the Yukon-Northwest Territories border (Fig. 1.1). The section of highway from km 450 to km 465 is locally named *Hurricane Alley* (Fig. 1.2) as it experiences strong easterly winter winds measured up to 137 km h^{-1} and blowing snow. Downslope flow of easterly winds creates turbulence and locally severe conditions (Wahl *et al.* 1987).

The highway was built upon a gravel bed 1 to 2.5 m thick to prevent degradation of the permafrost that underlies most of the route (Vyalov 1979; Burn *et al.* 2015). Such an embankment may alter air flow causing snow accumulation near the roadway (Hiemstra *et al.* 2006). The N-S alignment of the Dempster Highway in Hurricane Alley promotes snow accumulation at the side of the embankment, especially on the west side where there are tall shrubs near the road (C. Brais, pers. comm. 2018). Warming of the ground in response to increased snow depth is well established in the literature (Kinsley 1963; Judge 1973; Mackay and MacKay 1974; Burn *et al.* 2009).

In Hurricane Alley, high wind speeds and blowing snow have led to highway closures and serious disruption of driving conditions. The development of snowdrifts on the road and right-of-way (ROW) is a common maintenance problem in tundra environments and is particularly problematic in the study region (C. Brais, pers. comm., 2018). The cost of snow clearing and snow management along the Dempster Highway in

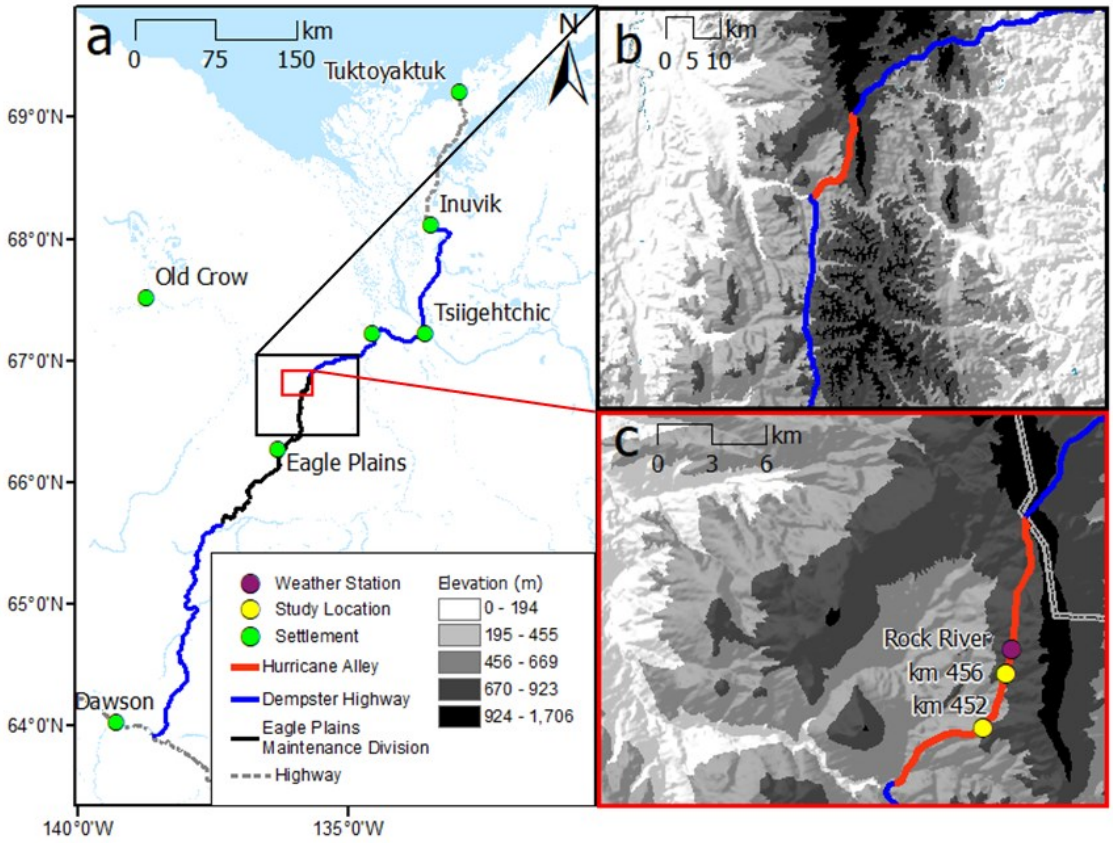

Figure 1.1. Field sites (a) in relation to the Dempster Highway, (b) west of Richardson Mountains, and (c) within Hurricane Alley.

Figure 1.2. Tundra landscape of Hurricane Alley in August looking south from the Yukon–NWT border. Photo by C. R. Burn (2016), reproduced with permission.

the Eagle Plains Maintenance Division increased by ~$72,000 per year between 2006 and 2016 (C.R. Burn, pers. comm., 2019).

When wind flows over an obstacle such as a snow fence, shrub thicket, road embankment or topographic feature, the streamlines of wind direction and speed diverge and separate from the surface, creating eddies that dissipate kinetic energy and reduce wind velocity (Mellor 1965). As the potential volume of snow transported is related to wind speed, and wind velocity decreases with contact of an obstacle, snow is dropped out of suspension when wind velocity decreases (Mellor 1965). The structure of the obstacle controls how air flow is disrupted, leading to the formation of snowdrifts in predictable areas. Wind speeds decrease immediately downwind of a snow fence, producing a zone of deposition where a drift will accrete (Fig. 1.3). Small drifts may also develop immediately upwind of the fence where small eddies form. Downwind of the deposition zone is an area of snow protection, where wind speed is comparatively low and relatively little snow is transported. A well-designed snow fence placed off the road may be used to protect the roadway by accruing wind-transported snow in the adjacent terrain.

1.2 Rationale

Snow fence design in the last two decades has been dominated by an increasing ability to model wind disturbance (Naaim-Bouvet *et al.* 2002; Liston *et al.* 2007) and by development of better criteria to evaluate snow-fence performance (Sanudo-Fontaneda *et al.* 2011; Basnet *et al.* 2015). Despite advances in fence design, snow fences often fail to reduce snow accumulation in a desired area because limited consideration is given to site-specific analysis (Tabler 1980; Blanken 2009). Snowdrift development has been

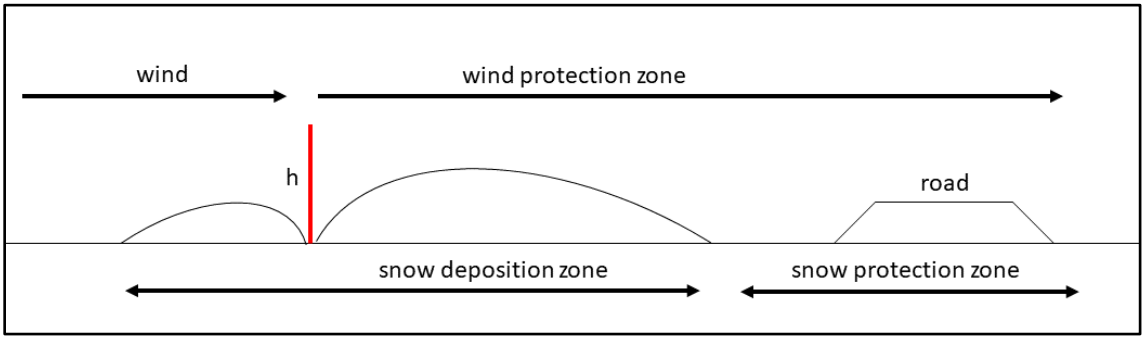

Figure 1.3. Generalized zones of snow deposition and snow protection produced by snow fencing.

examined at two sites along the Dempster Highway, km 452 and 456, to evaluate the site-specific potential of snow fences to redistribute snow accumulation away from the roadway and mitigate the rising costs of mechanical snow removal. The response of ground temperature to snow fencing has also been evaluated to support the integrity of the road embankment over the long-term. Infrastructure that accumulates snow limits winter cooling and may cause permafrost degradation and thaw subsidence (O'Neill and Burn 2017a), therefore snow management can assist in preventing degradation. This thesis is a response to the need for improved maintenance practices and guidelines for managing climate-change related hazards along the Dempster Highway. It addresses the rising cost of snow removal in this section of the highway by evaluating a snow management strategy with respect to the local environment. In this context, snow fences were installed upwind of the road to investigate the impacts of fencing on snow conditions and ground temperatures in contrast with natural snow-cover conditions.

1.3 Research objectives

The purpose of this research is to investigate how snow fences alter snow cover and to examine their impacts on the ground thermal regime in Hurricane Alley. The research objectives of this thesis are to:

1) Characterize the snow cover (e.g., depth and density) under a natural snow accumulation regime, and under various artificial regimes involving 1, 2 or 3 snow fences;
2) Compare natural snow-cover conditions with the effects of snow management on the snowpack;

3) Evaluate the impacts of the fencing on near-surface ground temperatures;
4) Develop recommendations for the control of blowing snow and the mitigation of permafrost degradation near the road through snow management in Hurricane Alley.

The hypotheses to be tested in this thesis are:

1) the installation of snow fences redistributes snow forming drifts, producing elevated snow depths in the zone of deposition and reduced snow depths in the zone of protection, with greater reductions in the zone of protection at plots with additional rows of fencing;
2) fence efficacy is site-specific, with steeper slopes at km 452 increasing snow fence drift height and length; and
3) increased snow deposition in drifts raises ground temperatures beneath the drifts and reduces them in the zone of snow protection.

1.4 Thesis structure

This thesis comprises six chapters. The following chapter outlines the properties of snow, the development of snowdrifts and controlling factors, and the influence of the snow cover on ground temperature. Chapter 3 presents the methodology and describes the study region. Chapter 4 presents the results from field observations and analysis. Chapter 5 extends the discussion of the results and leads to Chapter 6, which provides a summary of the conclusions and suggests future research directions.

Chapter 2: THE SNOWPACK

2.1 Introduction

A study of the winter snow regime and its management in Hurricane Alley requires an understanding of: (1) snow transport and deposition, especially in relation to fencing and other common obstacles, (2) the physical and mechanical properties of the snowpack, (3) the surface energy balance, and (4) permafrost and active-layer thermal regimes. This chapter provides background on the evolution of tundra snow cover over the winter season and its effects on the ground thermal regime.

2.2 Snow cover distribution

Snow cover is the total of precipitation fallen as snow, ice pellets, hoar frost, rain, and various contaminants, minus melt (McKay and Gray 1981). The structure of a snowpack is complex and highly variable, depending on: the weather during and immediately preceding deposition, nature and frequency of the parent storms, weather throughout the season, processes of metamorphism and ablation, and characteristics of the surface (i.e., topography, and vegetation) (McKay and Gray 1981).

The distribution of snowfall may be considered over macro-, and meso-scales, while the redistribution of snow following deposition is strongly associated with microscale effects (Pomeroy and Brun 2001). Macroscale variation in snow distribution are the differences in snow cover due to latitude or major physiographic factors such as regional moisture sources or mountains that disturb air flow over distances of 10^4 to 10^5 m and areas up to 10^6 km^2. Mesoscale (or local scale) variation in snow distribution

characteristically considers linear distances of 10^2 to 10^4 m and includes alterations to air flow such as cooling or warming of air with elevation or convective precipitation from lakes. At this scale, the distribution of snowfall occurs due to wind and deposition occurs due to elevation, slope, aspect, and characteristics of the vegetation cover. Microscale variation in snow distribution considers linear distances of 10 to 10^2 m, with accumulation patterns primarily related to processes of erosion, transport, sublimation, and deposition.

Precipitation, deposition, condensation, turbulent transfer of heat and moisture, radiative exchange and air movement, as well as ground surface characteristics control snow redistribution at the microscale (McKay and Gray 1981). A snow cover's resistance to erosion is the result of interparticle bond strength and cohesion, and is related to snowpack temperature (Schmidt 1980; Li and Pomeroy 1997). Older, wind-hardened, dense, and/or wet snow have greater interparticle bonds and cohesion that resist erosion. When air temperature is near 0 °C and snow falls, the cohesive forces between the 'wet' snow particles are much greater (Li and Pomeroy 1997). Snowfall is comparatively dry, and more easily erodible at lower temperatures. Density and age are important as they both lead to increases in the number of intercrystal bonds, and overall resistance to erosion (Li and Pomeroy, 1997).

2.2.1 Redistribution by wind

Following the initial deposition of snow, wind erodes and transports fresh loose snow, redepositing it in drifts and banks. There are three modes of snow transport at the surface of the snowpack: creep, saltation, and suspension (or turbulent diffusion) (Mellor 1965)

(Fig. 2.1). Creep refers to grains that remain in contact with the surface as they move laterally, i.e., they roll. Saltation refers to grains that bounce along the surface, rising to heights of 10 to 100 cm. Grains held in suspension experience no ground contact.

The mode of transport depends on particle size and wind speed (Kok *et al.* 2012). As wind speed increases, some grains are moved by fluid drag force. Once the grains have been lifted, they saltate along the surface. As wind speeds increase, suspension becomes the dominant mode of transport (Fig. 2.2). However, entrainment by saltation is necessary before snow can enter suspension (Schmidt 1980). At wind speeds of 8 m s^{-1}, 75% of the total snow transport is by suspension for a fallowed field with a complete snow cover (Pomeroy and Male 1992). Creep and saltation are forms of drifting that occur regularly near the ground surface along highways (Mellor 1965).

Transportation, erosion, and deposition

Wind speed is a particularly important consideration for snow drifting. The earth surface exerts frictional drag on the air flowing above it, resulting in shear stress and turbulence within the layer of air affected by the surface, e.g. the planetary boundary layer (PBL). Within a neutrally stable PBL, the logarithmic wind profile estimates mean wind speed (u_z) at height z over flat ground (Oke 1987):

$$u_z = \frac{u_*}{\kappa} \ln\left(\frac{z}{z_0}\right) \quad [1]$$

where u_z, is the wind speed (m s^{-1}) at height z (m) above the ground, z_0 is the aerodynamic roughness length (m), κ is the von Karman's constant (0.4), and u_* is the friction velocity (m s^{-1}). The aerodynamic roughness length is the hypothetical height above the surface of zero wind speed. It characterizes the ground surface roughness – the

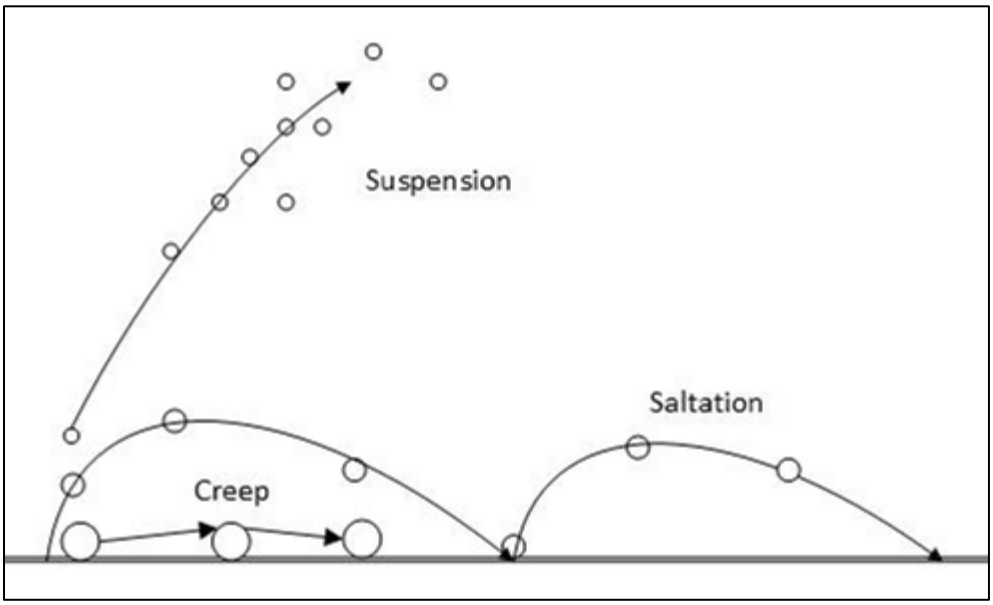

Figure 2.1. The three modes of snow transport. After Presley and Tatarko (2009, Fig. 3, p. 3).

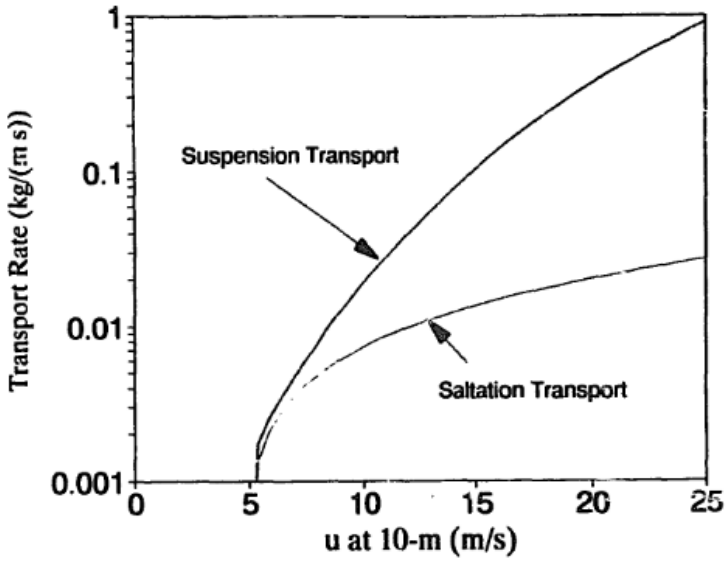

Figure 2.2. The modelled snow transport rates for both saltation and suspension as a function of the wind speed at a height of 10 m. Reprinted from Pomeroy, J.W., and Male, D.H. Steady-state suspension of snow. *Journal of Hydrology*, 136: 275–301, Fig. 9, p. 297. © 1992, with permission from Elsevier.

obstacles on the ground that exert drag on air flow (Table 2.1) (Oke 1987).

Friction velocity is a measure of shear stress, caused by the drag on airflow by the ground:

[2] $$u_* = \sqrt{\frac{\tau_0}{\rho_0}}$$

where, τ_0, is the shear stress (kg m^{-1} s^{-2}), and ρ_0, is the density of air. If z_0, and u(z), are known, u_*, can be calculated for a given atmospheric stability regime. There have been numerous formulae developed to estimate the quantity of snow transport using u_*or u. The general principle is that the transport rate of blowing snow increases with wind speed and is inversely related to surface roughness. Tabler *et al.* (1990) developed a practical formula for the downwind transport rate of snow:

[3] $$q_T \approx 1.4 \times 10^{-6} \cdot u_{10}^{4.2}$$

where q_T (kg m^{-1} s^{-1}) is the total transport rate in the first 10 m above the surface, and u_{10} is the wind speed (m s^{-1}) at 10 m height.

Snow is eroded if the wind speed or surface roughness change to create a shear force on the surface great enough to break the bonds between the snow grains and initiate movement. Shear stress is mainly a result of wind speed, topography and vegetation (Pomeroy *et al.* 1997). For example, near-surface wind accelerates when it flows over the crest of a ridge, so these areas are typically scoured. In contrast, as air flows over vegetation protruding from the snow, the rougher surface (Table 2.1) results in a decrease in wind speed and snow is typically deposited rather than transported away from these locations. The minimum friction velocity required to initiate movement of a particle is

called the threshold friction velocity. The value varies with the size of the snow grains, the amount and type of bonding, and their frictional properties (Mellor 1965; Li and Pomeroy 1997). The corresponding wind speed is called the threshold wind speed.

Pomeroy *et al.* (1993) reported that threshold friction velocities range from 0.15 to 0.25 m s^{-1} for fresh, loose, dry snow, and 0.25 to 1.0 m s^{-1} for older, wind-hardened dense or wet snow. Threshold wind speeds at 10 m height reported by Mellor (1965) range from 3 to 8 m s^{-1} (11 to 29 km h^{-1}) for fresh unbonded snow, while wind speeds greater than 30 m s^{-1} are required to dislodge snow particles bonded by freeze-thaw processes. The values reported by Pomeroy *et al.* (1993), and Mellor (1965) are similar to estimates by Liston *et al.* (2007), who reported threshold wind speeds for new, cold (−2 °C), dry snow between 4 to 5 m s^{-1} at 10 m height, or a threshold friction velocity of 0.2 to 0.3 m s^{-1} (0.7 to 1.1 km h^{-1}) for a given roughness length.

Snow cover distribution reflects the patterns of turbulence created by surface features. The amount of snow accumulation in windswept environments can be calculated by using a mass balance equation (Pomeroy *et al.* 1997):

$$Q_A = Q_S - Q_L - \frac{dQ_T}{dx}(x) \quad [4]$$

where Q_A represents the snow accumulation flux at the ground surface (kg m^{-2} s^{-1}), Q_S is the snowfall flux (kg m^{-2} s^{-1}), Q_T is the transport flux for horizontal blowing snow (kg m^{-2} s^{-1}), Q_L is the flux for sublimation (kg m^{-2} s^{-1}), and x is the fetch length (m). Fetch is the distance of ground over which the wind has blown, and sublimation is the conversion of snow grains to vapour, thus when Q_L is positive, it represents a loss of snow to the atmosphere due to change of phase. Q_A is negative where a surface is being eroded, and

positive where a surface is accumulating snow. Q_S and Q_L represents atmospheric terms of addition and loss, and dQ_T/dx (x) represents the transport change term, where net horizontal transport of snow is either into an area (negative) or out of an area (positive). A surface experiences a net loss of snow when the horizontal transport change term is greater than the atmospheric terms, dQ_T/dx (x) > ($Q_S - Q_L$). While accumulation occurs when the transport change term is less than the atmospheric change, Q_S less Q_L.

Overall, transport of snow particles occurs when the wind speed increases, or surface roughness decreases, enough to raise the shear stress over the threshold required to break the interparticle bonds and initiate movement. This threshold friction velocity increases with increasing snowpack density, increasing grain bonding, snowpack temperatures, and time since deposition, which all reduce the erodibility of the snow surface. Deposition occurs as the transportation rate decreases when wind speed declines, the surface roughness increases, or the rate of snowfall increases. Wind speed may decline with changes in synoptic weather systems, if katabatic effects dissipate at the foot of a slope, or by obstacles impeding flow (Mellor 1965; Tabler 2003).

Sublimation

Sublimation, Q_L, is a key component in determining the balance of snow accumulation in tundra and prairie environments (eq. 4). In tundra environments, such as Hurricane Alley, snow cover is thinner than in southern environments as it is reduced by sublimation owing to snow particles being in suspension for long periods of time in the unobstructed wind flow (Sturm *et al.* 1997). Within non-alpine tundra settings, sublimation of the total snowfall has been estimated to be 25–47% (Essery *et al.* 1999), though estimates vary widely depending on the approach (Liston and Sturm 2004).

Sublimation rates increase with wind speed, decreasing monthly minimum temperatures, decreasing relative humidity, and increasing snowfall and snow depth (Pomeroy and Gray 1994).

2.2.2 Interception and deposition

When wind flows over an obstacle such as vegetation, hills, or roads, the streamlines separate from the surface. The separation of flow from the surface creates a low pressure region which pulls the air towards it and can generate swirling flow structures called eddies. The eddies form a turbulent wake, where more kinetic energy is dissipated by rotation resulting in reduced wind speeds. The separation of flow and subsequent eddy formation also occurs when the wind faces abrupt obstacles such as a fence or shrubs.

The structure of the obstacle and the wind speed impacts the nature and location of eddies in a wake (Tabler 2003). In the case of snow fences, pressure increases ahead of the fence. At the fence line, streamlines are forced to converge to get over the fence (Fig. 2.3), causing a brief acceleration (Oke 1987). Separation of flow from the surface (of the fence) occurs at the top of the fence. There is significant room for expansion immediately after the flow crosses the fence, but the air cannot fill it instantaneously (Oke 1987). This low pressure zone immediately downwind of the fence pulls air in, creating lee eddies. The eddies dissipate energy, reducing wind speed, and allow for deposition of wind transported snow. Snow fences reduce windspeeds and create turbulence in predictable areas and can be used to direct distribution of snow to adjacent terrain, protecting, for instance, a highway.

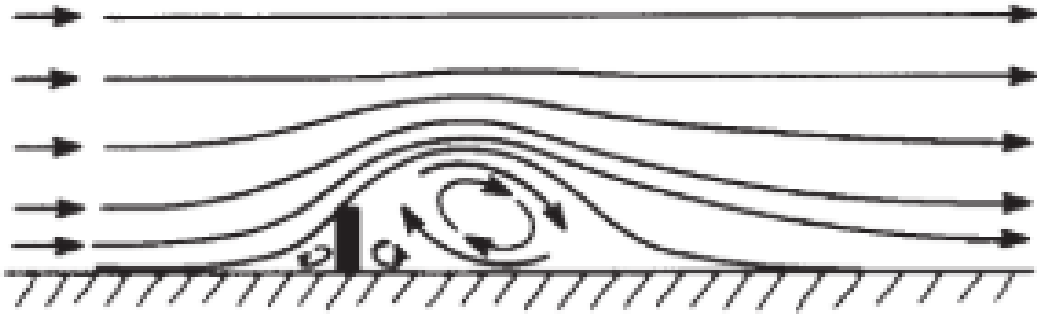

Figure 2.3. Streamlines around a solid fence, showing the separation of flow and associated eddies beginning from the fence line. Republished with permission of Taylor & Francis Informa UK Ltd – Books, from Oke. T.R., 1987, *Boundary Layer Climates*, Second Edition. Routledge, London. 435 pp, Fig. 7.6, p. 243; permission conveyed through Copyright Clearance Center, Inc.
.

Effect of topography on snow cover

In open environments such as Arctic tundra and prairie environments with long winter seasons and unobstructed wind flow, the combination of vegetation and terrain type uniquely influences snow accumulation (Pomeroy and Gray 1995; Morse *et al.* 2012). Snow is relocated from open, unvegetated areas or windward slopes to those with vegetation, valley sides, or other wind protected areas.

If a snow transport axis flows perpendicular to a ridge, the highest snow accumulation is seen on the lee slope (Fig. 2.4), with about twice the accumulation on the lee slope as the windward slope (Föhn and Meister 1983). The location of deep snow and its depth increase with the size of the ridge and the steepness of the lee slope. If the lee slope is especially steep (i.e., > 25°) the point of maximum depth is at the ridge peak. As the steepness of the lee slope decreases, the point of maximum snow depth moves further downslope. Pomeroy and Gray (1995) observed similar snow accumulation patterns along a valley side in Trail Valley Creek, a small catchment in the western Arctic (Fig. 2.5). If the aspect of the valley sidewall was perpendicular to a major snow transport axis, then drift formation occurred along the valley side, otherwise topographic accumulation did not occur.

Pomeroy *et al.* (1997) classified a forest–tundra transition zone into sources and sinks of blowing snow with vegetation and slope as criteria, simulating the accumulation regime for the various sites. Drift areas, defined as slopes exceeding 9° or stream channels near source areas, took an additional three months to reach maximum snow accumulation, and maximum accumulation was ~9 times greater than tundra sites. Drifts in wind protected zones, such as those near vegetation, mountain crests, or valley sides

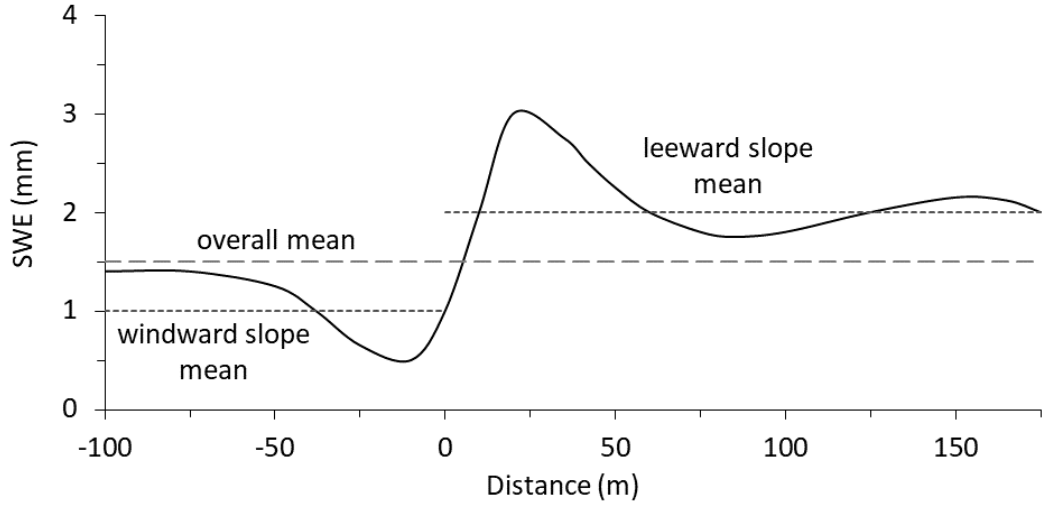

Figure 2.4. Generalized snow deposition pattern on ridges from snow survey transects in Switzerland with perpendicular wind flow from the right in this diagram. Reproduced for clarity with permission of Cambridge University Press from Föhn, P.M.B., and Meister, R., 1983, Distribution of snow drifts on ridge slopes: Measurements and theoretical approximations. *Annals of Glaciology*, 4: 52–57, Fig. 7a, p. 55.

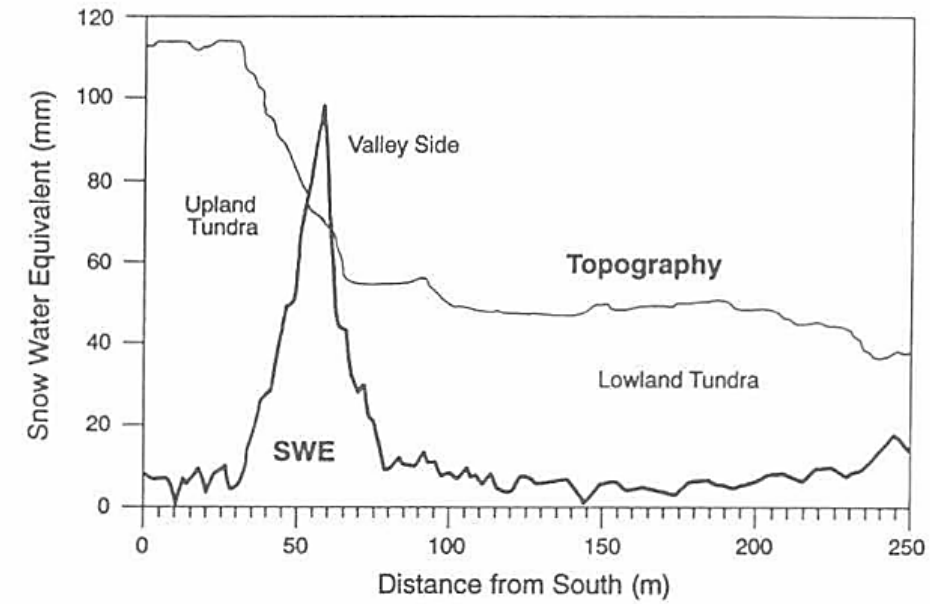

Figure 2.5. Cross-section from an upland tundra plateau, along the valley side (incline > 25°) to a sheltered tundra lowland, Trail Valley Creek, NWT. Republished with permission of Government of Canada, from Pomeroy, J.W., and Gray, D.M., 1995, *Snowcover: Accumulation, relocation, and management.* National Hydrology Research Institute (NHRI), Saskatoon, SK, NHRI Science Report No. 7. Environment Canada, Saskatoon – Saskatchewan, Fig. 16, p. 25. This figure is a copy of an official work published by the Government of Canada and has not been produced in affiliation with, or with the endorsement of the Government of Canada.

persisted much later than adjacent snow covers in spring, delaying meltwater supply (Föhn and Meister 1983).

Effect of fencing on snow cover

The idealized drift shape formed by a vertical slat fence is parabolic (Fig. 2.6), as with most structural fences of open construction. Notable characteristics are the uneven snow accumulation on either side of the fence, and the change in shape over a winter season. When fencing or any obstacle is placed perpendicular to the prevailing wind direction, the windward and lee sides accrue different amounts of snow, with approximately twice as much snow on the lee side (Mellor 1965). The windward side has a higher snow density and hardness from wind compaction (Mellor 1965). As the drift builds, the zone of accumulation lengthens until the fence reaches saturation. Reaching saturation implies the storage capacity of the snow fence has been met and it no longer promotes deposition.

Major changes to drift shape occur with the design of the fence, wind conditions, and characteristics of the local environment. Tabler developed the most common protocols for snow fence design beginning in 1968 (e.g., Tabler 1968, 1973, 1986, 1991, 1994, 2003, 2004). Two main recommendations are a porosity, which is the percentage of open space, from 40 to 60%, and setting the fence back a distance of 35H from the region to be protected, where H is the height of the fence (Tabler 2003). Drift development is typically controlled by modifying the porosity, bottom gap, and height of structural fences (Mellor 1965; Tabler 2003; Basnet *et al.* 2015).

The capacity of a fence scales with height, so the higher the structural fencing the larger the drift (Basnet *et al.* 2015). A gap between the bottom of a structural fence and

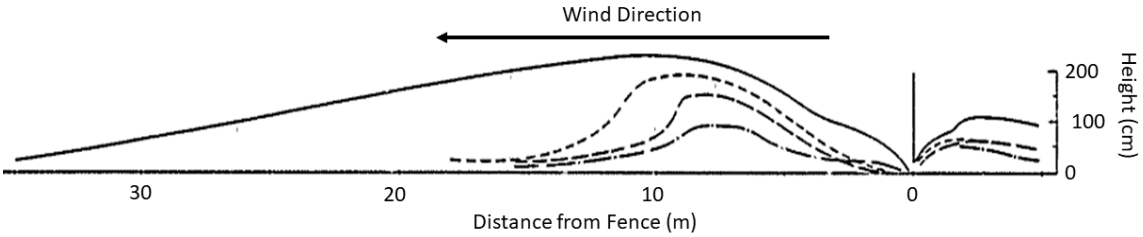

Figure 2.6. Snowdrift formation for vertical slat fencing of 1.87 m high with a gap of 20 cm. Reproduced from Mellor, M., 1965, *Blowing snow*, U.S. Army Cold Regions Research and Engineering Laboratory (CRREL), Hanover, NH, CRREL monograph, Part III, Section A3c, Fig. 46, p. 46.

the surface is another way to raise the apparent fence height, with the recommendation being 0.15 to 0.40 m (Mellor 1965). The bottom gap allows a longer drift to form, raising the storage capacity and delaying the time to reach saturation (Tabler 2003). Another common method to raise the storage capacity is to install multiple rows of structural fences. This method is preferable when the required fence heights are impractical, the volume of snow trapped is large, or the goal is dispersing snow cover over a larger area (Tabler 2003).

Fences used for infrastructure protection commonly have a porosity from 40 to 60% (Tabler 2003). Structural snow fences with a higher porosity produce longer wake zones, accruing the maximum amount of snow (Mellor 1965; Basnet *et al.* 2015). In such fences with open, porous construction, air flows over top and *through* the fencing, which reduces the drop in pressure behind the fence and reduces the pressure gradient driving air flow into the wake zone. Wind speeds in the lee are not as slowed as behind a solid fence but the turbulent wake zone is extended (Oke 1987). A fence of solid construction will prevent any air flow through the fencing, which reduces the number of eddies and the size of the wake zone (Mellor 1965; Tabler 2003). Fencing with low porosity forms downwind drifts that are concentrated close to the obstacle, and a larger proportion of the drift settles upwind.

Effect of vegetation on snow cover

Vegetation affects snowfall or transported snow by creating turbulence above and within the vegetation canopy (Table 2.1) that leads to variable snow distribution, and by directly intercepting snow (Pomeroy and Gray 1995). Despite vegetation structure being significantly more variable than wooden fencing, snow accumulation in shrubs is

dependent on the same factors of height and porosity (Essery and Pomeroy 2004; Pomeroy *et al.* 2006; Lantz *et al.* 2009). While height and porosity govern the amount of snow accumulated in both structural and living fences, vegetation does not accumulate snow in the same manner (Peterson and Schmidt 1984; Naaim-Bouvet and Mullenbach 1998; Heavey 2013). Deciduous shrubs with a porosity of 50%, grown as a living snow fence had a greater drift area than wooden structural fencing in early winter but by the end of the winter the structural snow fence had a larger drift area, 27 m^2 compared to 23 m^2 (Naaim-Bouvet and Mullenbach 1998). The shrub snowdrift was lower, and more evenly distributed. The drift of the wooden fence mirrored that of Figure 2.5, a ballistic curve with a break in deposition directly at the fence, a peak in accumulation a few meters downwind of the fence, and a long zone of deposition (Naaim-Bouvet and Mullenbach 1998).

2.3 The role of snow in the energy balance

Seasonal snow cover influences the exchange of energy between the ground and the atmosphere and therefore has a large impact on ground temperatures. The energy balance of a snowpack, can be written as (Oke 1987):

$$\Delta Q = Q^* + Q_G + Q_H + Q_E + Q_M \quad [5]$$

where ΔQ (W m^{-2}) is the rate of change in energy storage in the snowpack, Q* is the net radiative energy flux (energy gained or lost by the surface from solar and longwave radiation), Q_G is the ground energy flux (heat gained or lost by conduction), Q_H is the sensible energy flux (heat transfer between the snow surface and atmosphere), Q_E is the latent energy flux (heat gained or lost from the surface due to phase change) and Q_M (W

m^{-2}) is the advective energy flux (heat gained from precipitation or lost into the soil from meltwater flow).

The impact of a snow cover on ground temperature depends on the storage and transport of energy between the ground, snow, and atmosphere. The exchange of energy between these media involves radiative energy transfer, thermal conduction within the ground and snow, and turbulent transfer within the atmosphere (Oke 1987). Internal mass and energy balances drive water movement and phase change, and further complicate the surface energy balance (Oke 1987). The processes of conduction, melting/refreezing, percolation, metamorphism, and settling in the snowpack are all driven by temperature and vapour density gradients within the snowpack. The temperature and vapour density gradients are driven by energy fluxes at the snow cover–atmosphere and snow cover–ground surface interfaces.

Seasonal snow cover acts to: (1) cool the ground surface due to its high albedo and emissivity, (2) insulate the ground due to its low thermal conductivity, and (3) release heat during snowmelt due to its high latent heat (Zhang 2005). The net effect is generally reduced ground heat loss and higher ground temperatures in comparison to a site where snow is absent (Mackay 1978; Goodrich 1982). However, in the case of a very thin snow cover with relatively high albedo, the result is a cooling effect at the soil surface (Zhang 2005). In the case where snow cover is sufficiently deep and has a warming effect on the ground surface, the elevated ground temperatures in winter mean less energy is required to thaw the soil in the summer, and more heat is available to warm the soil. Overall, increases to snow cover thickness tend to raise average annual soil temperatures (Hinkel *et al.* 2003). Despite this general effect, the overall impact on the ground surface energy

balance varies with characteristics of the snow (e.g., density, thickness, or timing), and the interaction of the snow with the atmosphere and ground surface (Zhang 2005).

2.4 Snowpack evolution

2.4.1 Metamorphism

Over the course of the winter, the grains within the snow cover interact with the soil and atmosphere to undergo transformations in size, shape, and cohesion (Colbeck 1982). Snow metamorphism is controlled by the water content and the temperature gradient (Sturm and Benson 1997). The evolutionary path the snow takes determines the metamorphic state of the snow and its physical properties, such as density, grain shape, hardness (Colbeck 1982; Colbeck *et al.* 1991). The presence of liquid water in the snowpack distinguishes the two types of evolution—dry and wet snow metamorphism (Colbeck 1982). When the temperature is below 0 °C there is an absence of liquid water and snow is dry, although the melting point can vary slightly (Colbeck 1982). Wet snow is further subdivided by the liquid water content. At low liquid contents there are typically tightly packed grain clusters, whereas at higher liquid water contents particles are well-rounded, and cohesionless. Dry snow is further subdivided based on the crystalline shape, which is either an equilibrium form, or a kinetic growth form (Colbeck 1982).

Dry snow metamorphism can be further divided depending on the magnitude of the temperature gradient that extends vertically through the snowpack (Colbeck *et al.* 1991). Low, medium, and high temperature gradient metamorphism occurs when the temperature gradient is less than 5 °C m^{-1} , between 5 °C m^{-1} and 15 °C m^{-1}, and greater

than 15 °C m^{-1}, respectively (Colbeck 1983). The size of the temperature gradient is the result of the radiative cooling of the snow surface, warm and/or wet soils, and the low thermal conductivity of the snow cover (Zhang 2005). The low thermal conductivity of the snow allows the soil to stay warmer than the atmosphere and induces a temperature gradient. Because water vapour is saturated in the snowpack, a temperature gradient produces a vapour pressure gradient, with vapour diffusion from warmer to the cooler grains (Colbeck 1983). Vapour pressure depends on the snowpack temperature and ice surface curvature; the vapour pressure over an ice surface increases with temperature (Colbeck 1983). As such, the efficiency of metamorphism depends on the temperature of the snowpack, with fast metamorphism occurring around the melting point, and negligible changes occurring towards −40 °C.

At low temperature gradients, equilibrium growth, also called destructive metamorphism, dominates, as it erodes newly precipitated particles down to rounded grains (Pomeroy and Brun 2001). In the case of wind-transported snow, grains have already been broken down mechanically by wind action. Low temperature gradients form small and rounded grains (0.1 to 0.4 mm) with pores of comparable size, sintered and strongly bonded by ice (Colbeck *et al.* 1991). The smaller the grains are at the beginning of the process the faster sintering occurs. Wind crust or wind slab is classified as an equilibrium growth type of snow as it forms when small wind-eroded snow grains are deposited in densely packed layers that quickly sinter, to develop a layer of high strength (Colbeck 1982). As thermal conductivity increases with density (Li and Pomeroy 1997), a high density snow has a lower temperature gradient than a porous one, and thus more heat may be transported by conduction, less is used for phase change, and metamorphism

occurs at a slower rate.

At larger temperature gradients, kinetic growth metamorphism dominates. This is typically called constructive metamorphism, as it changes rounded particles to faceted crystals under relatively high temperature gradients. Within the snowpack, the saturated vapour pressure is highest at the base of the snow cover, at the ground surface, where snow temperature is highest. Vapour sublimates from the crystals there and is transported along the vapour pressure gradient until it reaches the bottom surface of the upper snow layer where it recrystallizes. Medium temperature gradients form faceted crystals ranging from 0.3–1 mm, these crystals are linked by both ice bonds and by brittle chains, experiencing intermediate properties (Colbeck *et al.* 1991). At the largest temperature gradients large crystals form with grain sizes ranging from 2–10 mm, and pore sizes that are comparably large (Colbeck *et al.* 1991). Grains are linked by brittle chains to form piles. In a natural snow cover, these transformations occur each time a new snowfall occurs, and the temperature gradient is often variable, which results in intermediate snow types (Pomeroy and Brun 2001). Equilibrium and kinetic growth metamorphoses can both work within the same layer, and their relative effect may change depending on the weather conditions.

Main morphological classes

The main morphological grain shape classes are precipitation particles, decomposing and fragmented precipitation particles, rounded grains, faceted grains, depth hoar, surface hoar, melt forms and ice (Fierz *et al.* 2009). In the initial stages of metamorphism, the characteristic shapes of the precipitating particles are still recognizable. Rounded particles are produced by low temperature gradient

metamorphism, and their growth increases with higher temperature, and lower density snow. Wind packed snow forms at the surface and involves the packing and fragmentation of wind-transported snow crystals that round due to abrasion during saltation. High wind speed and small particle sizes lead to denser wind packed layers, i.e., wind slabs or crusts. Wind slabs and crusts are distinguished by depth, with wind crusts tens of millimeters thick, and wind slabs tens of centimeters thick (Colbeck 1991). Faceted crystals have flat faces with sharp angles and form under moderate temperature gradients (Fierz *et al.* 2009). They involve grain-to-grain vapour diffusion by a sufficiently large temperature gradient that allows for kinetic growth. Depth hoar is also formed by grain-to-grain vapour diffusion but is driven by a large temperature gradient. It develops within the snowpack, in dry snow.

Metamorphism exhibited in tundra snow covers

Sturm *et al.* (1995) classified seasonal snow covers into six main divisions: tundra, taiga, alpine, prairie, maritime, and ephemeral, based on the stratigraphic characteristics and climate conditions associated with each. In the western Arctic, the snow cover would usually be considered as tundra or taiga. A tundra snow cover is typical north of tree line in areas with low precipitation (<250 mm water equivalent/year). Tundra snow cover is thin, with a maximum depth of 75 cm, but dense (~0.4 g cm^{-3}), and develops from cold, wind-blown snow. There is characteristically a basal layer of depth hoar overlain by one to multiple hard wind slabs of small, rounded grains. Layers of faceted crystals or ice may separate wind slabs. The taiga snow cover is also formed in low temperature climates but is deeper, with maximum depths of 120 cm, and forms in environments with low wind speed, and has low snow density. By late winter 50 to 80%

of the pack has metamorphized into depth hoar, with the upper portion covered by low-density new snow.

2.4.2 Physical properties of a snow cover

Hardness of the snowpack increases from time of *snowfall* (not deposition) onwards, with the largest increases immediately following the event. Following the precipitation event, metamorphism modifies the snow to induce a wide range of hardness and densities (Colbeck 1989). The range of reported densities, as well as the mean density, and reported snow particle size for various tundra snow types are shown in Table 2.1.

Fresh snowfall has low hardness, and a low density (0.01 to 0.2 g cm^{-3}) (Table 2.1). In high wind speed environments, erosion and transportation form small round grains (Mellor 1965). The small grains deposit in layers with a high density (0.2 to 0.5 g cm^{-3}), hardness, and strong cohesion due to wind packing. High wind speeds and older snow both contribute to increased hardness and density of a snow cover. Snow densities in the late winter ranged from 0.35 to 0.4 g cm^{-3} at Garry Island, NWT over two years (Mackay and MacKay 1974). These densities are typical of Arctic stations with low temperatures and strong winds (Gold and Williams 1957).

The characteristics of a snow cover also differ with topographic setting (Benson and Sturm 1993). Over flat tundra a thin veneer of snow develops, but topographic depressions can be filled by deep drifts. In such veneers, the basal layer develops into depth hoar, covered by dense wind-blown snow. The cohesion, hardness, and density (0.15 to 0.35 g cm^{-3}) of depth hoar or faceted grains are low relative to the layers of wind-blown snow. In drift facies, the snow is deeper, denser, and the stratigraphy is more

Table 2.1. Physical properties of various snow types, including grain size, density (ρ), and thermal conductivity (λ). After Dominé *et al.* (2008, Table 1, p. 176).

Snow Type (symbol)	Grain Size (mm)	ρ Range (g cm^{-3})	Mean ρ (g cm^{-3})	λ Range (W $m^{-1} K^{-1}$)	Mean λ (W $m^{-1} K^{-1}$)
Fresh snow (+)	0.5–1.0[7]	0.01–0.2[3]; 0.05–0.09[8]; 0.07–0.2[9]; 0.01–0.2[11]	0.1[7]	0.03–0.12[9]	0.07[9]
Recent snow particles (/)		0.06–0.25[1];0.17–0.35[9]; 0.07–0.35[11]	0.16[10]	0.06–0.2[9]	0.13[9]
Small rounded grains: wind packed (•)	<0.4[1]; 0.5–1.0[7]; 0.1–0.8[10]; 0.25[12]	0.3 to 0.56[9], <0.61[6]; 0.35–0.40[2]; 0.28–0.35[8]; 0.17–0.52[11]; 0.35–0.52[10]	0.38[7]; 0.4–0.5[7]; 0.35–0.48[10]	0.2–0.6[1]; 0.05–0.6[9]; 0.06–0.65[9]	0.17–0.45[9]
Large rounded grains: low temp. met. (●)	0.1–1[10]; 1–2[7]; 0.3–1.5[10]	0.15–0.35[1]; 0.2–0.35[5]; 0.3[10]	0.2[7]	0.08–0.3[9]	0.16[9]
Faceted Crystals (□)	0.2–3[10]; 0.5–2[1]	0.19–0.4[11]	0.3[10]	0.08[1]	
Depth hoar (∧)	2–20[1]; 5–10[7]; 3-15[10]	0.15–0.28[10]; 0.2–0.35[11]	0.15–0.25[7]; 0.2[10]	0.02–0.14[9]	0.07–0.18[9]
Melt-forms (○)	0.5–2[4]		0.17–0.3[11]	0.1–0.45[9]	0.19–0.25[9]

[1] Domine *et al.* (2008). Table 1, or text.
[2] Mackay and MacKay (1974). Garry Island, NWT (1969–70 and 1970–71).
[3] Judson and Doesken (2000) in Dominé *et al.* (2008).
[4] Raymond and Tusima, (1979) in Dominé *et al.* (2008).
[5] Albert and Shultz (2002); Dominé *et al.* (2003) in Dominé *et al.* (2008).
[6] Domine *et al*. (2008, Unpublished data).
[7] Benson and Sturm (1993).
[8] Gray (1978), Table 4. Density of fresh snow (+) was: (1) ordinary new snow, (2) settling snow, and (3) slightly toughened by wind.
[9] Sturm *et al.* (1997). Table 5, where fresh snow was type 1.0, decomposing snow was 2.0, small rounded grains were types 3.1 and 9.1 to 9.4, depth hoar was types 5.1, and 5.2, and melt freeze crusts were considered to be type 6.1 and 6.2.
[10] Dominé *et al.* (2002). Used values from Table 1.
[11] Legagneux *et al.* (2002). Estimated based on Figure 8.

complex. As the snowpack undergoes metamorphism, the density of an Arctic or subarctic snowpack lessens and becomes more permeable, with coarser grained crystals, as snow types such as large rounded grains, faced crystals, and depth hoar develop (Table 2.1).

The thermal conductivity (λ, W m^{-1} K^{-1}) of a snow cover is its ability to conduct heat. With the snow cover being a composite of air and ice, the thermal conductivity of snow must lie within the thermal conductivities of those two materials, which at −15 °C are 0.023 and 2.2 W m^{-1} K^{-1}, respectively (Sturm *et al.* 1997). The insulating capacity of the snow cover depends on its depth, crystal structure and density (Sturm *et al.* 1997) because the thermal conductivity of snow increases with the square of density, excluding very low-density snow (Li and Pomeroy 1997). Sturm *et al.* (1997) report that effective thermal conductivity ranged from 0.05 W m^{-1} K^{-1} for low density (0.1 g cm^{-3}), fresh snow, to 0.6 W m^{-1} K^{-1} for dense (0.5 g cm^{-3}) drifted snow. Snow with densities below 0.2 g cm^{-3} exhibits no relation between thermal conductivity and density as net thermal conductivity of the snowpack is controlled by depth hoar in this case (Sturm *et al.* 1997).

2.5 The influence of ground surface temperature on permafrost

2.5.1 Permafrost and the active layer

In many regions, long winters, and short summers lead to the development of a ground layer that does not thaw. This perennially frozen ground is permafrost, defined as ground (soil or rock) with a temperature that remains at or below 0 °C for at least two years (French 2007). The relations between the ground thermal regime and different ground layers are shown in Figure 2.7.

The depth to the base of permafrost (Fig. 2.7) depends on the mean annual surface temperature, the geothermal heat flux, and the thermal conductivity of ground material (French 2007). The mean annual ground surface temperature, and the heat loss from the ground surface, are the result of the energy balance, described in Section 2.4. Heat flows from the interior of the Earth, known as the geothermal flux, and generally ranges from ~0.05 W m^{-2} in the Canadian Shield to ~0.2 W m^{-2} in the Canadian Cordillera (Burn 2011). The ground layer above permafrost, which freezes and thaws annually, is known as the active layer.

2.5.2 The thermal regime of the active layer

Within the annual thermal cycle in the active layer there are four distinct periods based on the heat-transfer processes that occur in each. These are: (1) snowmelt in early spring, (2) thaw season in spring and summer, (3) freezeback in fall and early winter, and (4) frozen season in mid to late winter (Outcalt and Hinkel 1996) (Fig. 2.8). In early spring, the onset of snowmelt brings rapid increases in active-layer temperatures. Later in spring when the snow cover has melted and the ground surface temperatures rise above 0 °C, the active layer thaws from the surface downwards. Active-layer thickness is determined from penetration of the 0 °C isotherm. The maximum thickness is typically reached in late August to early September in northern Yukon.

Freezeback of the active layer begins once the ground surface temperatures fall below 0 °C, which happens shortly after the air temperatures fall below 0 °C in autumn. Freezeback occurs downwards from the ground surface but can also occur in lesser,

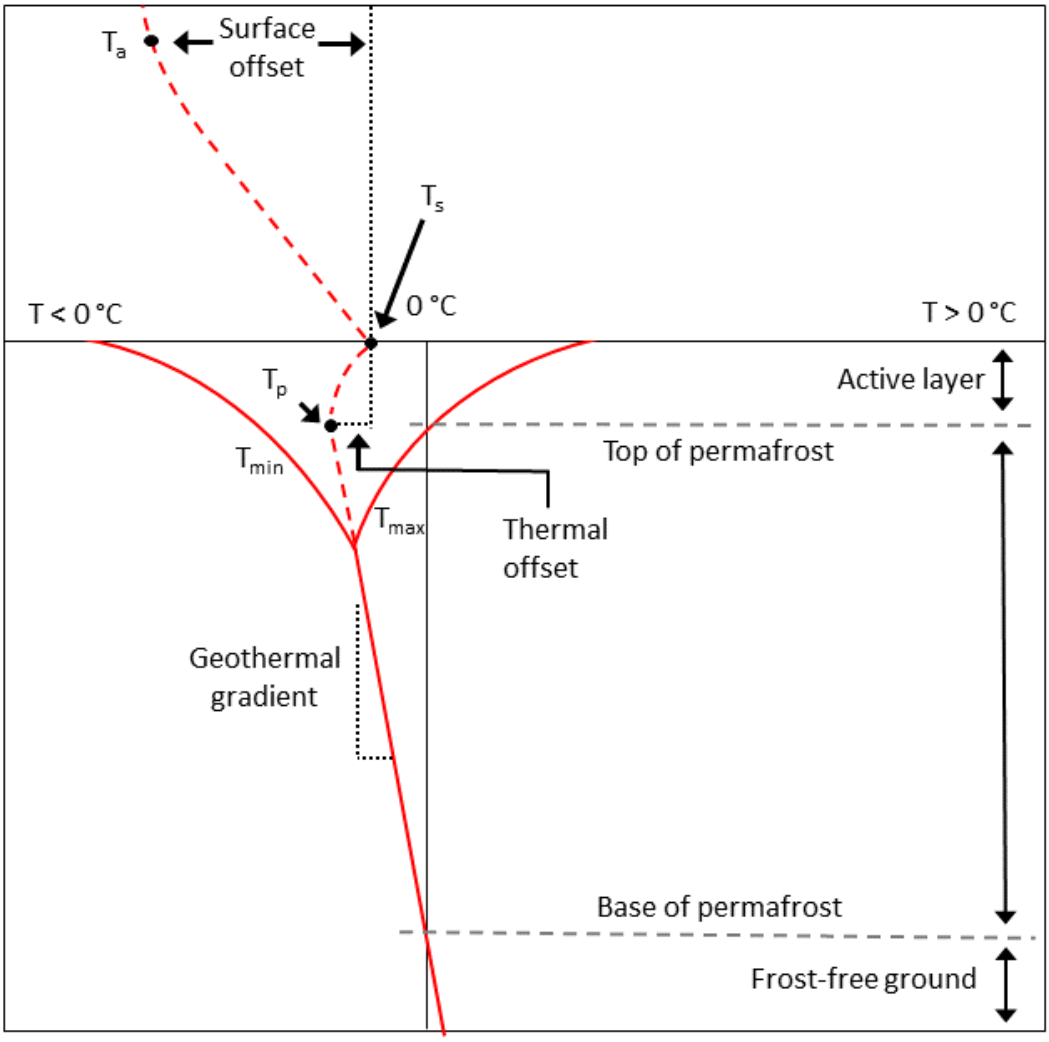

Figure 2.7. Ground thermal regime typical of a periglacial environment. After French (2007, Fig. 5) and Osterkamp and Burn (2003, Fig. 1, p. 1717). Where T_a, T_s, and T_p are the annual mean temperature of the air, ground surface, and top of permafrost, while T_{max} and T_{min} represent the annual maximum and minimum temperatures, respectively, and the dashed line represents the annual mean temperature.

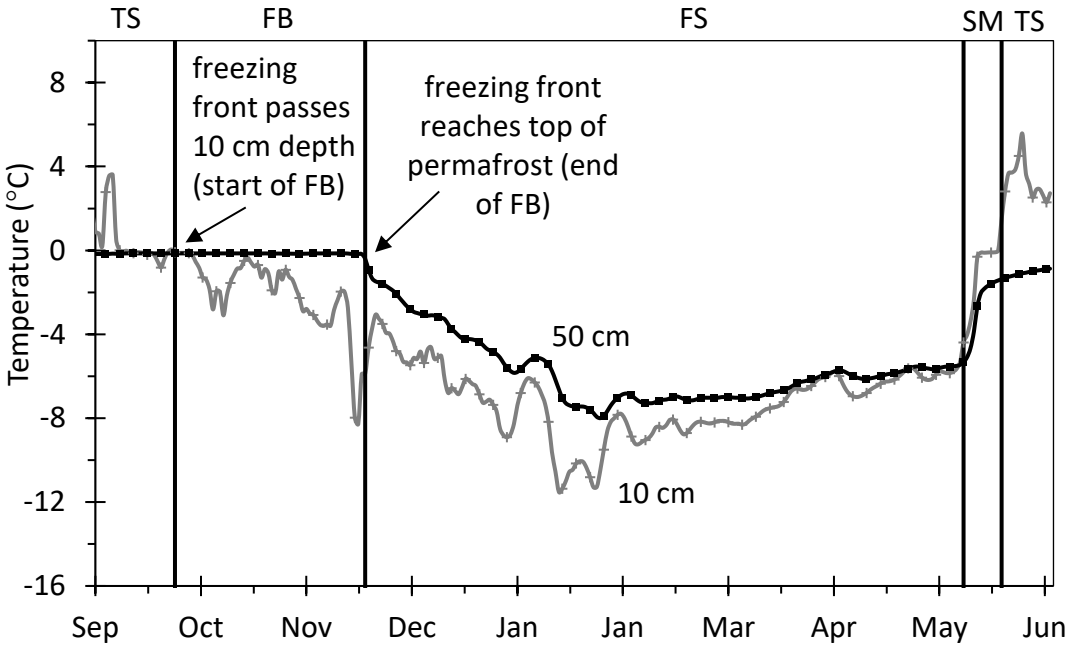

Figure 2.8. Daily mean ground temperatures at km 452 (P0L3), September 2018 to June 2019. With surface temperature in grey, and ground temperature in black. The thermal seasons of the active layer, as shown at the top of the graph: snowmelt (SM), thaw season (TS), freezeback (FB), freezing season (FS).

amounts from the top of permafrost upwards (Mackay 1983; Osterkamp and Romanovsky 1997). During active-layer freezeback, the freezing of soil water releases latent heat that may maintain the ground temperature at, or slightly below 0 °C for an extended period. This effect, the zero-curtain, is prolonged in soils with high water contents (Williams and Smith 1989). Closure of the zero-curtain occurs when most soil water has frozen, and there is a rapid decline in ground temperature within the upper portion of the active layer. Temperatures decline when sensible heat, rather than latent heat, is conducted out of the ground (Romanovsky and Osterkamp 1995). The closing of the zero-curtain corresponds to the end of the freezeback period, when the temperature at the top of permafrost begins to fall.

2.6 Controls on ground temperature and active-layer freezeback

2.6.1 Air temperature, and the role of the surface and ground offsets

The mean annual temperature of the air is distinguished from the mean annual temperature of the permafrost by the surface offset and the thermal offset (Lachenbruch *et al.* 1988). The surface offset is the difference between the annual mean temperature at the ground surface and the annual mean air temperature; the thermal offset is the difference between the annual mean temperature at the ground surface and the annual mean temperature at the top of permafrost (Lachenbruch *et al.* 1988) (Fig. 2.7).

The magnitude of the surface offset depends on the characteristics of the vegetation, snow cover, and moisture availability, which impact the energy balance at the surface (Eaton *et al.* 2001; Beltrami and Kellman 2003). Snow cover significantly influences the surface offset, and generally the greater the snow depth the greater the

difference between the air temperature and the ground surface temperature. Snow cover can insulate the ground from low winter air temperatures, which reduces cooling of the ground and can increase mean annual ground surface and permafrost temperatures by several degrees (Zhang 2005). The thermal offset is a result of the ratio of frozen and thawed ground conductivities and the length of the freezing season (Romanovsky and Osterkamp 1995; Riseborough 2002).

2.6.2 Physical and thermal properties of ground

Physical properties of a soil include texture, structure, density, porosity, temperature, colour, and moisture. Soil texture is the relative proportion of primary particles (i.e., sand, silt, and clay), while structure is the arrangement of solid particles and the pore spaces. Soil texture and structure determine porosity, density, water absorption and movement, and aeration of a soil. The main thermal properties of a soil are volumetric heat capacity, thermal conductivity, and thermal diffusivity. Typical values for the three thermal properties for various soil materials are shown in Table 2.2.

Thermal conductivity was introduced in section 2.4.2. The specific volumetric heat capacity (C) of a soil is the amount of heat which must be added or released to unit of volume of the material to change the temperature by 1 K (J K^{-1} m^{-3}, or J $°C^{-1}$ m^{-3}). While the thermal diffusivity is ratio of the thermal conductivity to the specific heat capacity and represents how quickly temperature may change through a material.

The physical properties of a soil influence the thermal properties and mediate the relations between the ground surface and the permafrost thermal regime (Andersland *et al.* 2003). Differences in the properties of water and ice are particularly important for the

Table 2.2. Thermal properties of various soil materials. Adapted with permission of Springer Nature Customer Service Centre GmbH from C.R. Burn, The Thermal Regime of Cryosols, In *Cryosols*, Edited by J. M. Kimble, Table 3.3.1, p. 394, © Springer-Verlag Berlin Heidelberg 2004.

Material	Thermal Conductivity (W m^{-1} $°C^{-1}$)	Volumetric Heat Capacity (J m^{-3} $°C^{-1}$)	Thermal Diffusivity (m^2 s^{-1})
Air (10 °C)	2.2×10^{-2}	8.6×10^{2}	2.6×10^{-5}
Water (10 °C)	5.6×10^{-1}	4.2×10^{6}	1.3 x 10-^{7}
Ice (0 °C)	2.2×10^{0}	1.9×10^{6}	1.16×10^{-6}
Quartz	8.0×10^{0}	2.1×10^{6}	3.81×10^{-6}
Mica	3.0×10^{0}	2.4×10^{6}	1.25×10^{-6}
Feldspar	2.0×10^{0}	2.0×10^{6}	1.0×10^{-6}
Peat (dry)	6.0×10^{-2}	5.8×10^{5}	1.03×10^{-7}
Peat (wet)	5.0×10^{-1}	4.0×10^{6}	1.25×10^{-7}
Peat (wet, frozen)	1.1×10^{0}	1.6×10^{6}	6.9×10^{-7}

ground thermal regime. Pore ice has a higher thermal conductivity than unfrozen soil moisture, and makes heat transfer more efficient in the winter, creating a thermal offset (Smith and Riseborough 2002). This is the cause of the inflection in the profile of mean annual temperature within the active layer (Fig. 2.7). Soil particle-size distribution and specific surface area, both physical properties of a soil, determine the unfrozen water content at a given temperature (Burt and Williams 1976).

2.7 Summary

The distribution of snow cover is a major control on its condition and evolution. Obstructions to wind flow, including road embankments, topographic features, vegetation, and snow fences, dissipate kinetic energy and allow for the deposition of wind-transported snow, often in predictable patterns. In tundra, porous snow fences produce both up and down-wind snow drifts, with stratified layering and varying properties. Snow distribution and conditions control the physical and thermal properties of the snowpack. The insulative effect of a snow cover, which increases with depth and decreases with density, reduces ground cooling during freezeback and the frozen season, and can increase mean annual ground temperature. Rising ground temperatures may thaw near-surface ground ice causing subsidence (Burn and Kokelj 2009). Permafrost degradation in response to ground warming is particularly important along northern highways where snow may accumulate alongside the road (O'Neill and Burn 2015), increasing the risk of thaw subsidence and damage to infrastructure.

Chapter 3: STUDY AREA AND METHODOLOGY

3.1 Introduction

This chapter describes the location, physiography, regional climate, and characteristics of the two field sites discussed in this thesis, which are located at km 452 and km 456 (Fig. 1.1). Following the description of the sites, the field methods used to install the snow fencing, as well as to collect data on snow conditions and ground temperatures, are presented. Finally, the methods used to analyze the data are described, and limitations of the study design are discussed.

3.2 Study area

The field sites are located along the Dempster Highway in Yukon, 9 and 13 km south of the Yukon–Northwest Territories border (km 465 YT/km 0 NT). The sites are within Hurricane Alley, where the road is parallel to a valley side wall. Hurricane Alley is midway (~80 km) between Eagle Plains to the south and Fort McPherson to the northeast. The area is bounded by 66.91° N, 67.04° N, 136.36° W, and 136.21° W (Fig. 1.1).

3.2.1 Regional setting

The study area lies within the British–Richardson Mountain ecoregion (165) of the Taiga Cordillera ecozone (Ecological Stratification Working Group 1995). The ecoregion includes Richardson and British mountains, as well as Arctic Plateau between them (Bostock 1948a) (Fig. 3.1). Richardson Mountains are a straight narrow belt with a broad

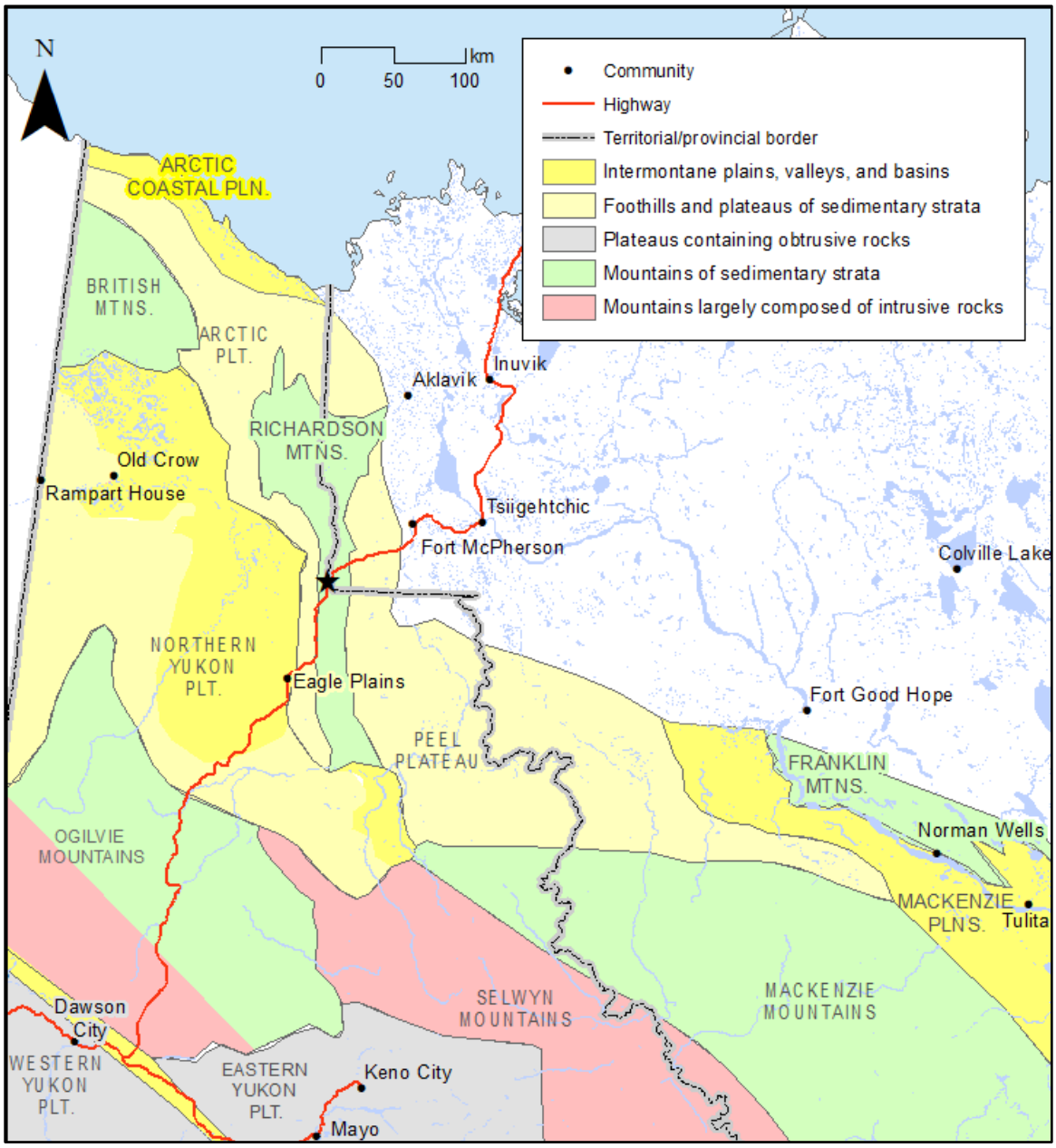

Figure 3.1. Subdivisions of the Canadian Cordillera, including the north–south oriented Richardson Mountains. After Bostock (1948b, "A" Series Map no. 922). The black star indicates Hurricane Alley.

northern end confined by Peel Plateau to the east and Arctic Plateau to the west (Bostock 1948a) (Fig. 3.1). Hurricane Alley is situated on the western face of the Richardson Mountains (Fig. 3.1). The Richardson Mountain belt, is widest (80 km), and highest at 68° N (Catto 1996), just north of the Dempster Highway territorial border crossing at 67° N.

Glacial limits recognized by McConnell (1891), Ogilvie (1890), Hughes (1972), and Bostock (1948) established that Richardson Mountains represent part of the limit of continental glaciation in northern Canada. Hughes (1972) and others (Bostock 1948a; Rampton 1982, 1988) suggest that ice pushed up from the south and glaciation terminated in a line slightly east of Richardson Mountains. There is no evidence of glaciation along the western slopes of Richardson Mountains where Hurricane Alley is located (Bostock 1948a; Hughes 1972; Catto 1996).

The ecoregion, including Richardson, British, and Barn mountains is composed of folded sedimentary strata (McConnell 1891). Richardson Mountains are generally a series of steep smoothed ridges of north–south orientation separated by relatively broad valleys (Catto 1996). Resistant quartzites and sandstones make up the ridges, while weathered siltstones and shales compose the valleys (Norris 1985). Middle and low elevation areas are covered by residual rock, weathered rock, and solifluction or colluvial materials, forming fans or gentle slopes (Yukon Ecoregions Working Group 2004). Turbic Cryosols are the dominant soil type over most of the northern Yukon, including Hurricane Alley, with rock and/or ice possibly nearer to the mountain ridge (Soil Classification Working Group 1998).

Shrub tundra is the dominant vegetation of the Richardson Mountains (Zoltai and

Pettapiece 1973; Scudder 1997; Yukon Ecoregions Working Group 2004). The highway in Hurricane Alley is just above the ~ 600 m ASL treeline, where the shrub tundra (subarctic alpine tundra) is a combination of low and dwarf shrubs, graminoids, forbs, bryophytes, and lichens. Trees are generally limited to river valleys and low slopes with favourable aspects, and shrub thickets to moist sites along creeks, drainage areas and regions of snow accumulation (Yukon Ecoregions Working Group 2004) (Fig. 3.2a). Low slopes support sedge tussock communities (Fig. 3.2b). Tussocks often form from tussock cottongrass (*Eriophorum vaginatum*), beautiful cottongrass (*E. callitrix*), narrow-leaved cottongrass (*E. angustifolium*), and spruce muskeg sedge (*Carex bigelowii ssp. lugens*) and are commonly seen with shrub birch (*Betula glandulosa*), Labrador tea (*Rhododendron tomentosum* subsp. *decumbens*), bog bilberry (*Vaccinium uliginosum*), lingonberry (*V. vitis-idaea*), and mosses (Fig. 3.2c). Upper and middle slopes range from dry to moist conditions and support a mix of low shrub and heath tundra (Fig. 3.2d) and are composed of microsites with variable moisture (3.2e, 3.2f).

3.2.2 Climate

The climate of Yukon is characterized by long cold winters, short warm summers, and an annual mean daily temperature below freezing (Wahl *et al.* 1987). Storms typically move west to east across the Yukon due to the general circulation pattern and the eastward progression of pressure systems (Wahl *et al.* 1987). In January, a major cell of high pressure prevails over the central Yukon and Mackenzie Mountains, stabilizing weather and leading to clear skies and low temperatures.

The continental climate, modified by the topography and elevation of Richardson

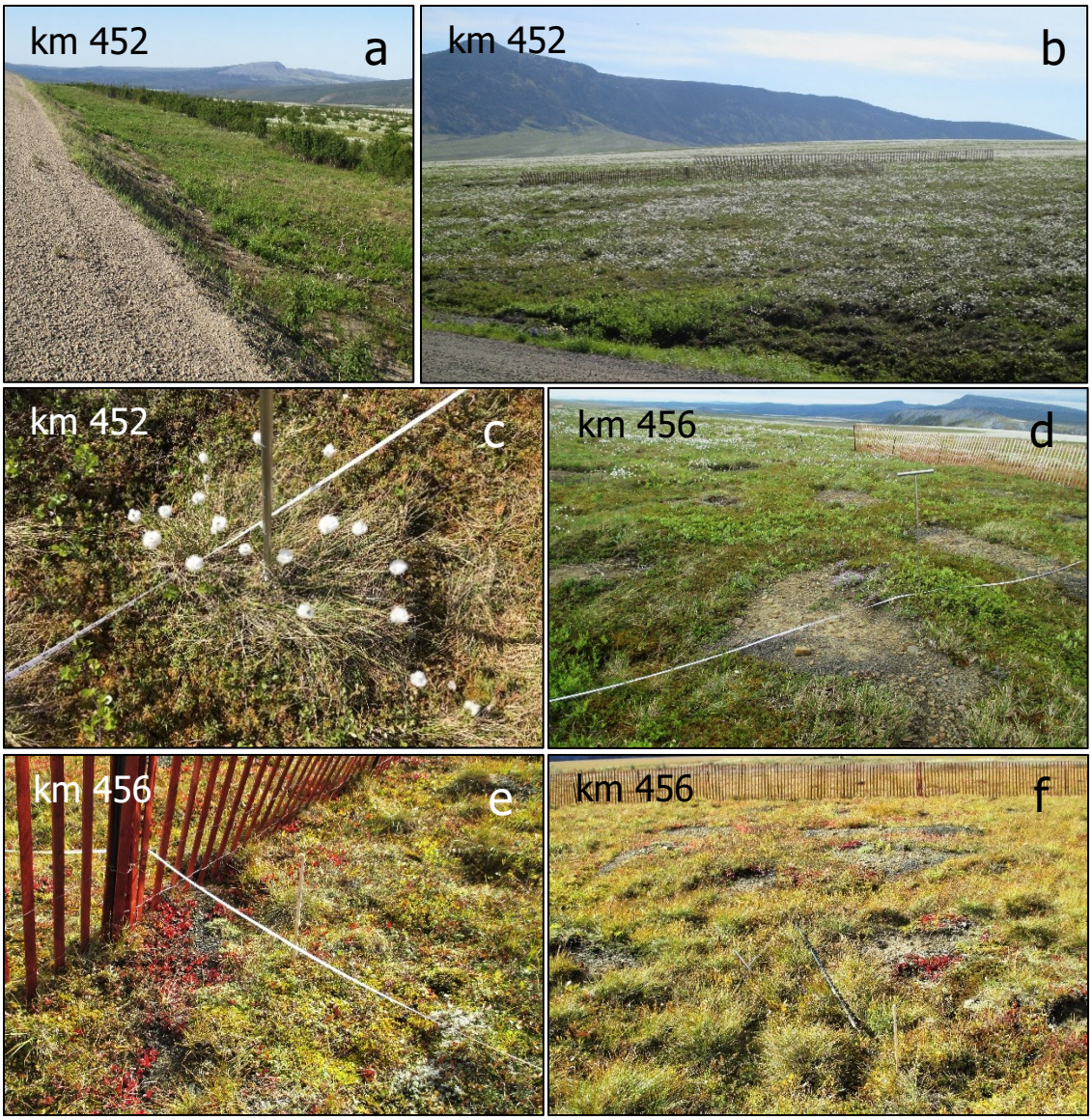

Figure 3.2. Vegetation communities in Hurricane Alley, showing (a) shrub thicket in the western right-of-way at km 452, (b) sedge tussock east of the road at km 452, and (c) a tussock in greater detail, as well as (d) microsites east of km 456, some of which are dominated by (e) lichen, mosses and herbaceous plants, while others support (f) sedge tussock.

Mountains in Hurricane Alley and the surrounding region, is classified as Northern Mountains by Wahl *et al.* (1987). This climate is characterized by moderate precipitation of 300–400 mm annually with most occurring in the summer, mild winter temperatures due to air temperature inversions, and unstable weather due to the proximity to the Beaufort Sea. The area near the border often experiences poor visibility, and a low cloud ceiling, as well as strong easterly winds as observed at the Rock River weather station (km 457) (Klock *et al.* 2001; Humphries *et al.* 2019) (Fig. 3.3), which are examples of downslope foehn winds (Ribberink *et al.* 2020).

The climate of northern Yukon is represented by conditions observed at Old Crow (252 m ASL), 170 km from the field sites, and Fort McPherson (25 m ASL), 95 km from the field sites in Peel Plateau (Fig. 1.1b). At Old Crow for 1981–2010, the mean annual air temperature (MAAT) was −8.3 °C, mean annual total precipitation (MATP) was 278.6 mm, and mean annual total snowfall (MATS) was 141.4 mm (Environment Canada 2018a). At Fort McPherson, MAAT was −7.3 °C for 1981–2010, MATP 297.7 mm, and MATS 152.5 mm (Fig. 3.4) (Environment Canada 2018a). More recently, the MAAT at Old Crow for 2015–2017 was −6.2 °C (Environment Canada 2018b). In comparison the MAAT from nearby weather stations at km 421 and 457 (Rock River) in Yukon, and km 8.5 and 51.5 in Northwest Territories for 2015–17 were −4.5 °C, −4.5 °C, −5.1 °C and −4.8 °C, respectively. The higher mean annual air temperatures than at lowland communities indicate the influence of winter inversions on the study area's climate mentioned by Wahl *et al.* (1987) and observed in Peel Plateau by O'Neill *et al.* (2015a).

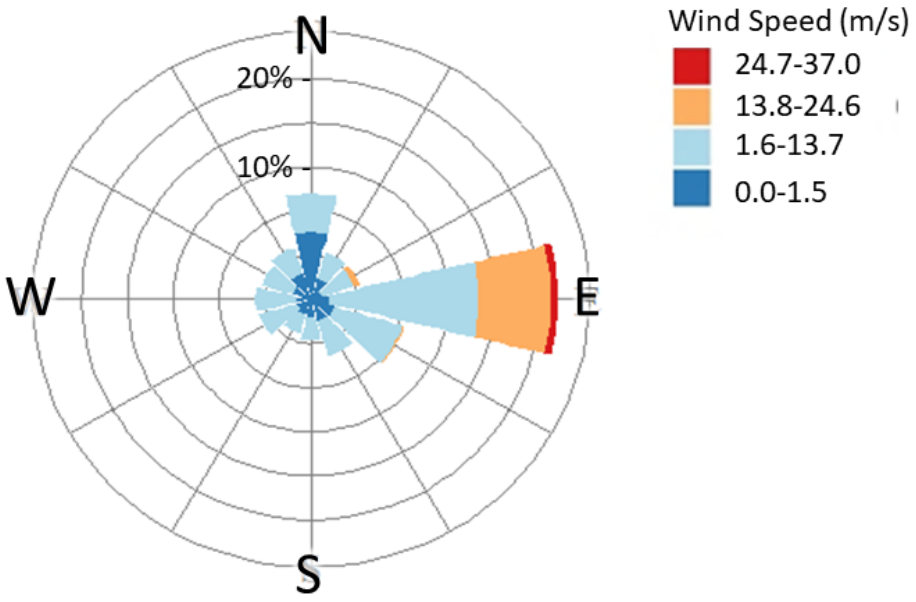

Figure 3.3. Frequency of wind speed by direction, Rock River weather station 730 m ASL, km 457 (66.98° N, 136.21° W), 2014-2018.

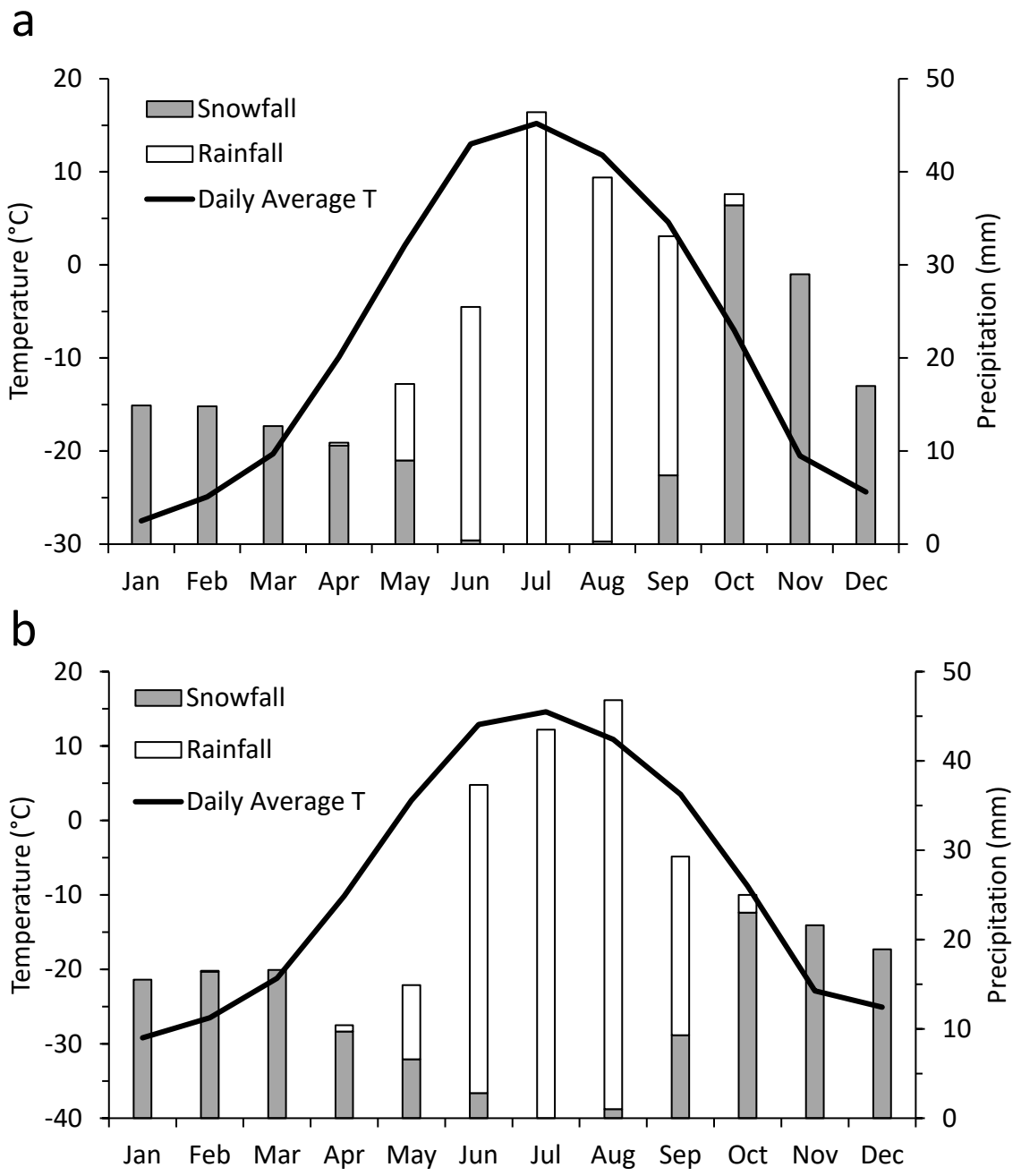

Figure 3.4. Monthly climate normals (1981–2010) for (a) Fort McPherson (66.97° N, 135.43° Wand 29 m ASL) and (b) Old Crow (67.57° N, 139.84° W, and 255 m ASL). Canadian climate normals 1981–2010 data from Environment Canada (2018b).

3.2.3 Ground temperature

The study region is within the continuous permafrost zone (Heginbottom *et al.* 1995) and largely unglaciated (Catto 1996; Lacelle *et al.* 2013). Geomorphic indicators of the severe frost action throughout the Quaternary in this area include patterned ground, solifluction lobes, frost-shattered rocks, and cryoplanation terraces (Lauriol 1990; Yukon Ecoregions Working Group 2004). Undisturbed ground temperatures are relatively moderate in the tundra of Peel Plateau due to winter air temperature inversions producing warmer winter temperatures in elevated regions; at 5 m depth mean annual ground temperature (MAGT) for 2013/14 is −1.8 °C and −2.6 °C at NT km 51 and 60, respectively (O'Neill and Burn 2017b). South of Hurricane Alley, at YT km 421, MAGT over 2014/15 at 8 m depth was −3.6 °C (Idrees *et al.* 2015). Mean annual temperature at the top of permafrost between 2014–18 was −1.9 °C at km 421, −0.7 °C at km 8.5, and −0.3 °C at km 51.5 (Stockton *et al.* 2019). MAGT was −3.8 °C at 10 m depth in 2012/13 at the territorial border (Burn *et al.* 2015).

3.3 Study design

3.3.1 Site selection

Following an initial site visit, two field sites known for high wind speeds and a history of high maintenance requirements due to blowing snow were selected at km 452 and 456. The locations were chosen from a set of locations identified by Cathy Brais, Road Foreman, Eagle Plains. The sites, with distinct topographic features, were selected to evaluate the site-specific fence efficacy.

3.3.2 km 452

Hurricane Alley is situated within a 13 km-wide and 12 km-long valley where the Richardson Mountains make up the eastern valley wall. The Dempster Highway lies on a lower slope of this wall. The highway runs northeast–southwest at km 452 (Fig. 3.5a). The 400 m-long study area at the entrance to Hurricane Alley is on a hillslope facing northwest (Fig. 3.5b). The area is in low shrub tundra overlying gravel and bedrock. The hillslope peaks at ~723 m ASL, declining to ~670 m ASL at the highway (Fig. 3.6), and continuing to ~550 m ASL in the valley floor. The average slope within 50 m of the highway is 5.6°.

Soil stratigraphy comprised 30 cm of vegetation and organic matter, on top of silt and clay high in organic matter, and coarse material. Nearby at km 454, drilling in July 2017 revealed a 30 cm organic layer overlying silty sand to 1 m depth (Calmels *et al.* 2018). The sediment transitions to a silt with sand and gravel at 1.3 m depth, returning below to a silty sand, and ending in sediment with greater than 50% gravel content at 2.8 m (Calmels *et al.* 2018). Ice lenses were visible at a depth of 30 cm at the borehole and indicate proximity of the top of permafrost (Calmels *et al.* 2018).

On the eastern side of the roadway the vegetation is tussock sedge, 10 cm tall on average, composed of cottongrass and a variety of graminoids (Fig. 3.7a). On the western side of the highway the snow accumulates in large drifts creating a moist, wind-protected environment where willows have proliferated, growing up to 2.5 m tall. The willows have been cut back in the western right-of-way (wROW), i.e., the area extending 15 m west of the road, as part of regular highway maintenance, revealing an understory of forbs and grasses (Fig. 3.7b). The active layer in early October 2018 was thickest in the wROW,

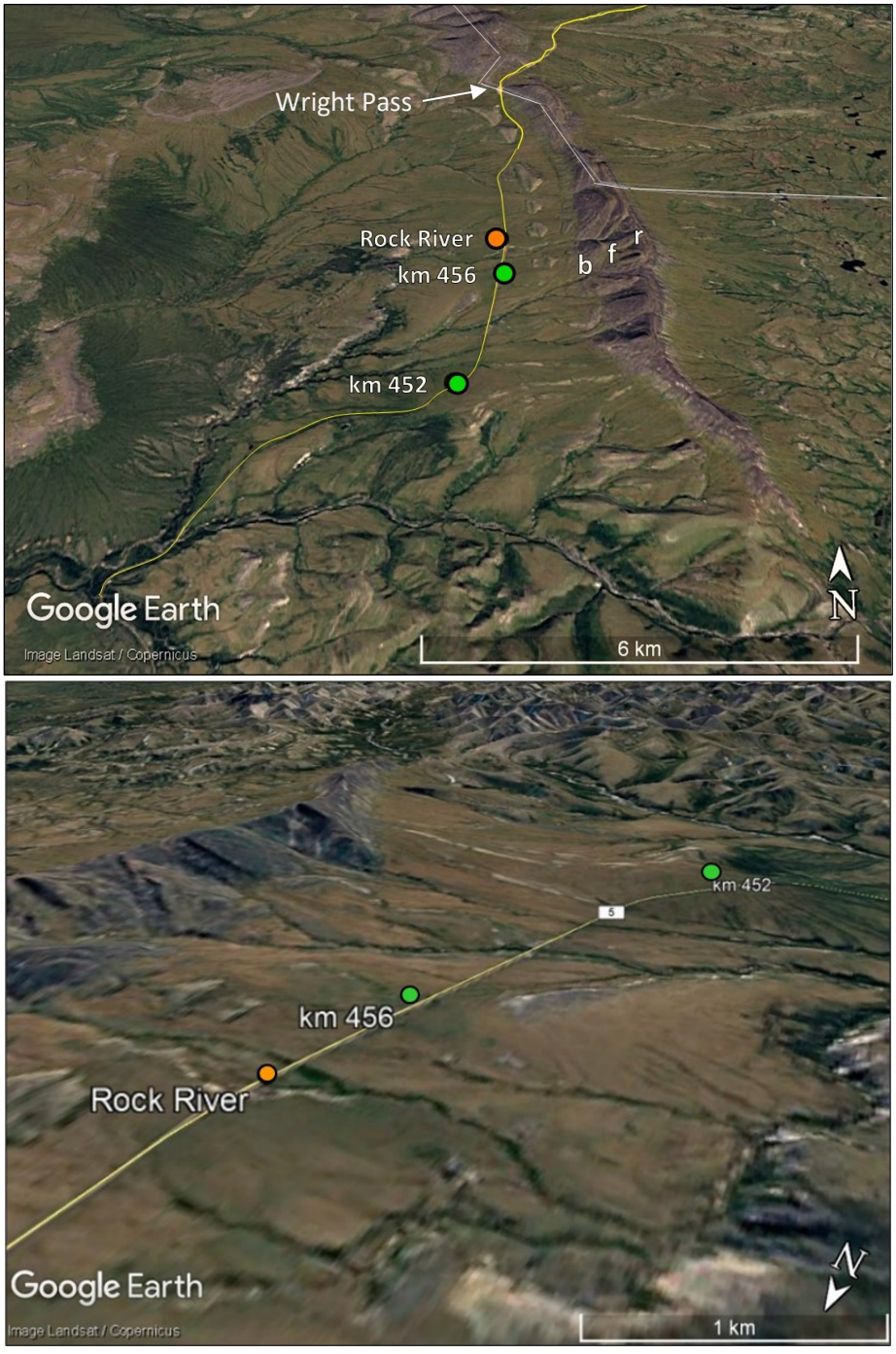

Figure 3.5. Overview of the sites and their position relative to the single ridge running N–S, a part of the Richardson Mountain belt, showing: (a) km 452 to the west of ridges' southern end, and (b) the road cutting across the foot slope of a large hill at km 452. Where r, f, and b are the mountain ridge, flank, and base. Rock River weather station is west of the road at km 457. Satellite imagery from a) Google Earth (2015), and b) Google Earth (2014).

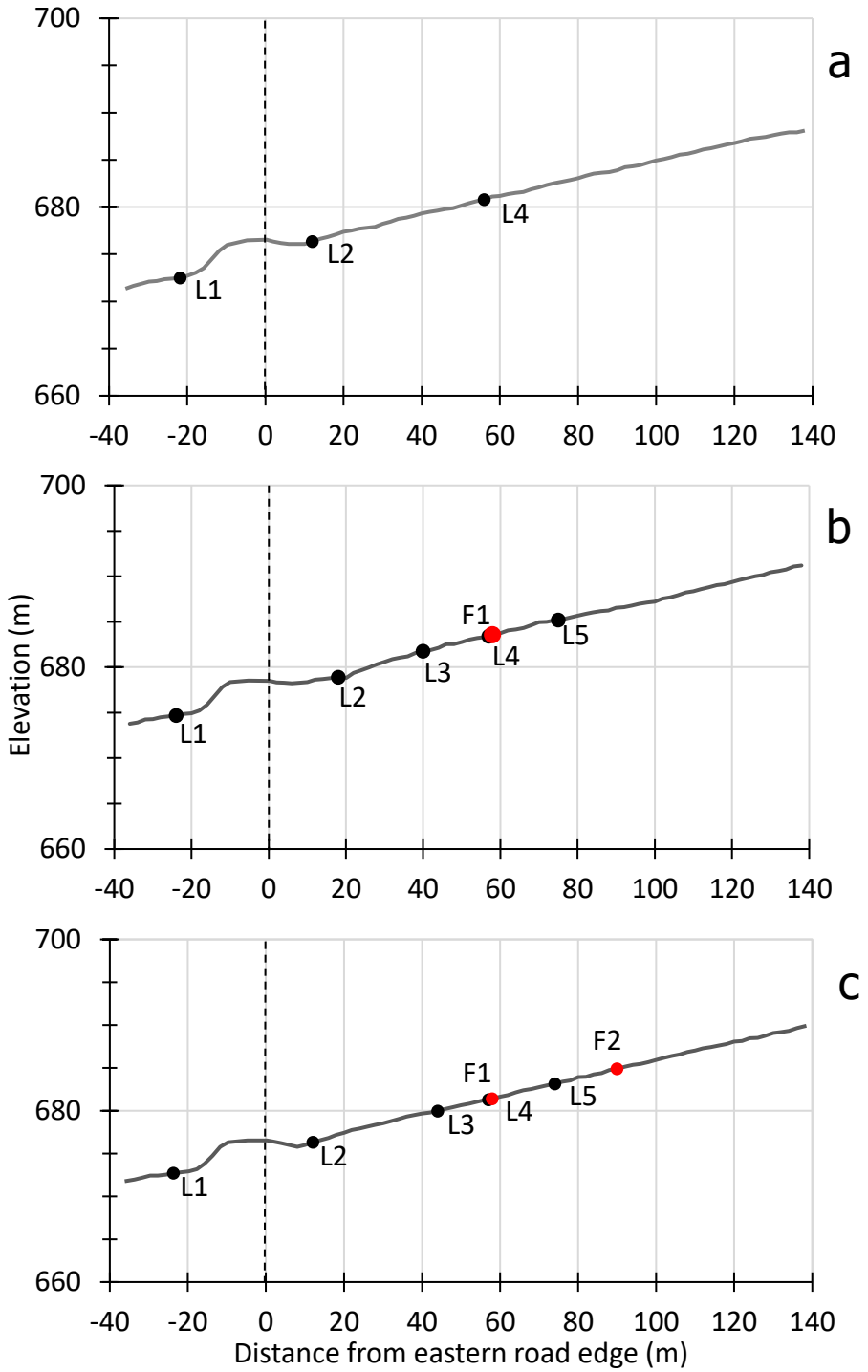

Figure 3.6. Km 452 elevation profiles at a) the control plot (P0) with no fences, b) plot 1 (P1), with one fence row, and c) plot 2 (P2) with two rows of fence. Black circles represent the location of ground temperature loggers (L1–L5) and red circles the fence row (F1–F2). Vertical scale is displayed with an exaggeration of 4.5.

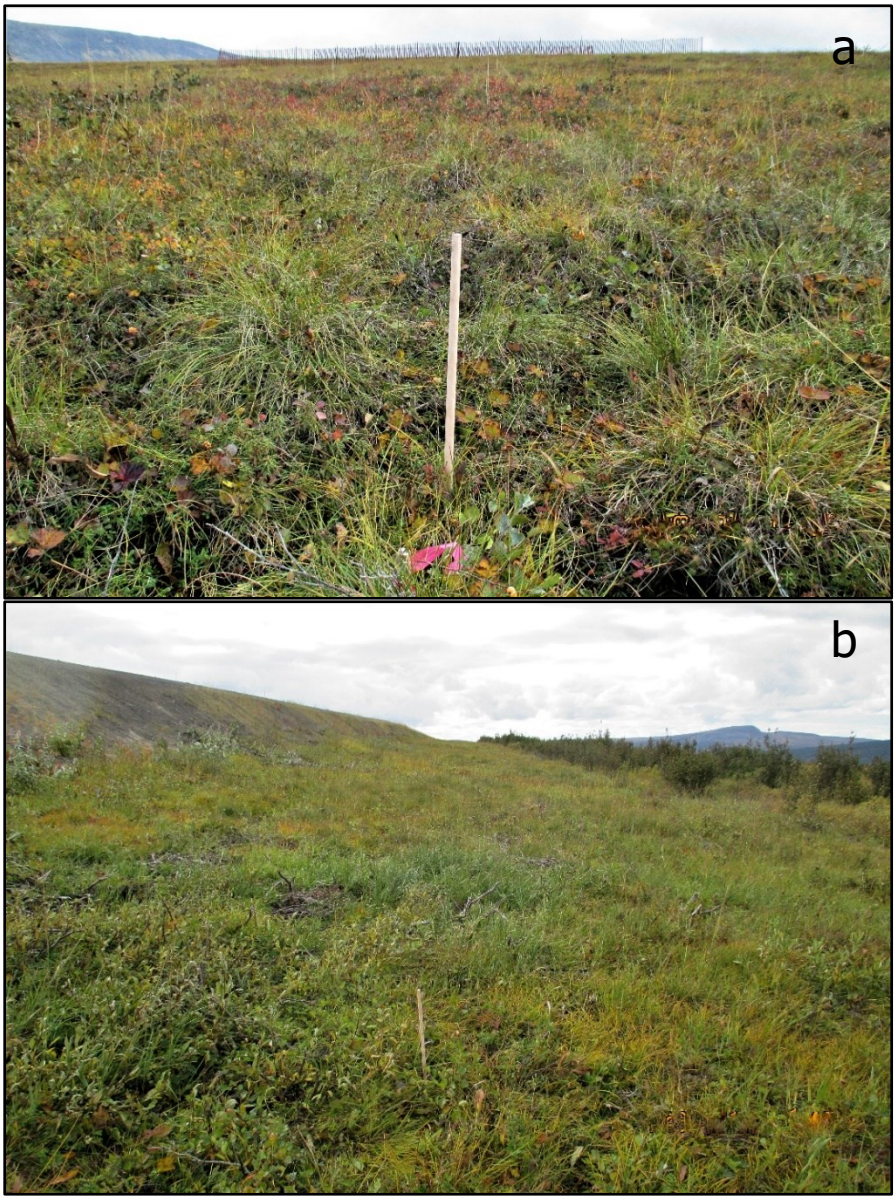

Figure 3.7. Vegetation at km 452 in 2018: (a) tussock-sedge community upslope of the road, and (b) understory of cutback shrub thickets downslope of the road. The road embankment is on the left side of the photograph.

followed by the eastern right-of-way (eROW), i.e., the area up to 15 m east of the road, and finally the eastern hill slope in the tundra, with mean values of 60 cm (n=12), 45 cm (n=18) and 40 cm (n=102), respectively.

3.3.3 km 456

Km 456 was chosen as the second study area for its history of high snow accumulation along the highway ROW. The highway runs ~north to south at km 456, towards Wright Pass at the territorial border and follows closely along the western slope of Richardson Mountains (Fig. 3.5b). The 400 m-long study area was set atop a gravel outcrop, with a west-facing bank (Fig. 3.8). East of the road the elevation of the ridge of Richardson Mountains peaks at ~1100 m ASL, descends to ~710 m ASL at the highway (Fig. 3.9), and continues down to ~590 m ASL in the valley bottom. Upslope of the gravel cut the average slope of tundra was 4.7°.

The soil stratigraphy is comprised of an organic layer 25 cm deep, which sits on an organic silty sand to 50 cm depth and then colluvium. The colluvial material is a heterogenous mixture of coarse granular, and fine-grained (typically sand), materials (Calmels *et al.* 2018). Mud boils, upwellings of mud from differential heave of frost susceptible soils (ACGR 1988), occur sporadically over the tundra east of the road. Wind flows downslope uninterrupted from the ridge of Richardson Mountains. Frequent scouring of snow in winter and drier site conditions contribute to a low shrub tundra vegetation community with proportionally less tussock forming grasses, and more shrubs, forbs and lichen than occur at km 452 (Fig. 3.10a). Clearcutting of the ROW was not necessary at this site as the vegetation was mostly tall grasses and shrubs (Fig. 3.10b).

Figure 3.8. The gravel bank east of the road in 2018 at km 456.

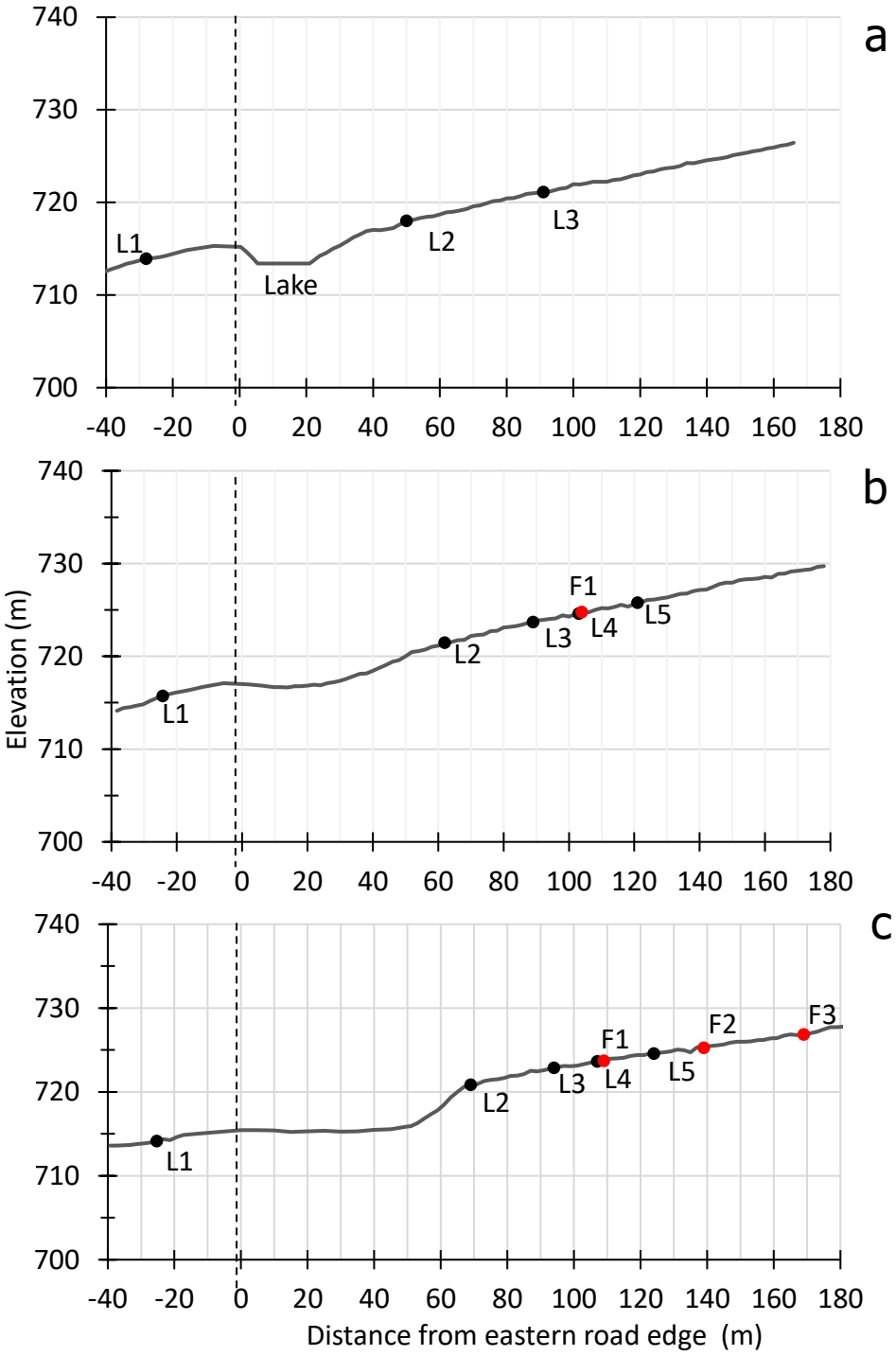

Figure 3.9. Km 456 elevation profiles at a) the control plot (P0) with no fences, b) plot 1 (P1) with one fence, and c) plot 2 (P2) with two rows of fences. Black circles represent the location of ground temperature loggers (L1–L5) and red circles the fence row (F1–F2). Vertical scale is displayed with an exaggeration of 6.

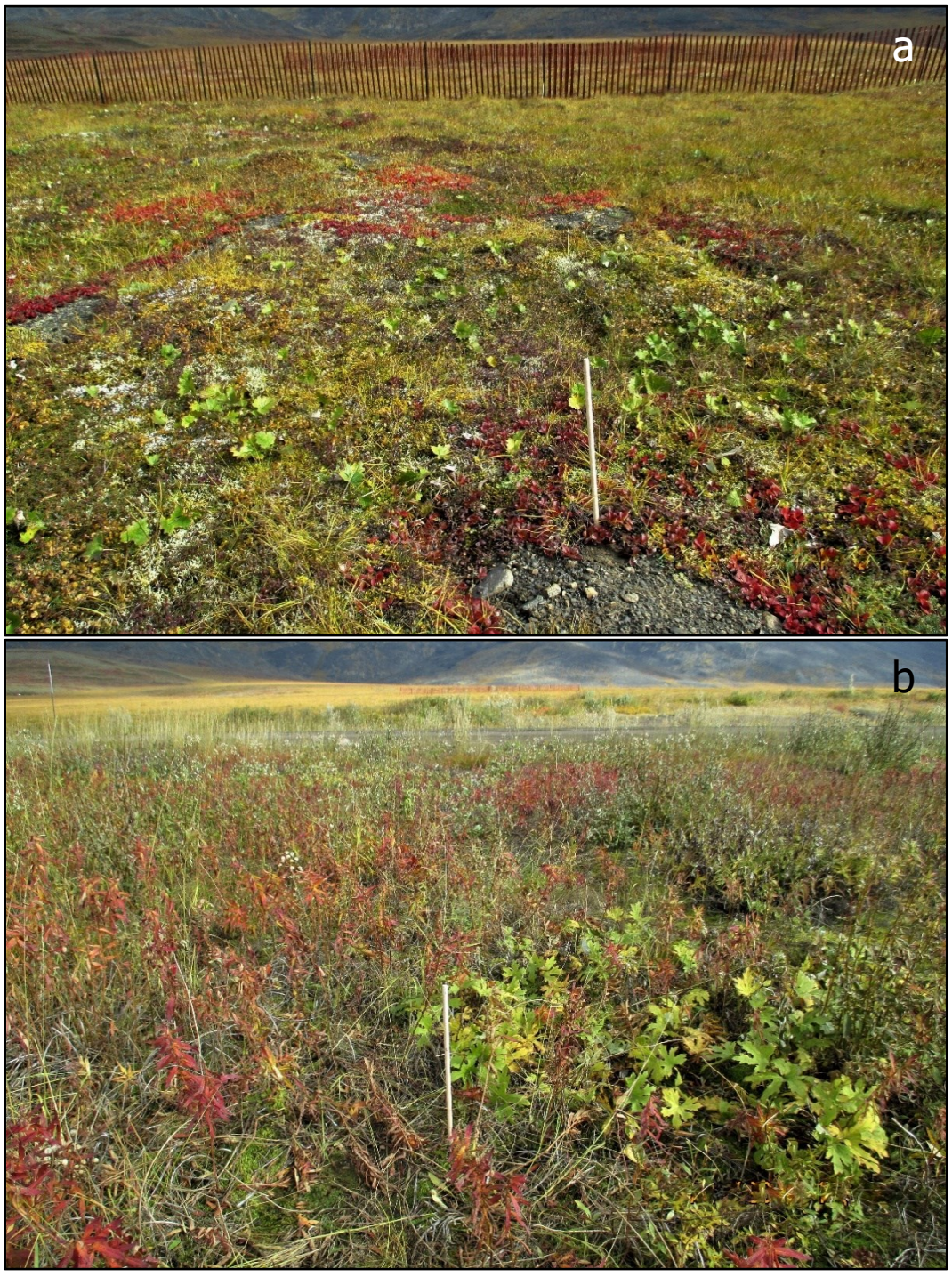

Figure 3.10. Vegetation at km 456 in 2018: (a) exposed ground materials, and the dominance of short, annuals upslope of the road, and (b) the prevalence of tall non-tussock forming grasses and shrubs downslope from the highway.

The ground material was too rocky to measure active-layer thickness within the ROW. In the tundra, active-layer thickness in early October 2018 varied from 46 to 80 cm and was 63 cm on average (n = 120).

3.4 Field methods

Field work was conducted between June 2018 and June 2019. Field visits took place in late August 2018, early October 2018, mid-December 2018, mid-March 2019, and June 2019 to investigate the efficacy and impacts of fencing along the Dempster Highway in Hurricane Alley. Traditional vertical wood slat snow fencing arranged in multiple rows with a minimal bottom gap was chosen over a tall fence of a single row as the traditional slat snow fencing is widely available and easy to install, making it a likely choice for use along a remote northern highway with limited personnel. It also serves as a good starting point to examine the general applicability, as well as any potential implications of installing fences alongside the highway.

3.4.1 Fence Installation

3.4.1.1 km 452

Three plots were established at km 452, a control with no fence rows (P0), a plot with a single row of fencing (P1), and a plot with a double row of fencing (P2) (Fig. 3.11). Fencing was installed in August 2018. Each row of fence was 30 m long, and 1.22 m tall, and constructed from traditional vertical wood slat snow fencing with no bottom gap (Fig. 3.12). This fencing type is composed of slats 3.8 cm wide, spaced 6.3 cm apart, with a porosity of 60%. The fencing was placed at an angle perpendicular to the average

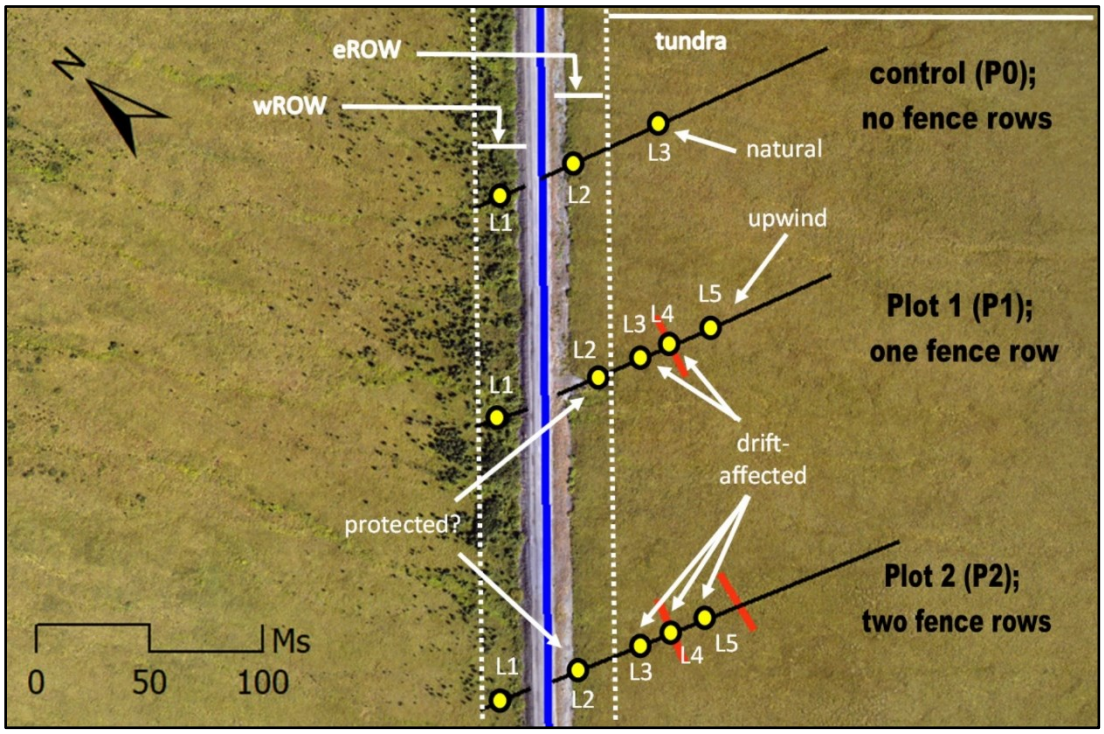

Figure 3.11. Experimental layout at km 452, with the blue line representing the Dempster Highway, red lines indicating the fence rows, black lines indicating the transects, and yellow circles the locations of ground temperature loggers. Aerial photograph from Yukon Government (2014a).

Figure 3.12. A row of traditional vertical wooden slat snow fencing installed at km 452.

winter wind direction, determined from meteorological data retrieved from the Rock River weather station, and satellite imagery (Digital Globe, Inc. 2016) that showed snowdrift formation.

The most common wind direction was easterly (Fig. 3.3), and the fences were oriented NNE–SSW (Fig. 3.11). The primary fence, nearest the road, was placed 35H, equivalent to 42 m from the end of the eastern ROW, or 60 m from the road's edge. The secondary and tertiary fences were set back an additional 35 m (30H) from the primary fence to trap the maximum amount of snow. Fence position was based on guidelines by Tabler (2003) to position the road and wROW in the zone of snow protection.

One transect was established at each plot, beginning from 20 m to the west of the road and extending 100 m to the east, in order to place the instrumentation as well as to conduct repeated winter snow surveys. At P1 and P2 ground temperature loggers were placed: in the wROW (L1); in the eROW (L2); 45 m from the eastern edge of the road, 15 m west of the primary fence (L3); at the primary fence (L4); and 15 m east of the primary fence (L5). Ground temperature loggers at P0 were placed at positions L1, L2 and L3 only (Fig. 3.6, 3.11).

The locations of the loggers were chosen to examine the impact of altered snow cover due to fencing on the ground thermal regime (Fig. 3.6, 3.11). L1 was positioned beneath the snow drift that develops west of km 452. L2 was positioned in the eROW to represent the ground thermal regime beneath: (1) the potential zone of snow protection at P1 and P2, or (2) the natural snow cover in the eROW at P0. L3 was positioned to represent the ground thermal regime beneath: (1) the downwind snow drift at P1 and P2, or (2) the natural tundra at P0, while L4 represented the ground thermal regime beneath

the fence line at P1 and P2. L5 represented the ground thermal regime beneath: (1) the tundra upwind of the fence at P1, i.e., upwind tundra, or (2) the downwind drift of the secondary fence at P2.

3.4.1.2 km 456

Like km 452, three plots were established at km 456 in late August 2018. A control plot with no fencing (P0), a plot with a single row of fencing (P1), and a plot with a triple row of fencing (P3) (Fig. 3.13). Three rows were installed at P3 because that is highest number of rows that might reasonably be used for snow protection along the highway. The fencing was again placed perpendicular to the prevailing winter wind direction, east, and ran NNE–SSW. The large gravel cut (Fig. 3.8) extends ~70 m east of the road, and the primary fences were placed a further 42 m upslope from the top of the gravel cut. At each plot, two transects, one extending east and the other extending west, were established. East of the road, the transect began at the top of the gravel cut, ~70 m, and extended 100 m eastward. To the west, the transect began at the western road's edge and extended 20 m.

Instrumentation was placed in the same configuration as at km 452 (Fig. 3.11, Fig. 3.13). However, at km 456 the eastern transect began from the top of the gravel cut, as opposed to the eastern road edge. At P1 and P3 ground temperature loggers were placed: in the wROW (L1); at the top of the gravel cut, ~70 m from the road edge (L2); 85 m from the road's edge, equivalent to 15 m in front of the primary fence (L3); at the primary fence (L4); and 15 m upslope of the primary fence (L5) (Fig. 3.9). Ground temperature loggers at P0 were placed at locations L1, L2 and L3 only.

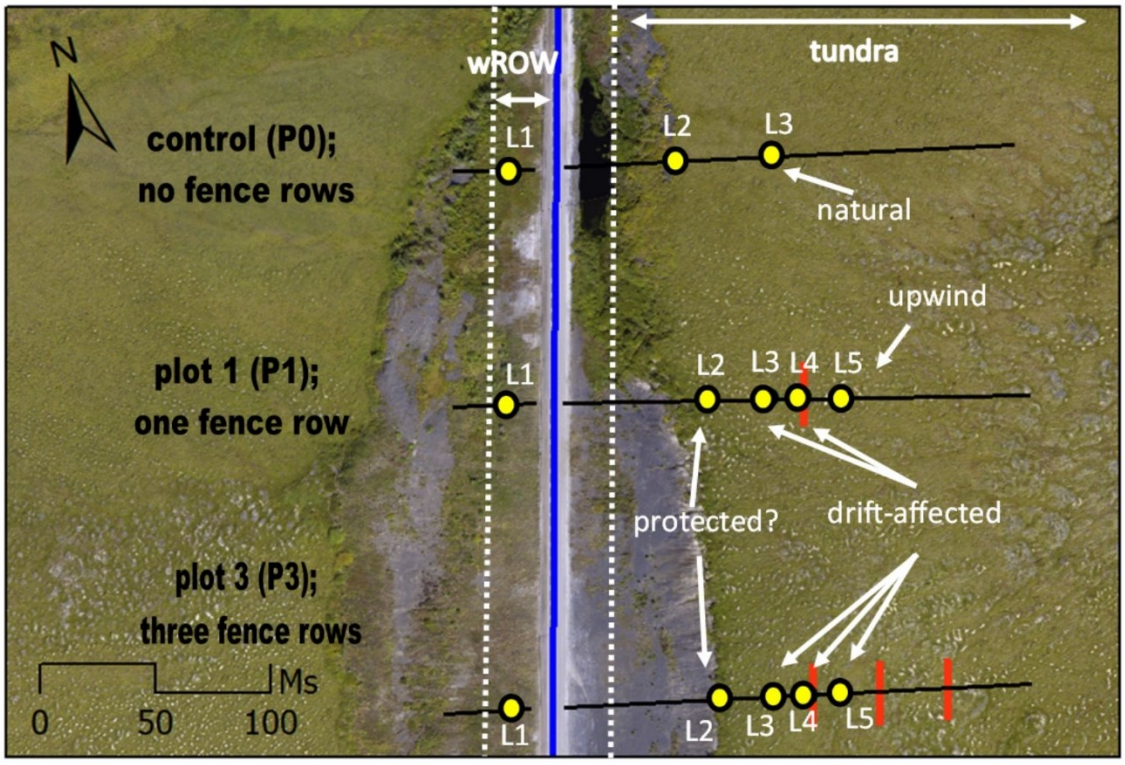

Figure 3.13. Experimental layout at km 456, with the blue line representing the Dempster Highway, black lines representing the transects, red lines the fence rows, and yellow circles the location of ground temperature loggers. Aerial photograph from Yukon Government (2014b).

3.4.2 Ground temperature

Ground temperatures were measured to determine the timing and rate of active-layer freezeback and the thermal differences that exist between the plots. Ground temperature sensors were mounted on wooden dowels that were placed directly into 5 cm diameter holes in the ground (Fig. 3.14). Ground temperatures were measured at 10 and 50 cm depths. 50 cm was the greatest possible depth for consistency among sites given the rocky ground materials. The sensors installed at 10 cm depth (T_{10}) are hereby referred to as surface temperature, and those at 50 cm depth (T_{50}) are referred to as ground temperature.

Surface and ground temperatures were measured using Onset HOBO Pro v2 2x External Temperature Data Loggers and U23-003 external temperature sensors. The accuracy of the sensor was ±0.4 °C at −40 °C, and ±0.2 °C at 0 °C. The resolution was ±0.02 °C at 25 °C. The sensor operation range was −40 to 100 °C and the logger operating range was −40 to 70 °C. The loggers were programmed to record temperatures every 20 minutes beginning August 2018 and were downloaded in June 2019.

3.4.3 Snow measurements

Snow depth and density were measured to determine the variability in snow cover across the sites. Measurements of snow depth and density were made on 14 to 17 December 2018 and 9 to 11 March 2019, with snow depth also measured on 2 to 4 October 2018. Snow depth was determined with a probe to the nearest 0.5 cm. Three measurements were taken every 1 m along the transects perpendicular to the road, as well as at the fencing.

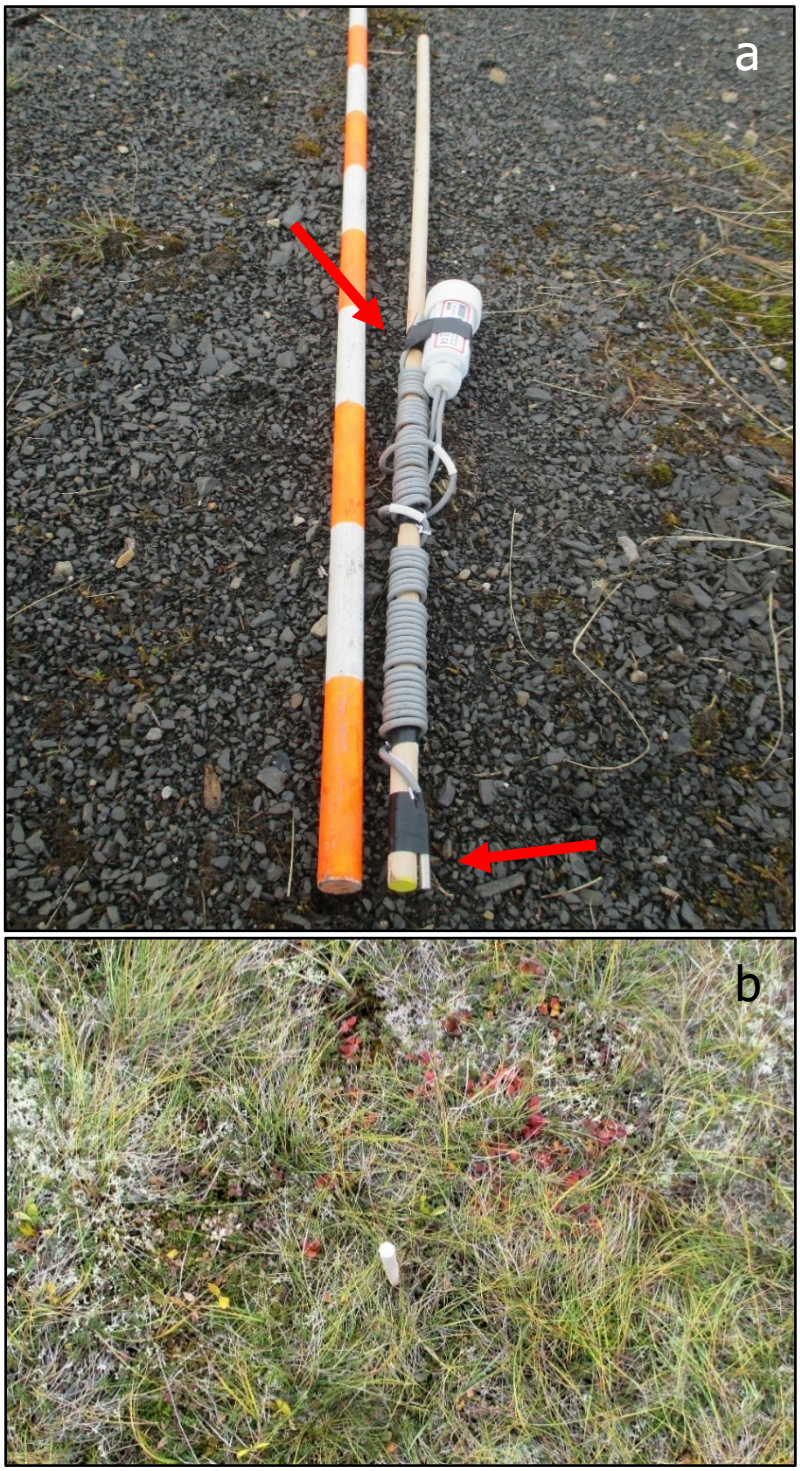

Figure 3.14. (a) Ground temperature loggers fixed to a wooden dowel 40 cm apart, indicated by red arrows and (b) minimal disturbance of the ground surface immediately following installation of the loggers in August 2018.

Snow cover generally reaches maximum depth between March or April in the western Arctic (Mackay and MacKay 1974; Burn and Kokelj 2009). Snow depth and density were measured in mid-March, the time of maximum snow depth. Densities were measured using a Mount Rose snow sampler, which consisted of an aluminum snow sampling tube, driving wrench, spring scale, and cradle. The sampling tube was 1.3 m long with a diameter of 6 cm. Determining the snow density involved weighing the empty sampling tube using the cradle and spring scale. The tube was then inserted into the snowpack, where snow depth was measured using graduations on the outside of the tube, and the tube was removed with a core of snow inside. The sample and snow tube were then weighed. The centimetre snow water equivalent (SWE) was determined from the tared scale, and snow density of the full snowpack was calculated using:

$$\rho_s = \frac{SWE}{h_s}\rho_w \quad [7]$$

where ρ_s is snow density, SWE the snow water equivalent, h_s the snow depth, and ρ_w the density of water. Measurements were made at 5 m intervals along the transects. These measurements contributed to understanding the spatial variability of the snowpack along the transects and across plots.

In addition to measuring the density of the snowpack in March, detailed measurements of the snowpack density and structure were determined from snow pits located immediately downwind of primary fences or open tundra at each plot in December 2018 and March 2019. These measurements were done to examine the snowpack development in natural tundra and fence drifts in mid- and late-winter. In both December and March one snow pit at each plot was dug to the ground surface. Snow pits

were dug at the peak of the downwind snowdrift at fenced plots, and in a representative area in the control plots. Pits were dug wide enough to stand in, with one wall vertical, smooth, and free from obstruction (Fig. 3.15).

At each pit, slope aspect was determined using a compass and slope angle using a clinometer. Additional data including the weather conditions and a description of the area were recorded. The snowpack was visually and physically inspected to identify major snow strata, representing snow deposition and weather events. The bottom and top of each layer were marked with flat sticks (Fig. 3.15b). The thickness of each layer was recorded with the ground surface representing the beginning of the first layer at 0 cm, up to the snow surface.

The temperature of each layer was determined to the nearest 1 °C using a dial stem thermometer, beginning from the layer nearest the ground surface to the top of snow surface. The temperature gradient (°C m^{-1}) for each pit was calculated by subtracting the temperature of the uppermost snow layer (T_u) from the bottom most snow layer (T_b), dividing by the total snow pit depth, and multiplying by 100. Snow hardness readings were taken from the center of each layer using the Hand Test (The Canadian Avalanche Association 2014). The layer was considered very soft, soft, medium, hard, very hard or ice depending on if a closed fist, four horizontal fingers, an index finger, the sharpened end of a pencil, a knife, or nothing, respectively, was able to penetrate the layer of snow. For each layer, snow grain size and type were determined and recorded. A laminated card with mm lines and a hand lens were used to measure three crystal grains. Grain type was determined as one of the basic grain form classes described by Fierz *et al.* (2009).

Snow density of each layer was determined by using an aluminum box density

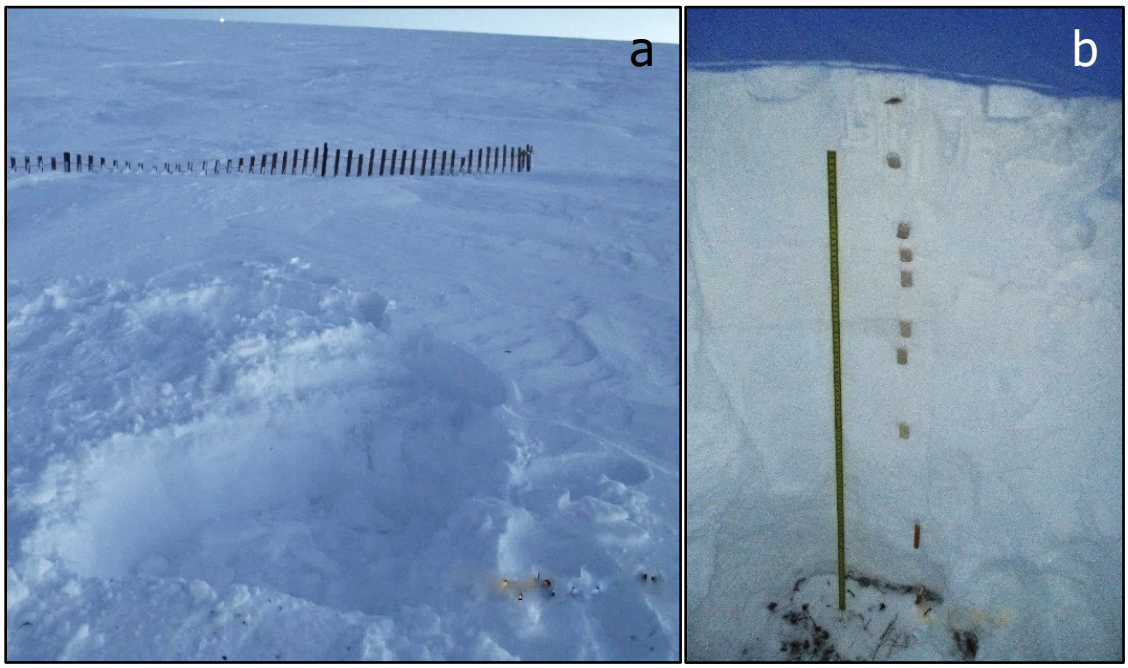

Figure 3.15. Snow pits (a) being dug downwind of a snow fence at km 452 and (b) a completed snow pit, with distinct snow layers identified on vertical wall in December 2018.

cutter, of a known volume (3 x 6 x 5.5 cm) and a spring scale. The density could only be measured for layers with a height greater than 3 cm (the height of the density cutter). The density cutter was inserted into the snow face, and a shave plate covered the front and back openings. The snow sample was then transferred and weighed in a nylon bag using a tared spring scale. The mass of the snow was recorded in grams and the density determined using the equation:

$$\rho_s = \frac{m_s}{V_s} \quad [8]$$

where ρ_s is the snow density, m_s the mass of snow, and V_s the volume of snow sampler.

3.4.4 Elevation

Elevation surveys were completed at each transect to better understand the topographic influence on snow accumulation. Surveying was completed in June 2019, with four surveys completed at each site. Transects were used to create an elevation profile for each plot (Fig. 3.11, 3.13). In addition, a survey along the east edge of the road was completed to allow the elevation profiles at each plot to be referenced to one another. As there were no known elevation control points in proximity to the sites, the elevation of the east edge of the road at P0 of km 452 and P0 of km 456 were estimated, and all elevations were derived from those points. Estimates were determined by averaging three elevations obtained by GPS (Garmin etrex 20x) over the course of the year.

A levelling procedure was used to determine the elevation at regular distances from the road (Fig. 3.17) (Donald and Entine 2002) using a Wild Heerbrugg NA2-144030 level which has a SD of 0.7 mm km^{-1} . Surveys began at the eastern end of the

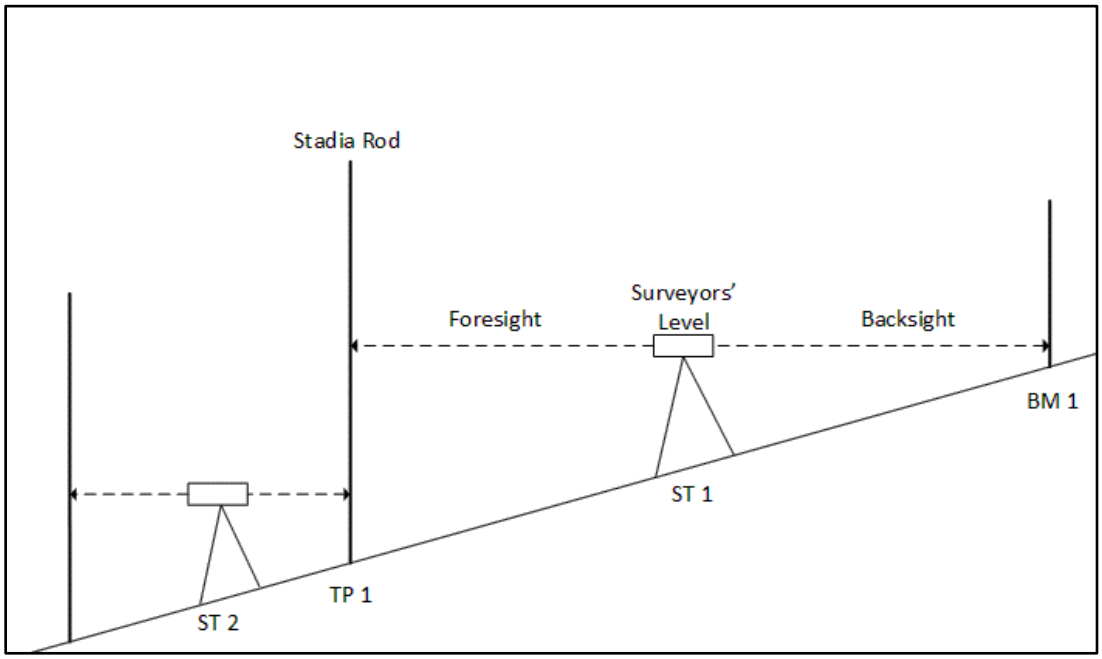

Figure 3.16. Survey protocol down a slope. Beginning from a benchmark (BM 1), back sight measurements are used to calculate height of instrument at station 1 (ST 1), and fore sight measurements are used to determine the elevation of an unknown point.

transect, moving towards the road and finishing at the west end of the transect (Donald and Entine 2002). A level rod marked to the centimeter was used to measure the vertical distances. Back sight measurements to a known benchmark (BM 1) were used to determine the elevation of the levels eye piece, i.e., the height of instrument, and foresight measurements were then used to determine the difference in elevation points (Fig. 3.17). The surveyors' level remained at station 1, and the rod was moved progressively further down the transect until no longer visible from the level by the surveyor. At this point, the elevation was "carried" to a new location by using a turning point. The leveling rod remained in place, at a turning point, a fore sight to that point was taken, and the surveyor level was moved to a second station on the other side of the turning point. A new back sight reading was taken to determine the new height of instrument, and fore sight measurements were continued.

3.4.5 Soil and vegetation measurements

Shallow soil pits were dug in October 2018 to determine soil type. One soil pit was dug at each plot, for a total of three pits per field site. Pit depths were ~30 cm, and typically restricted by ground ice. Starting from the top, the profile was observed, and soil horizons were identified and described according to standard methods (ECSS 1983).

To understand the influence of vegetation on snow accumulation, surveys of vegetation height at each plot were completed in June 2019. The maximum vegetation heights to the nearest cm were recorded at 5 m intervals along each transect.

3.5 Data analysis

3.5.1 Fence efficacy

Snow depths were averaged by zone, including the wROW, protected zone, drift affected zone, and tundra. Fences were considered to be efficacious if average snow depth in the zone of snow protection (see details below) was reduced in comparison to the average snow depth of natural tundra. Average drift depth was determined by identifying the beginning of the drift (i.e., where deposition began to occur upwind of the fence), and the end of the drift (i.e., where deposition tapered off downwind of the fence), and averaging the snow depths over the drift affected area. At P2 of km 452 and P3 of km 456, which had multiple fence rows, the upwind drift of the primary fence overlapped with the downwind drift of the secondary fence, so the average drift depth was determined over a greater distance.

The average snow depth of the tundra was the average of snow depths sufficiently upwind of the snow fences as to be considered unaffected by upwind drifts. The maximum upwind drift length of a similar fence, a horizontal slat snow fence of 60% porosity is 13H (Tabler 1980). This approximation was used to determine the minimum distance upwind tundra began. For a 1.22 m tall snow fence, upwind tundra was considered to begin 14 m from the fence.

Snow depths increased in proximity to the road, which required the zone of protection have the same defined length at all plots. The zone of snow protection was defined as the area from the 5 m east of the road to the end of the longest drift (~30 m east of the road) at km 452. From 0 to 5 m east of the road the ground was cleared in the winter and was excluded from the average. At km 456 the fences were considered

separate from the road because of the gravel bank, and the zone of snow protection was from L2 to the end of the drift and varied in length. While the wROW was the area extending 15 m from the western edge of the road. Average snow depth of the wROW was not calculated at km 452, where snow depths were not measured.

3.5.2 Ground and surface temperatures

Daily mean ground and ground surface temperatures, T_{50} and T_{10}, respectively, were calculated, and used to determine the minimum temperature at each sensor, as well as the average temperature over the winter season. The winter season was defined as 1 December 2018 to 28 February 2019 corresponding to meteorological winter.

3.5.3 Freezing season

The beginning of the freezing season can be defined in several ways at different temporal (hourly, daily, multi-day averages) and spatial scales (single sensor, multiple sensors, an entire area using air temperature). For this thesis, the beginning of the freezing season was determined at sensor-level, obtaining a freezeback date unique to each location. Daily averages were used because ground surface temperature was measured at 10 cm depth which is within the layer of diurnal fluctuation in October. How the beginning of the freezing season is defined has a considerable influence on freezeback duration (FBD), but only marginally influences FDD. When determining FBD, each day represents a value of one, but for FDD daily mean temperatures are near 0 °C in this period and have negligible impact on the seasonal sum.

Daily mean air temperatures (T_a) from the Rock River weather station were used

to determine the start and end of the air freezing season (FS_a). The FS_a began the first day of autumn when T_a fell and remained below 0 °C for three consecutive days (unless it was followed by a warming period of equal or greater length, in which case the freezing season would restart) and ended on the last day in spring with three or more days with T_a above 0 °C (Sladen 2017). Similarly, the ground freezing season (FS_{10}) began when the daily mean ground surface temperature (T_{10}) fell below 0 °C unless it was directly followed by a warming period of equal or greater length, in which case the freezing season would restart. The freezing front (FF_{50}) was considered to have passed at depth when daily mean ground temperature (T_{50}) fell below −0.25 °C and declined steadily afterwards. The duration of freezeback (FBD) was the number of days between the start of the ground freezing season and the freezing front passing 50 cm depth. While the zero-curtain referred to the period in the freezing season when T_{50} remained near 0 °C before dropping below −0.25 °C.

During the analysis of ground temperatures, the definition of freezeback used above was shown to be insufficient at km 456. At km 452, daily mean ground temperatures remained near −0.1 °C and then abruptly fell, indicating the freezing point and end to freezeback. However, at km 456 freezing occurred gradually potentially due to differences in ground materials, and ground temperatures did not begin to fall rapidly until −1.0 °C was reached. The end of freezeback was redefined at km 456 as when T_{50} fell below −1.0 °C and continued to decline.

3.5.4 Freezing degree-days

The effect of snow fence drifts on ground temperatures during the freezing season was

represented by the difference in freezing degree-days in ground below the tundra and drifts. Freezing degree-days are the accumulated daily departures of temperatures below 0 °C during the freezing season. Freezing degree-days of the ground surface (FDD_{10}) and ground (FDD_{50}) were calculated at each sensor, from T_{10}, and T_{50}, respectively, using the equation:

$$[9] \qquad FDD_{10} = \int_{0}^{\theta_s} (T_f - T_{10})\, dt$$

where FDD_{10} (or FDD_{50}) is the freezing degree-days of the surface (or ground) (°C days); θ_s is the length of freezing season for the surface (or ground) (in time t; typically days); T_{10}, or T_{50}, are the surface (or ground) temperatures (°C; typically daily means); and T_f is the freezing temperature (0 °C) (Karunaratne and Burn 2004).

FFD_{10} were averaged by group in each of the: wROW, eROW or protected tundra, natural tundra, or drift affected tundra. The FFD_{10} of the natural tundra less FDD_{10} of the drift is the effect of the snow drifts on surface temperatures over the freezing season. FDD_{50} were also averaged by group to determine the impact of drifts on ground temperatures over the freezing season.

3.5.5 Estimated annual ground temperature effect

As FDD and TDD approximate ground temperature over the freezing and thawing seasons, respectively, estimates of the effect of snow drifting on MAGT can be produced from measures of FDD and TDD at T_{10} and T_{50} if certain assumptions are met. First, it is assumed that ground temperatures are close to 0 °C at T_{50} during the thawing season due to the proximity of permafrost below, thus, the effect of snow cover on thawing degrees

days (TDD_{50}) is assumed to be 0 °C days. Second, as the effect of the snow drift on the ground thermal regime may differ if the active-layer deepens over time, this assumes no active layer response in the first season. Dividing the FDD_{50} by 365 days then estimates the MAGT, and on an annual basis, the temperature effect of snow fence drifts on ground temperature can then be calculated from the equation:

$$\bar{F}_{50} \approx \frac{\Delta FDD_{50}}{n} \quad [10]$$

where $\bar{F}_{50}$ is the difference in ground temperature (°C) between the drift affected tundra and the unaffected tundra; ΔFDD_{50} is the difference in freezing degree-days of the ground surface at 50 cm depth between affected and unaffected tundra (°C days); and n is the number of days in a year.

At T_{10} the effect of snow cover on MAGT can be estimated if ground surface conditions are similar among transects. Vegetation was similar across the tundra at both sites, with the max height of vegetation in tundra ranging from 7 to 12 cm across the six transects over two field sites. In this case, the effect of the snowdrift is restricted to the time for which it is on the ground, and we may assume that during the thawing season ground temperatures between tundra and snow fence drift areas are similar. Ground temperatures in the thawing season are assumed to be unaffected in this short-term study. With this assumption, the temperature effect of snow fence drifts on surface temperature can then be calculated from eq. 10 using FDD_{10} to approximate the difference in surface temperature ($\bar{F}_{10}$) between drift affected and the unaffected tundra.

3.5.6 Thermal properties

Snow depth and density values collected in March 2019 were used to determine thermal conductivity and thermal resistance values for the snowpack above each logger in late winter. Thermal conductivity, was calculated from:

[11] $$\lambda = c\rho^2$$

where ρ is the bulk density of snow (kg m^{-3}), and c is a unitless constant, with a value of 2.9 x 10^{-6} (Morse and Burn 2014, p. 204). This approximates the equation presented in Geiger (1980), using 0.007 for c, and units of g cm^{-3} for ρ and Cal cm^{-1} s^{-1} $°C^{-1}$ for λ. The thermal resistance of a snowpack, is a measurement of how a material resists flow of heat, and the arithmetic mean was calculated from (Morse and Burn 2014, eq. 1, p. 204):

[12] $$R = L/\lambda$$

where R is the thermal resistance (m^2 K W^{-1}), reported as RSI in SI units, L is the material thickness, which in this case is the snow depth in March (m).

3.5.7 Ground temperature relations

Two correlation matrices were produced using Spearman's rank correlation in R ('Hmisc' package, F. Harrell, 2020) to describe the relationships among the variables. The matrices incorporated all environmental variables collected or calculated including: active-layer depth, vegetation height, snow depth in October, December and March, March snow density, March thermal resistance, freezeback duration, FDD_{10}, minimum temperatures at 10 and 50 cm depth, and average winter temperatures at 10 and 50 cm depth. The analyses were conducted separately for km 452 (n=13) and km 456 (n=13) to investigate the differences between the sites.

3.5.8 Limitations

Field visits over winter 2018−19 were four to five days in length, which limited the number of *in-situ* measurements possible. Snow depths on the eastern side of the road at km 456 were collected from L2 and did not encompass the eROW and gravel cut. Snow depths west of the road at km 452 were only for the first few meters, as the snowpack exceeded the depth of the 1.20 m long snow probe in December, and 2.40 m long probe in March. Snow densities were measured using the Mount Rose Snow Tube and gave a bulk measurement for the profile. Snow pits provided a detailed representation of the stratigraphy. In order to survey the snow cover throughout the field sites it was necessary to use the Mount Rose bulk method. As a result values for thermal conductivity dependent on density had limited detail on snowpack stratigraphy. In addition, the combination of variable wind direction with short fences led to variable drift development at each fence. It is likely that snowdrift lengths downwind of the fences may have been uneven, with shorter drifting towards the midline of the snow fence. As a result, the snow surveys that were conducted across the midline do not capture the potential variation in snow conditions that are likely present across the drifts.

Chapter 4: RESULTS

4.1 Introduction

The purpose of this chapter is to characterize the snow cover in Hurricane Alley under natural conditions and with snow fences, and to evaluate the impacts of snow fencing on the ground thermal regime. The first section of this chapter examines snow accumulation, snow characteristics, and air temperatures during the study period as these factors are the major drivers of active-layer freezeback. The ground thermal regime and variability in freezeback at the field sites are then presented and related to snow characteristics.

4.2 Air temperature

Daily mean air temperatures recorded by the Rock River weather station at km 457 during the study period are shown in Figure 4.1. Six thawing events (daily mean air temperatures exceeding 0 °C after the freezing season had begun) ranged from one to three days in length. Four of the thawing events occurred in October, one in mid-March, and the last in late April. Over 2006–19, there were an average of three thawing events per season: the majority (81%) occurring late (April and May) or early (September and October) in the season. Table 4.1 summarizes the start and end of the freezing seasons and the monthly and seasonal mean air temperatures. The freezing season began in late September and ended in early May over winter 2018/19. The mean air temperature (FS_a) from October to April, was 3 °C higher in 2018/19 than the 2006–19 average (Table 4.1). Monthly mean air temperatures were 2.0 to 3.5 °C higher in 2018/19 than over 2006–19 (Table 4.1). Mean air temperature in March was 9.7 °C higher than the long-term mean.

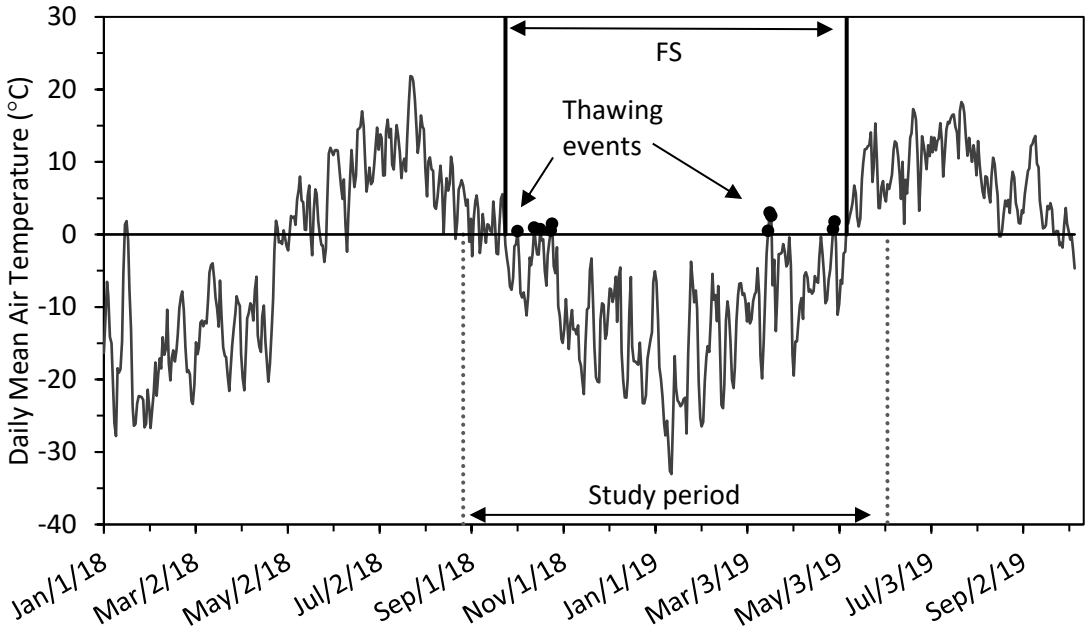

Figure 4.1. Daily mean air temperatures at Rock River weather station, from January 2018 to October 2019. The study period, indicated by dashed vertical lines, denotes the period in which ground temperatures were recorded, 27 August 2018 to 4 June 2019. The freezing season, FS, marked by solid black vertical lines, denotes the period from the first day of autumn when the daily mean air temperature fell and remained below 0 °C for three consecutive days, to the first day in spring when the daily mean air temperature rose and remained above 0 °C for three consecutive days (Sladen 2017). Thawing events, marked by black circles, indicate when daily mean air temperature exceeded 0 °C after the freezing season had begun.

Table 4.1. Air freezing season mean temperature (FS_a), and freezing degree days (FDD_a) for the study area during the study period and comparable statistics for the available record, 2006–2019, from Rock River weather station, km 457 (Environment Canada 2019).

Period	Freezing Season				Mean Air Temperature (°C)[1]						
	Start	End	FS_a	FDD_a	Oct	Nov	Dec	Jan	Feb	Mar	Apr
2018/19	Sep 24	May 7	−11.0	2496	−4.4	−13.6	−14.3	−19.3	−14.5	−6.8	−7.4
2006–19	Sep 24	May 6	−14.0	3073	−6.4	−15.6	−17.8	−19.5	−17.4	−16.5	−7.7

[1] Monthly mean air temperatures were calculated for the 2006/07 winter season to the 2018/19 winter season.

4.3 Snow accumulation

4.3.1 Snow depth

4.3.1.1 km 452

Summary

Snow cover at km 452 was discontinuous in October, with elevated snow depths isolated to the area 10 m downwind of the fences. By December, undisturbed tundra had an average snow depth of 52 cm, and fences were nearing capacity, with average drift height ranging from 92 to 101 cm. There were minimal changes in drift length or maximum height from December to March, although snow continued to accumulate with increased average snow depth at the fences, in the snow protected zone, and in undisturbed tundra. There was no noticeable reduction in snow depth in the potential zone of snow protection due to fencing as compared to undisturbed tundra.

Plot 0

At km 452 a raised embankment obstructs wind flow down a hill, promoting snow accumulation along the road and in the ROWs. The snowpack development over the winter at the control plot (P0) is shown in Figure 4.2. A discontinuous snow cover had developed by early October, average depth was just 14 cm in the tundra of the control plot (Table 4.2) and snow depths were not elevated near the road (Fig. 4.2b). By December, average tundra snow depth at the control plot had increased to 52 cm, with notable snow accumulation in the areas immediately east and west of the road (Fig. 4.2b). Snow depth in the tundra reached an average of 90 cm in March (Table 4.2), with continued drift development along the roadside. Snow depth in the embankment east of the road reached a maximum depth of 164 cm in March, and west of the road snow depth

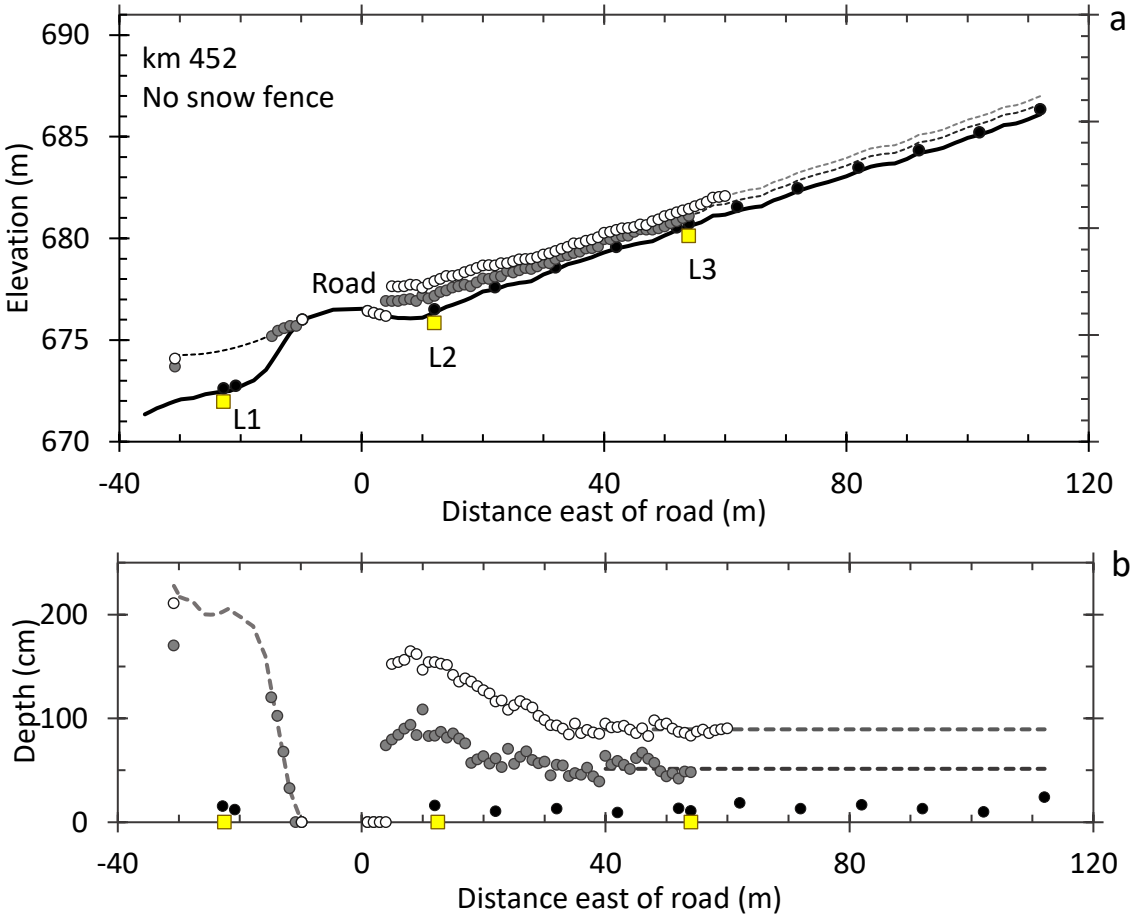

Figure 4.2. Snow depth profiles at km 452, with no snow fences (P0), (a) with elevation, and (b) normalized for elevation. Filled circles represent measured snow depths while dashed lines represent inferred snow depths based on field observations. Circles are black, grey, or open, to indicate measurements in October, December, and March 2018–19, respectively. Squares mark the location of ground temperature loggers at −22.5, 12.5, and 54 m from the eastern road edge (0 m).

Table 4.2. Average snow depth of fence drifts and natural tundra, at plots with no (P0), one (P1), or two (P2) rows of fencing at km 452, winter 2018–19. The number of measurements (n) is given in parentheses. The systematic variation in snow depth at P0 is shown in Fig. 4.2, and at P1 and P2 in Appendix A, Figs A.1 and A.2.

Plot	Average Snow Depth (cm)								
	Protected Zone[1]			Drift[2]			Tundra[3]		
	Oct	Dec	Mar	Oct	Dec	Mar	Oct	Dec	Mar
P0	13 (6)	74 (75)	135 (75)	-	-	-	14 (30)	52 (75)	90 (93)
P1[4]	15 (3)	104 (69)	193 (69)	19 (30)	92 (126)	126 (126)	12 (21)	40 (30)	101(24)
P2[4]	16 (9)	70 (78)	128 (78)	17 (57)	101 (180)	127 (180)	20 (9)	52 (12)	72 (51)

[1] Protected zone is ~5 to 30 m from the eastern edge of the road.
[2] Average of the entire drift affected area, both up- and down-wind of the fences. See Table 4.4 for the drift lengths throughout the winter.
[3] Areas unaffected by the fencing, including the area further upwind of the snowdrifts at fenced sites (P1 and P2), and P0 >30 m from the road's edge.
[4] In the protected zone snow depth was significantly different between P1 and P2 in Dec and March (t-test, $p<0.05$). Tundra snow depth differed significantly between P1 and P2 throughout the winter. Drift snow depth did not differ significantly between P1 and P2 at any time during the winter.

reached 214 cm in March at the shrubs 20 m from the western road edge. Enhanced snow accumulation to the east was visible up to 40 m from the road (Fig. 4.2b).

Plots 1 and 2

Maximum drift depth at each fence, and snowdrift lengths, are presented in Table 4.3, and Table 4.4, respectively. A discontinuous snow cover had also developed at P1 and P2 in early October (Fig. 4.3). Small snowdrifts had formed downwind of the fences at P1 and P2 (Fig. 4.4a), with maximum drift depths of 25–33 cm and downwind drift lengths of 7 to 10 m (Table 4.3, 4.4).

By December, large snowdrifts had formed at P1 and P2 (Fig. 4.5). Fence drifts had lengthened, up to 30 m in downwind length, and 11 m upwind (Table 4.4). The drift-affected area was on average 40 cm deeper than the tundra at P1, and 49 cm deeper at plot 2 (Table 4.2). Km 452 did not require or receive any snow clearing until December 16th, 2018 (C. Brais, pers. comm., 2018). Snow was cleared from the road and ~5 m of the eROW and it was blown towards the wROW. Snow clearing likely added to the snow depth observed in the wROW at all plots.

By March average snow depth of tundra in the control plot increased to 90 cm (Table 4.2) and there was little observable difference between tundra and fence induced drift areas in the field (Fig. 4.4b). Maximum drift depth at P1 and P2, changed less than 30 cm from December to March (Table 4.3). Average snow depth in the potential snow protection zone (5 to 30 m east of the road) at P1 and P2 were greater than or the same as the average snow depth in the equivalent area at P0 (Table 4.2, Fig. 4.5)

Table 4.3. Maximum snowdrift depth downwind of each fence at plots with one (P1), or two (P2) rows of fencing, km 452, winter 2018–19.

Plot	Fence	Maximum Drift Depth (cm)		
		Oct	Dec[1]	Mar
P1	F1	25	>120	141
P2	F1	33	>120	142
	F2	25	>120	150

[1] Snow depth probe was 120 cm long in December. Maximum snow depths in December would be less than or equal to those in March in the same area, with the maximum drift depth at P2 ranging between >120 and 130 cm at F1, and between >120 and 150 cm at F2.

Table 4.4. Up- and down-wind snowdrift length for each fence, at plots with one (P1), or two (P2) rows of fencing, km 452, winter 2018–19.

Plot	Fence	Drift Length (m)								
		Downwind[1]			Upwind[1]			Up- and Down-wind Total		
		Oct	Dec	Mar	Oct	Dec	Mar	Oct	Dec	Mar
P1	F1	9	30	30	0	10	11	9	40	41
P2	F1	7	18	18	0	9[2]	14[2]	7	27	32
	F2	10	22[2]	17[2]	0	9	9	10	31	26
	F1+F2							17	58	58

[1] Drift length was estimated based on field observations and snow depths.
[2] The upwind drift of fence 1 and downwind drift of fence 2 overlapped and there was no clear boundary between the fence drifts.

Figure 4.3. Discontinuous snow cover extending from the road to the fencing at P1, as well as the surrounding area in early October 2018. Photo was taken from the road, looking east.

Figure 4.4. Snowdrift development at km 452, P1 in a) October 2018 and b) March 2019. Black arrows indicate the ends of the fences

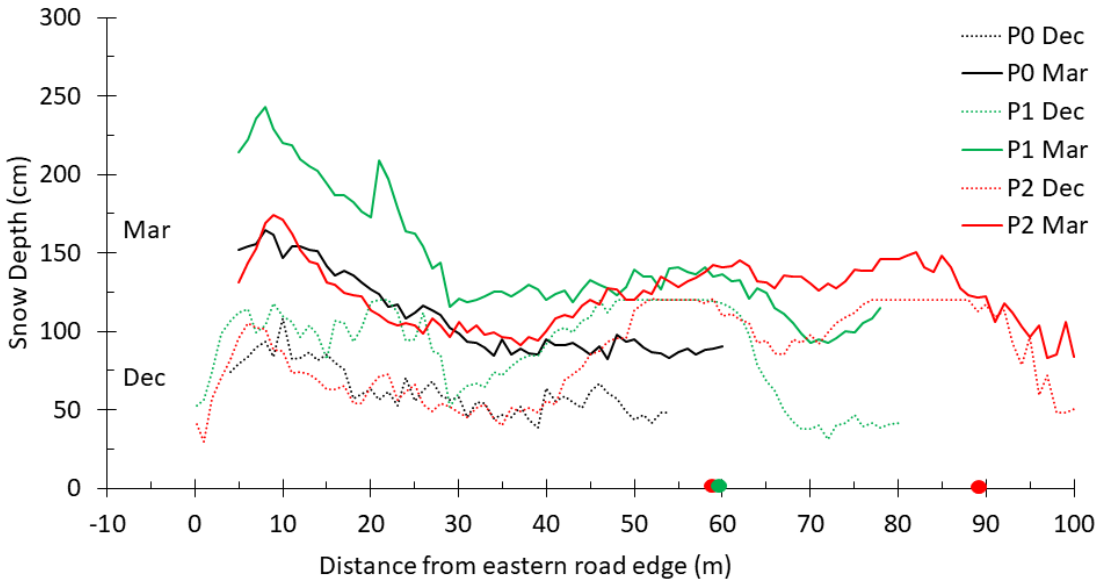

Figure 4.5. Snow depth profile comparison at km 452, showing snow depths at P0, P1, and P2 in December and March, beginning from the eastern edge of the road (0 m). The zone of snow protection extends from ~ 5 to 30 m east of the road. Circles represent the locations of the fences at P1 in green, and P2 in red.

4.3.1.2 km 456

Summary

The natural snow regime at km 456 consists of a shallow snow cover across the wROW and tundra. Clear drift development occurred at P1 and P3, and similar to km 452, fences approached capacity by December, with moderate increases in maximum drift height from December to March, when drift expansion occurred only at the multi-row plot (P3). Average snow depth was not reduced in the potential snow protection zone relative to the tundra.

Plot 0

The tundra at km 456 was raised above the road and separated laterally by a pond in the case of P0, or a gravel bank in the case of plots P1 and P3 (Fig. 3.7). Natural snow cover was thin across the length of the plot and remained so throughout the winter (Fig. 4.6). The snow cover of the natural tundra at km 456 (32 cm) was thinner than at km 452 (90 cm) in March (Table 4.2, 4.5). Snow cover at P0 in October was discontinuous, averaging 11 cm deep (Table 4.5). As the road was only gently elevated from the tundra to the west, snow depths in the wROW were the same as in the tundra east of the road throughout the winter (Table 4.5).

Plots 1 and 3

A sizable portion of the gravel area east of P1 and P3 was cleared of snow, preventing measurement of snow depth in the eROW at this site. Small snowdrifts 8 to 10 m in length and up to 70 cm high had begun to form downwind of the fenced plots at km 456 in early October (Fig. 4.7, Table 4.6, 4.7). Maximum drift height in October was 56

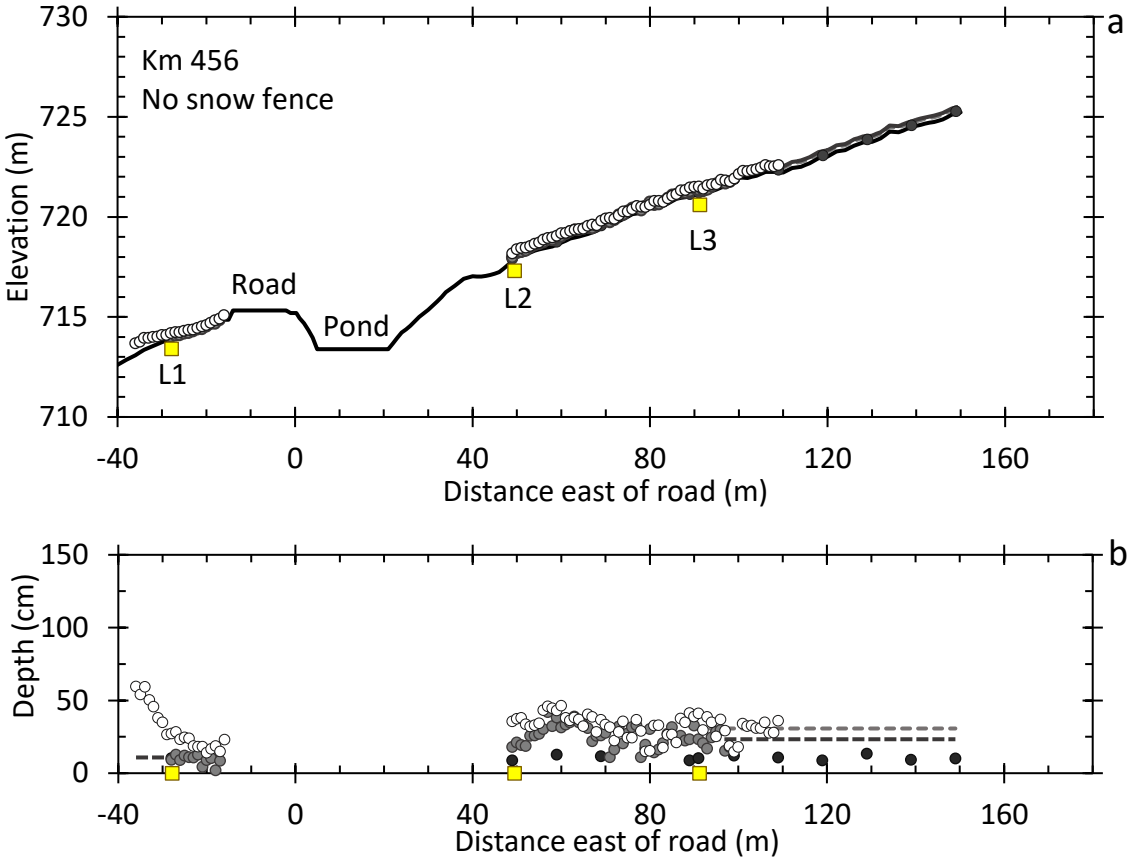

Figure 4.6. Snow depth profiles at km 456 with no snow fencing (P0), (a) with elevation, and (b) normalized for elevation. Filled circles are measured snow depths while dashed lines represent inferred snow depths based on field observations. Circles are black, grey, or open, to indicate measurements in October, December, and March 2018–19, respectively. Snow depths on the road surface were 0, and snow depths from 0–49 m east of the road were not measured as there was a pond. Squares mark the position of ground temperature loggers along the transect. Loggers were placed at −27.9, 49.5, and 91.2 m from the eastern road edge (0 m).

Table 4.5. Average snow depth in the snow protected snow, drift zone, and tundra at plots with no (P0), one (P1), or three (P3) rows of fencing, km 456, winter 2018–19. The number of measurements (n) is given in parentheses. Systematic variation in snow depth is shown for P0 in Fig. 4.6, and for P1 and P3 in Appendix A, Figs A.3 and A.4.

Plot	Average Snow Depth (cm)								
	Protected Zone[1]			Drift[2]			Tundra[3]		
	Oct	Dec	Mar	Oct	Dec	Mar	Oct	Dec	Mar
P0	11 (9)	28 (81)	36 (81)	-	-	-	11 (27)	23 (69)	30 (102)
P1[4]	13 (6)	26 (36)	44 (39)	36 (30)	74 (93)	83 (120)	14 (15)	38 (15)	41 (99)
P3[4]	15 (6)	20 (54)	30 (57)	33 (90)	74 (240)	91 (270)	-	17 (18)	45 (21)

[1] Protected zone is from L2 to the end of the downwind drift. Zone length was 30 m in December and March at P0, 19 m in December and March at P3, and 15 m in December and 12 m in March at P1.
[2] Average of the entire drift affected area, both up- and down-wind of the fences. See Table 4.7 for drift lengths at each plot throughout the winter.
[3] Areas unaffected by the fencing, including the area further upwind of the snowdrifts at fenced sites (P1 and P3), and all P0 above the gravel bank.
[4] In the protected zone snow depth was significantly different between P1 and P3 in March only (t-test, $p<0.05$). Tundra snow depth differed significantly between P1 and P3 in Dec only. Drift snow depth did not differ significantly between P1 and P3 at any time during the winter.

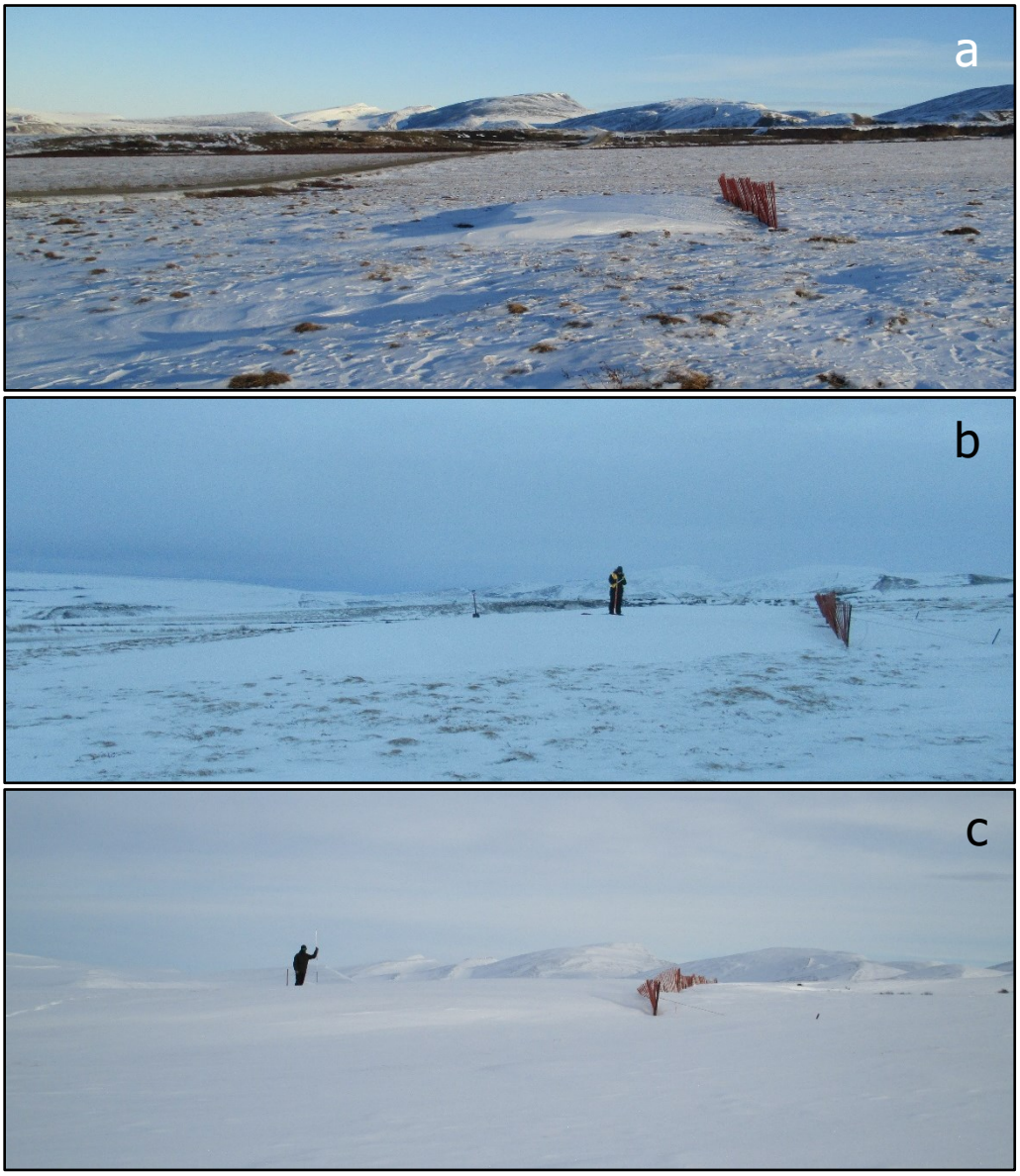

Figure 4.7. Snowdrift development at km 456, P1 with one fence, in a) October, b) December, and c) March.

Table 4.6. Maximum downwind snowdrift depth for each fence at plots with one (P1), or three (P3) rows of fencing, km 456, winter 2018–19.

Plot	Fence	Maximum Drift Depth (cm)		
		Oct	Dec	Mar
P1	F1	56	116	136
P3	F1	70	114	127
	F2	60	107	136
	F3	60	121	136

Table 4.7. Up- and down-wind snowdrift length for each fence at plots with one (P1), or three (P3) rows of fencing, km 456, winter 2018–19.

Plot	Fence	Drift Length (m)								
		Downwind[1]			Upwind[1]			Up- and Down-wind Total		
		Oct	Dec	Mar	Oct	Dec	Mar	Oct	Dec	Mar
P1	F1	9	32	35	0	8	9	9	40	44
P3	F1	8	21	21	0	3	8[2]	8	24	29
	F2	11	21	21[2]	0	7[2]	7[2]	11	28	28
	F3	9	21[2]	21[2]	0	9	7	9	30	28
	F1+F2+F3							28	82	85

[1] Drift length was estimated based on field observations and snow depths.
[2] The upwind drifts of fence 1 and 2 and downwind drifts of fence 2 and 3 overlapped, and there was no clear boundary between the drifts.

cm at P1, while at P3 peak drift height was 70 cm, downwind of the primary fence, and 60 cm, downwind of both the secondary and tertiary fences (Table 4.6).

Snowdrift development at km 456 followed a similar timeline as at km 452, with most snow accumulation at the fences having taken place by mid-December (Fig. 4.7b). Maximum snow depths downwind of fencing increased greatly from October to December, but less so from December to March (Table 4.6, Fig. 4.7c). The size and shape of the snowdrifts formed by fencing at P1 and P3 remained largely unchanged from December to March, with only upwind drifts of the first two fence rows at P3 further extending upwind (Table 4.7, Fig. 4.8). Average snow depth in the potential snow protection zone at P1 was 12 cm greater than the tundra at P0, while at P3 it was the same (Table 4.5).

4.3.2 Snow density

4.3.2.1 km 452

Summary

SWE and snow density were elevated within the snowdrifts in March. The deeper snowpack established at P1 and P2 earlier in the season was associated with a milder temperature gradient, and a thinner depth hoar layer, compared with P0. The snowpack at all plots consisted of small, round, wind-blown snow particles, deposited in layers and commonly separated by ice crusts. Much of the snow fence drift developed faceting by March. Less of the snowpack was faceted by late winter if snow continued to accumulate over the season as at P3.

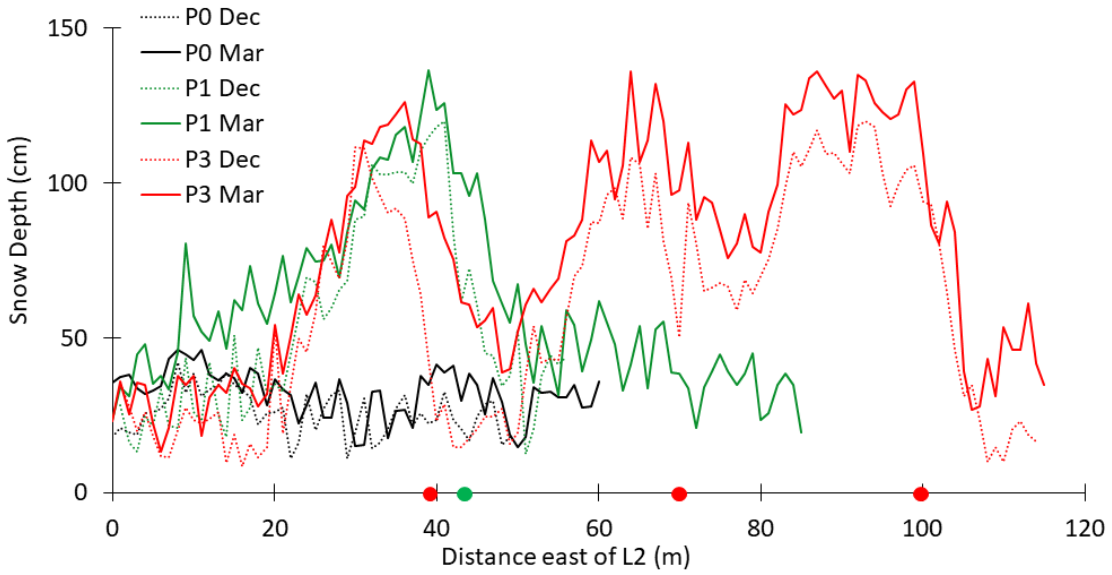

Figure 4.8. Snow depth profile comparison at km 456, showing snow depths at P0, P1 and P3 in December and March, beginning from L2 at the top of the gravel cut. The zone of snow protection is from L2 (0 m) to the end of the snowdrift, which was 15 m and 12 m east of L2 at P1 in December and March, respectively, and was 19 m in both December and March at P3. Circles represent the locations of the fences at P1 in green, and P3 in red.

Snow density profile

Figure 4.9 presents snowpack density, calculated from SWE and snow depth measured at 5 m intervals extending along transects at plots P1 and P2 in March 2019. Snow depth exceeded the length of the snow density sampler in the first 30 m of the eROW of P1 and prevented the determination of density. SWE followed a similar pattern to snow depth, increasing in the eROW and within snowdrifts at P1 and P2. Mean snowpack density of fence drifts was 0.42 g cm^{-3} at both P1 and P2, respectively (Table 4.8). Snowpack density was quite variable, ranging from 0.35 to 0.55 g cm^{-3} at P1, and 0.17 to 0.51 g cm^{-3} at P2. Mean snowpack density in natural tundra (0.28 g cm^{-3}, n=4) was less than the fence snowdrift (0.42 g cm^{-3}, n=21) in March. Only one SWE measurement, 60 m east of the road's edge, was obtained in P0 due to a densely packed slab (density of 0.84 g cm^{-3}, Table 4.9) preventing the insertion of the Mount Rose sampler; snow depth was 91 cm and density of the snowpack was 0.34 g cm^{-3}.

Snow pits

Temperature profiles showed a steep temperature gradient in December at all plots (Table 4.9). By March, temperature at the ground surface had decreased, and temperature at the snow surface had increased, to lower the temperature gradient. Depth hoar was present at the bottom of all snow pits in both December and March, with the thickest layer, 11 cm, observed at the shallowest plot, P0 (Table 4.9). In December at P1 and P2, wind-blown snow was deposited in layers above the depth hoar, with densities between 0.30 and 0.45 g cm^{-3}. Ice crusts separated the wind-blown layers. The highest density wind layers were immediately above depth hoar at P1 and P2 and density tended to decrease towards the air–snow interface. Constructive snow metamorphism was

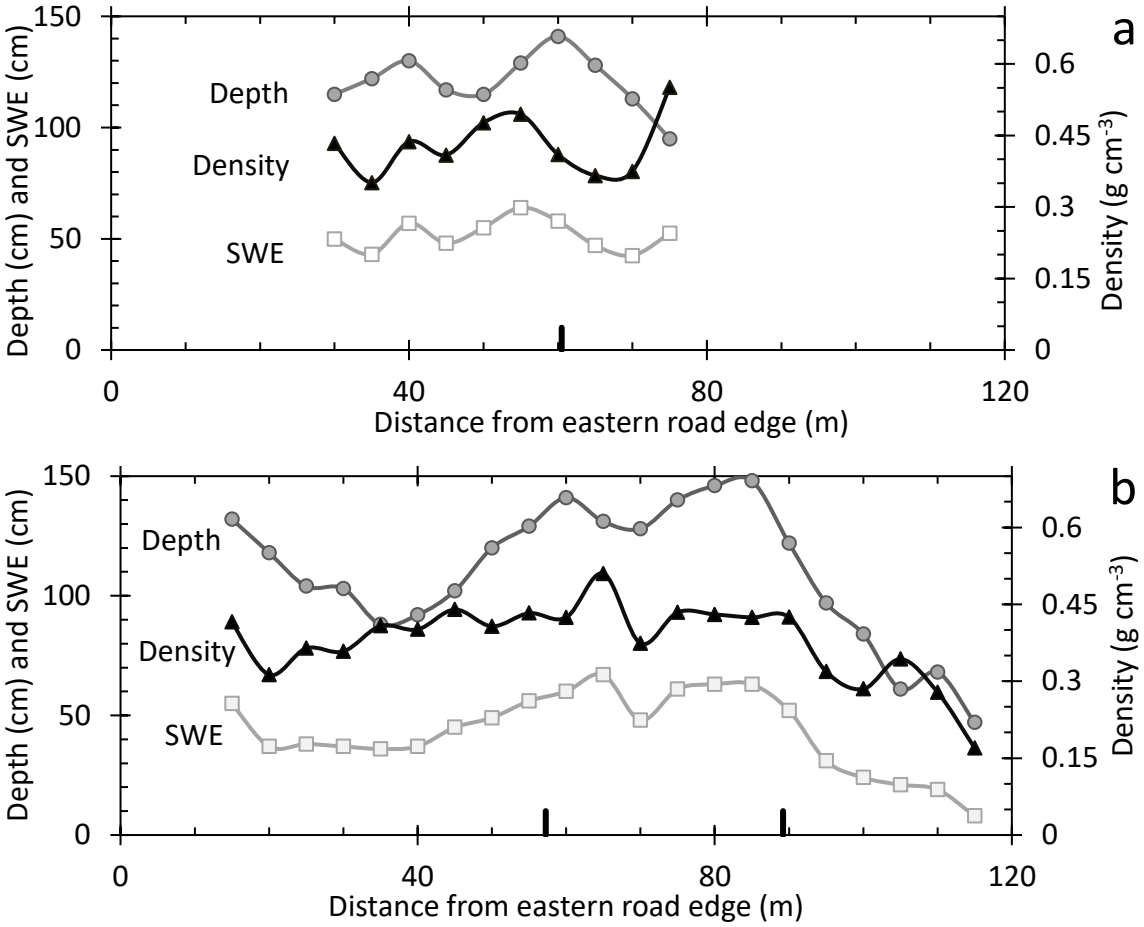

Figure 4.9. Snow density profiles at km 452 in March 2019, determined from SWE (cm) and depth (cm): (a) P1 and (b) P2. Black tick marks indicate the location of the fence rows.

Table 4.8. Average SWE and snow density in March 2019 at km 452. The number of measurements (n) is given in parentheses. The systematic variation in these variables is shown in Fig. 4.9.

Plot	Average SWE (cm)		Average Snow Density (g cm^{-3})	
	Drift[1]	Tundra[2]	Drift[1]	Tundra[2]
P0	-	31 (1)	-	0.34 (1)
P1	52 (9)		0.42 (9)	
P2	53 (12)	16 (3)	0.42 (12)	0.26 (3)

[1] Entire drift, both up- and down-wind of the fences. See Table 4.4 for drift lengths at each plot in March.
[2] Areas unaffected by the fencing, including the area upwind of the snowdrifts at fenced sites (P1 and P3), and P0.

Table 4.9. Snowpack characteristics of the primary downwind snowdrift at the plots of km 452 as observed in snow pits.

Plot	Month	Pit Density (g cm^{-3})	Pit Depth (cm)[2]	Faceted Snow Depth (cm)	Faceted Snow (%)	Wind-blown Snow Depth (cm)[1]	Wind-blown Snow[1] (%)	Temp. Gradient (°C m^{-1})	T_b (°C)[4]	T_u (°C)[5]	Depth Hoar (cm)
P0	Dec	0.32	50	10.5	21	30.5	61	−18	−9	−18	10.5
	Mar	0.45[3]	82	32.5	40	49	60	1	−11	−10	11
P1	Dec	0.39	140	5	4	131.5	94	−9	−5	−17	5
	Mar	0.31	127	100.5	79	25	20	−4	−7	−12	5
P2	Dec	0.35	111	24	22	85.5	77	−7	−5	−13	6.5
	Mar	0.39	127	114.5	90	11	9	−2	−10	−12	4

[1] Wind-blown snow was fine grained snow, with no observed faceting.
[2] Depth of faceted snow + depth of wind-blown snow ≠ pit depth as minor snow types (e.g., new snow, ice layers) are also present in the snowpack.
[3] In this snow pit there is a single layer of unusually high density (0.84 g cm^{-3}).
[4] T_b is the temperature of the bottommost layer of the snowpack.
[5] T_u is the temperature of the uppermost layer of the snowpack.

observed at each plot via the change in grain type and size that occurred between December and March. In December, the proportion of the snow classified as faceted, or partially faceted, ranged from 4 to 22% over the three plots (Table 4.9). By March, 40, 79 and 90% of the total snowdrift height at P0, P1 and P2, respectively, had developed faceting.

4.3.2.2 km 456

Summary

Snow density at km 456 peaked downwind of the fencing, and there were troughs immediately upwind of each fence row. Density at the control plot ranged between 0.13–0.30 g cm^{-3} in tundra. Enhanced snow accumulation at P1 and P3 reduced the temperature gradient, and depth hoar layers were thinner at plots P1 and P3 compared to P0. Most of the snow at P1 and P3 was wind packed, with total snowpack densities ranging from 0.34–0.36 g cm^{-3}. Snow layers generally ranged in density from 0.30 to 0.45 g cm^{-3}, although high density wind slabs, low density faceted layers, and ice layers were found throughout. Ice layers found in December correspond to melt periods in October which suggest they developed at the beginning of the snow season, and faceting developed over the winter at all pits.

Snow density profile

SWE was closely related to snow depth in March at km 456 (Fig 4.10). The average density of the tundra at P0 in March was 0.23 g cm^{-3}, while average snowpack density at the fence drifts of P1 and P3 were both 0.41 g cm^{-3} (Table 4.10). Mean snowpack density of the natural or upwind tundra (0.26 g cm^{-3}, n=21) was less than the

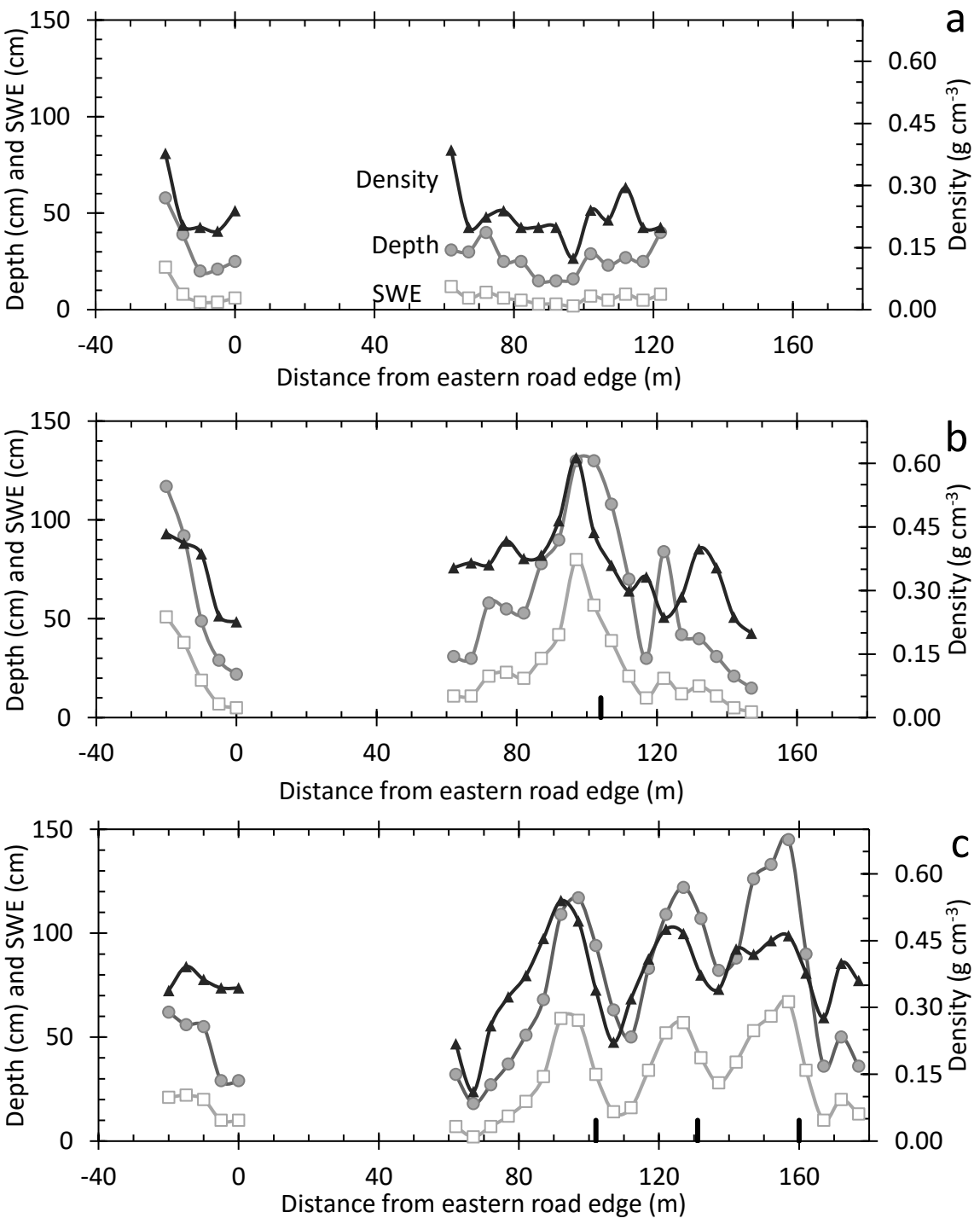

Figure 4.10. Snow density profiles at km 456 in March 2019, determined from SWE and snow depth a) P0, b) P1, and c) P3. Black tick marks indicate the location of the fence rows.

Table 4.10. Average SWE (cm), and snow density (g cm^{-3}) in March 2019 at km 456. The number of measurements (n) is given in parentheses.

Plot	Average SWE (cm)			Average Snowpack Density (g cm^{-3})		
	wROW[1]	Drift[2]	Tundra[3]	wROW[1]	Drift[2]	Tundra[3]
P0	6 (4)	-	6 (13)	0.21 (4)	-	0.23 (13)
P1	17 (4)	37 (9)	11 (6)	0.32 (4)	0.41 (9)	0.29 (6)
P3	16 (4)	41 (17)	17 (2)	0.36 (4)	0.41 (17)	0.38 (2)

[1] West side of the right-of-way from 0 and 15 m west of the road.
[2] Entire drift, both up- and down-wind of the fences. See Table 4.7 for drift lengths at each plot in March.
[3] Areas unaffected by the fencing, including the area further upwind of the snowdrifts at fenced sites (P1 and P3), and all P0 above the gravel bank.

fence snowdrift (0.41 g cm^{-3}, n=26) in March. As the average tundra snow depth was lower at km 456 than at km 452, the effect of fence drifts on density was more pronounced (Fig. 4.10). Average drift density and SWE in drifts were elevated compared to the tundra (Table 4.10). SWE at the fencing ranged from 37 to 41 cm, more than twice that of tundra, which ranged from 11 to 17 cm (Table 4.10). Snow density of the tundra across P0 was variable (Fig. 4.10a), ranging between 0.13−0.39 g cm^{-3}.

Snow pits

Snow pits were dug 90 to 100 m off the road in the tundra, at the peak of the primary fences' downwind drift. Snow pit depths at P1 were 114 cm in December and 115 cm in March, while snow pit depths at P3 increased to 114 cm in March from 88 cm in December. There was depth hoar at the bottom of all snow pits, with the thickest layer at P0 (Table 4.11). Unlike km 452, high density wind-blown layers were not found near the bottom of the snowpack, and density did not decrease towards the air–snow interface either. Most of the snow at P1 and P3 was wind packed with total snowpack densities ranging from 0.34−0.36 g cm^{-3} (Table 4.11). Snow layers generally ranged in density from 0.3−0.45 g cm^{-3}, although high density wind slabs, low density faceted layers, and ice layers ~ 0.5 cm were located throughout. Wind slabs with densities exceeding 0.50 g cm^{-3} were found at P1 in March and P3 in December, and thin (<10 cm) layers of faceted crystals with densities below 0.30 g cm^{-3} were found at P1 and P3 as well.

Classification of snow grain type highlights the snowpack evolution at each plot between December and March. For example, in December at P1, the upper 81 cm of snowpack alternated between layers of wind packed grains and ice layers, with two small layers totalling 8.5 cm of grains with faceting developed. By March small wind-blown

Table 4.11. Snowpack characteristics from snow pits of the primary downwind snowdrift at each plot of km 456.

Plot	Month	Pit Density (g cm^{-3})[2]	Pit Depth (cm)	Faceted Snow Depth (cm)	Faceted Snow (%)	Wind-blown Snow Depth (cm)[1]	Wind-blown Snow (%)	Temperature Gradient (°C m^{-1})	Tb (°C)	Tu (°C)	Depth Hoar (cm)
P0	Dec	0.25	9	8.5	94	0 (0)	0	n/a[3]	−7	n/a	8.5
	Mar	0.14	22	14	64	2 (9)	9	18	−11	−7	8
P1	Dec	0.36	113.5	40.5	36	69.5 (61)	61	−5	−4	−10	4.5
	Mar	0.35	115	91	79	14.5 (13)	13	1	−7	−6	0
P3	Dec	0.36	88	50	57	37 (42)	42	−10	−4	−13	6
	Mar	0.34	114	66	58	46.5 (41)	41	−2	−5	−7	5

[1] Wind-blown snow was fine grained snow, with no observed faceting.
[2] Depth of faceted snow + depth of wind-blown snow ≠ pit depth as minor snow types (e.g., new snow, ice layers) are also present in the snowpack.
[3] n/a as there was only a single layer of hoar beneath an ice crust.

snow grains were only found in the upper 20 cm of the snow cover. At the end of winter, 79% of the 115 cm downwind drift at P1 had developed faceting, but only 58% of the 114 cm downwind drift at primary fence of P3 had faceting (Table 4.11). The primary snow fence of P3 was the last of the fences at the multi-row plot to fill and showed the largest increase in snow depth from December to March (Fig. 4.9c). As snow depth continued to accumulate at P3 in late winter, there was little time for the snow at P3 to develop faceting.

4.3.3 Snowpack thermal properties

Snowpack density could not be measured for most of the tundra at P0, so there were few values to represent the thermal conditions of tundra at km 452. Arithmetic mean thermal conductivity of the fence drifts was estimated to be the same between km 452 and km 456 sites, with values of 0.51 and 0.50 W m^{-1} K^{-1} at km 452 and km 456, respectively (Table 4.12). The thermal conductivity of the natural tundra snow at km 456, 0.21 W m^{-1} K^{-1}, was less than at km 452, 0.35 W m^{-1} K^{-1} (Table 4.12). The arithmetic mean thermal conductivity of the tundra snowpack (including the upwind tundra) was less than the snow fence drift in March at both km 452 and km 456.

The highest resistance values were reported in the eROW at km 452 where snow accumulation was enhanced along the road, however greater values would be expected in the wROW if it had been sampled, due to a greater snow depth. Mean thermal resistance of the drift (2.51 m^2 K W^{-1}, n=21) was *lower* than that of the natural tundra snow cover (3.28 m^2 K W^{-1}, n=4) in March at km 452. However, no difference was found between the mean thermal resistance of the tundra snow (1.88 m^2 K W^{-1}, n=21) and the fence

Table 4.12. Average thermal conductivity (W m^{-1} K^{-1}) and resistance (m^2 K W^{-1}) of the snowpack in March 2019 at various locations, including the western right-of-way (L1), protected zone downwind of the fence and drifts (L2), and at drift and natural tundra (L3–L5). The number of measurements (n) is given in parentheses.

Location	Average Thermal Conductivity[2]		Average Thermal Resistance[2]	
	km 452	km 456	km 452	km 456
wROW	n/a (0)	0.30 (15)	n/a (0)	1.63 (15)
Protected Tundra[1]	0.39 (2)	0.24 (6)	3.40 (2)	1.94 (6)
Drift Affected	0.51 (21)	0.50 (26)	2.51 (21)	2.00 (26)
Natural Tundra	0.25 (4)	0.21 (21)	3.28 (4)	1.88 (21)
Δ (Drift – Tundra)	0.26	0.29	−0.77	0.12

[1] Refers to the protected area downwind of the fence and their respective drifts, including the eROW (0 to 15 m from the eastern road edge) at km 452, and the area at km 456 upwind of the gravel bank and downwind of the snow fence drifts.
[2] See section 3.5.6, for information on how values were calculated.

snowdrift (2.00 m^2 K W^{-1}, n=26) in March at km 456. Increases in snow depth at fence drifts were mitigated by increases in snow density, resulting in minimal difference in resistance values between tundra and fence drifts. This effect can be seen in Figure 4.11, where increases in snow depth are found to occur with increases in snow density (Fig. 4.11a), however for a given snow depth or density there was a wide range of potential thermal resistance values (Fig. 4.11b, 4.11c).

4.4 Ground conditions

4.4.1 Ground temperatures and freezeback

4.4.1.1 km 452

At km 452 freezeback of the ground surface occurred over two and a half weeks (Fig. 4.12a). T_{10} dropped below 0 °C for the first time on 7 September at three out of 13 locations at this site and remained below 0 °C at all sensors after 24 September. The highest ground temperatures at km 452 were measured at L1 in the wROW where a deep snow cover accumulated. Here T_{10} and T_{50} at all three plots in the wROW remained near, but just below 0 °C (Table 4.13, 4.14). Average minimum T_{10} and T_{50} in the wROW were −1.0 °C, and −0.2 °C, respectively, and were reached in May. The freezing front did not pass 50 cm at any plots in the wROW. Ground temperatures were also relatively high in the eROW, and freezeback occurred in January, later than all loggers at positions L3−L5 (Table 4.15).

Further from the road, in the tundra, the effects of snow fences and their drifts on ground temperature were localized. T_{10} and T_{50} beneath fence drifts were 3 to 4 °C higher than in tundra at 10 cm depth (Fig.4.12, Table 4.13) and 2 to 3 °C higher at 50 cm depth

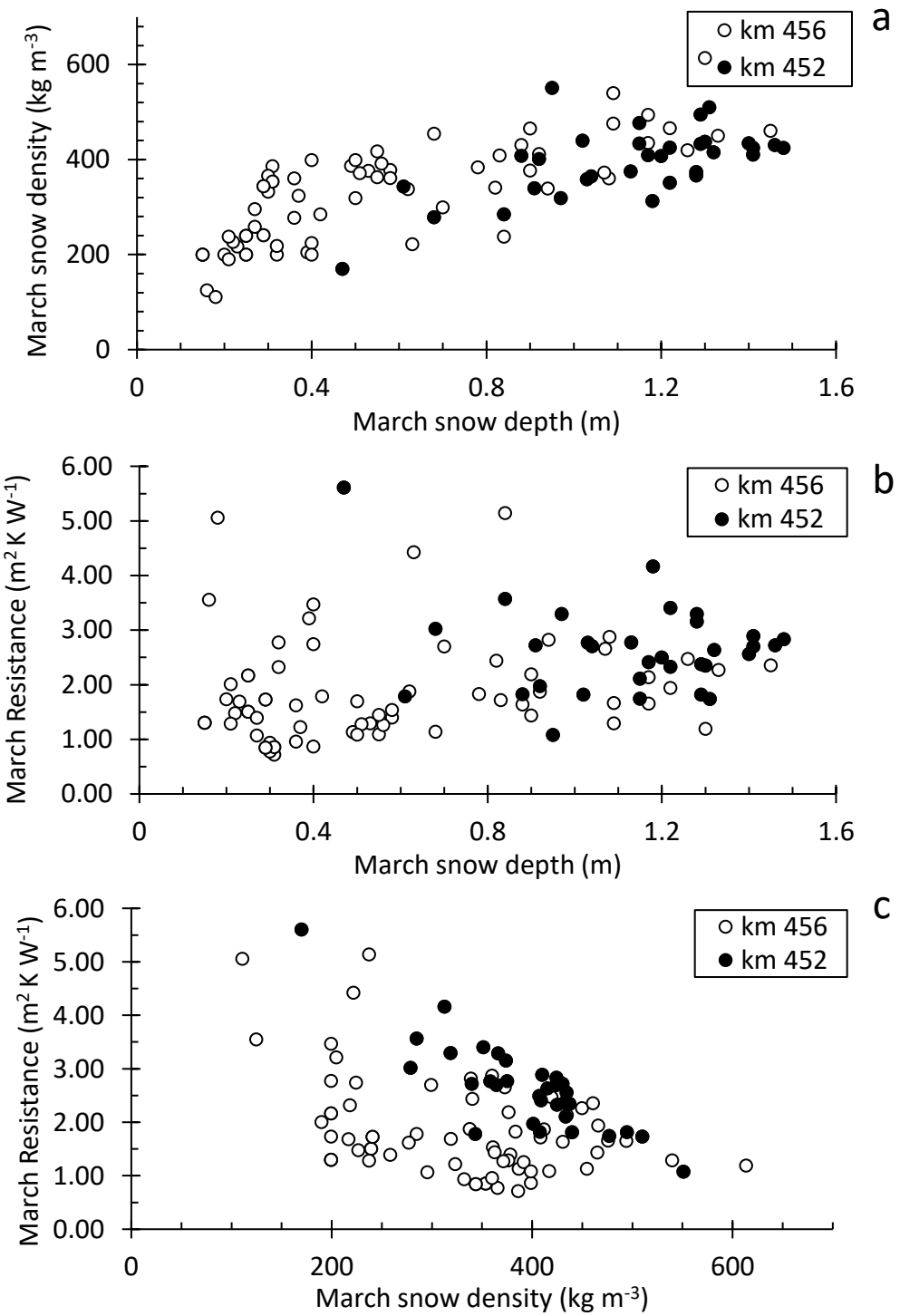

Figure 4.11. March thermal properties, (a) snow depth against density, (b) snow depth against thermal resistance, and (c) snow density against thermal resistance.

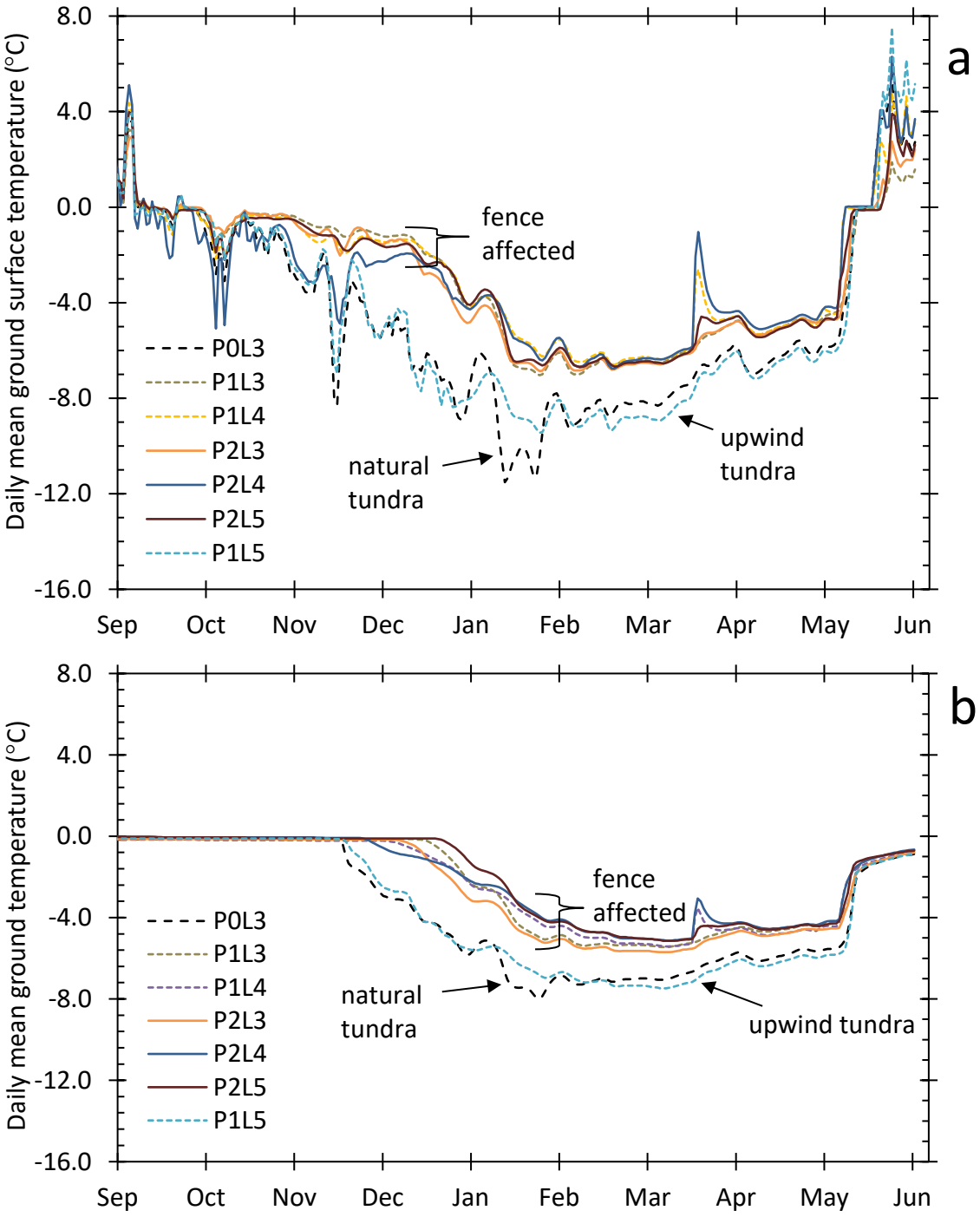

Figure 4.12. Temperatures of (a) the surface at 10 cm depth (T_{10}) and (b) the ground at 50 cm depth (T_{50}) at L3 to L5, km 452, from 1 September 2018 to 9 June 2019. Surface and ground temperatures are elevated at all fence affected loggers, compared to temperatures at P0L3 (natural tundra) and P1L5 (upwind tundra).

Table 4.13. Minimum and average ground surface temperatures at 10 cm depth (T_{10}) by general location, at km 452.

Logger	Surface Temperatures (°C)								
	P0[1]			P1			P2		
	Loc.	Min.	Avg. Winter	Loc.	Min.	Avg. Winter	Loc.	Min.	Avg. Winter
L1	wROW	−1.3	−0.8	wROW	−0.8	−0.6	wROW	−0.9	−0.7
L2	eROW	−5.1	−3.4	eROW	−4.5	−3.0	eROW	−3.8	−2.4
L3	Tundra	−11.7	−8.0	Drift	−7.1	−4.7	Drift	−6.9	−4.9
L4		-	-	Fence	−6.6	−4.4	Fence	−6.8	−4.7
L5		-	-	Upwind tundra	−9.5	−7.9	Drift	−6.7	−4.6

[1] L4 and L5 were not installed at the control plot, L3 of the control plot represents the ground temperatures of the natural tundra.

Table 4.14. Minimum and average ground temperatures at 50 cm depth (T_{50}) by general location, at km 452.

Logger	Ground Temperatures (°C)								
	P0[1]			P1			P2		
	Loc.	Min.	Avg. Winter	Loc.	Min.	Avg. Winter	Loc.	Min.	Avg. Winter
L1	wROW	−0.2	−0.0	wROW	−0.1	−0.0	wROW	−0.2	−0.1
L2	eROW	−3.8	−1.6	eROW	−2.0	−0.5	eROW	−3.0	−1.1
L3	Tundra	−8.0	−5.9	Drift	−5.4	−3.1	Drift	−5.7	−3.5
L4		-	-	Fence	−5.4	−3.0	Fence	−5.1	−2.9
L5		-	-	Upwind tundra	−7.5	−5.7	Drift	−5.1	−2.5

[1] L4 and L5 were not installed at the control, L3 of the control plot represents the ground temperatures of the natural tundra.

Table 4.15. Active-layer freezeback measurements including: the beginning of the freezing season at 10 cm depth (FS_g), the freezing front passing 10 cm depth ($FF_{-0.25}$) and the duration of freezeback ($FBD_{-0.25}$) for km 452, September 2018–May 2019.

Plot	Logger	Location	FS_g	$FF_{-0.25}$	$FBD_{-0.25}$
P0	L1	wROW	9/16	n/a	n/a
	L2	eROW	9/11	1/2	113
	L3	Tundra	9/8	11/18	71
P1	L1	wROW	9/16	n/a	n/a
	L2	eROW	9/16	1/22	128
	L3	Drift	9/11	12/18	98
	L4	Fence	9/8	12/4	87
	L5	Tundra	9/7	11/20	74
P2	L1	wROW	9/15	n/a	n/a
	L2	eROW	9/11	1/4	115
	L3	Drift	9/14	12/9	87
	L4	Fence	9/11	11/28	78
	L5	Drift	9/12	12/24	103

(Table 4.14). Freezeback was delayed by ~1 to 4 weeks at loggers beneath snowdrifts compared to loggers beneath natural tundra snow cover (Table 4.15). Ground temperature at 10 and 50 cm depth rise and fall sharply in late March at two loggers (Fig. 4.12). This corresponds to a thawing event on 17 to 19 March (Fig. 4.1). The ground temperature response is seen at P1L4 and P2L4, which are the loggers placed at the fence line, and suggests that snow melt is the cause.

4.4.1.2 km 456

Freezing of the ground surface at km 456 occurred over three weeks (Fig. 4.13a), with T_{10} dropping below 0 °C at one sensor on 7 September and T_{10} dropping and staying below 0 °C at all sensors by 30 September. Ground and surface temperatures at km 456 were lower than those at km 452. As the elevations of the road and wROW are flush at km 456, T_{10} and T_{50} in the tundra were similar to those in the wROW (Table 4.16, Table 4.17). Average winter ground temperatures beneath snow fence drifts were higher than natural tundra (Fig. 4.13). The minimum ground temperatures beneath fence drifts were higher than in tundra by an average of 7.7 °C at 10 cm depth, and 3.7 °C at 50 cm depth. Average winter T_{50} beneath fence drifts were 0 to 5 °C higher than natural and upwind tundra (Table 4.17).

Using the revised definition, freezeback was completed between 11 November and 26 December at km 456 and ranged in duration from 47 to 104 days (Table 4.18). Generally, the loggers with the shortest freezeback duration were in the wROW and protected tundra, where snow was scoured and average winter ground temperatures were comparatively low, while the longest freezeback periods were beneath drifts with

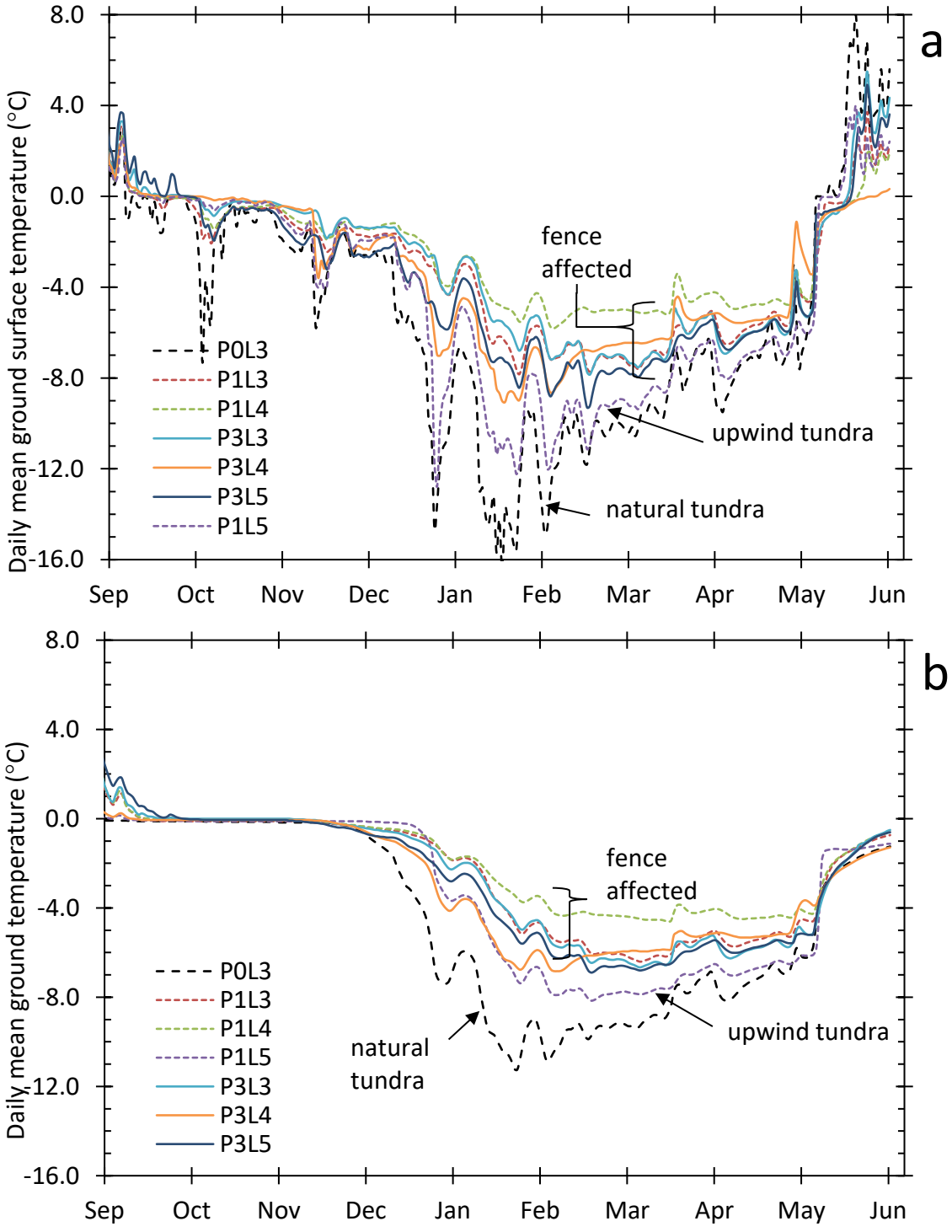

Figure 4.13. Temperatures of (a) the surface at 10 cm depth (T_{10}), and (b) the ground at 50 cm depth (T_{50}) at L3 to L5, km 456, from 1 September 2018 to 9 June 2019. Surface and ground temperatures are elevated at all fence affected loggers, compared to P0L3 (natural tundra) and P1L5 (upwind tundra).

Table 4.16. Minimum and average winter ground surface temperatures at 10 cm depth (T_{10}) by general location, at km 456.

Logger	Surface Temperatures (°C)								
	P0[1]			P1			P3		
	Loc.	Min.	Avg. Winter	Loc.	Min.	Avg. Winter	Loc.	Min.	Avg. Winter
L1	wROW	−16.9	−9.7	wROW	−10.3	−6.6	wROW	−10.9	−7.4
L2	Tundra	−14.6	−8.2	Tundra	−16.6	−9.7	Tundra	−16.3	−10.1
L3	Tundra	−17.6	−9.6	Drift	−7.9	−4.9	Drift	−7.9	−4.6
L4		-	-	Fence	−5.8	−3.8	Fence	−9.2	−5.9
L5		-	-	Upwind tundra	−15.0	−7.7	Drift	−9.4	−5.9

[1] L4 and L5 were not installed at the control plot, L3 of the control plot represents T_{10} of the natural tundra.

Table 4.17. Minimum and average winter ground temperatures at 50 cm depth (T_{50}) by general location, at km 456.

Logger	Ground Temperatures (°C)								
	P0[1]			P1			P3		
	Loc.	Min.	Avg. Winter	Loc.	Min.	Avg. Winter	Loc.	Min.	Avg. Winter
L1	wROW	−12.3	−7.4	wROW	−7.1	−4.7	wROW	−7.4	−5.2
L2	Tundra	−10.3	−6.0	Tundra	−12.0	−7.2	Tundra	−11.1	−6.9
L3	Tundra	−11.4	−7.2	Drift	−6.4	−3.2	Drift	−6.7	−3.3
L4		-	-	Fence	−4.6	−2.5	Fence	−6.8	−4.4
L5		-	-	Upwind tundra	−8.2	−4.6	Drift	−6.9	−3.8

[1] L4 and L5 were not installed at the control plot, L3 of the control plot represents T_{50} of the natural tundra.

Table 4.18. Active-layer freezeback measurements including: the beginning of the freezing season at 10 cm depth (FS_g), as well as the freezing front passing 10 cm depth (FF), and the duration of freezeback (FBD) using definitions of −0.25 °C or −1.0 °C, for km 456, fall 2018 to spring 2019.

Plot	Logger	Location	FS_g	$FF_{-0.25}$	$FBD_{-0.25}$	$FF_{-1.0}$	$FBD_{-1.0}$
P0	L1	wROW	9/16	10/31	45	11/16	61
	L2	Tundra	9/11	12/4	84	12/14	94
	L3	Tundra	9/7	11/23	77	12/4	88
P1	L1	wROW	9/16	10/26	40	11/11	56
	L2	Protected	9/29	11/13	45	11/17	49
	L3	Drift	9/13	11/22	70	12/24	102
	L4	Fence	9/13	11/25	73	12/26	104
	L5	Tundra	9/14	12/17	94	12/24	101
P3	L1	wROW	9/16	11/1	46	11/10	55
	L2	Protected	9/29	11/6	38	11/15	47
	L3	Drift	9/30	11/22	54	12/20	81
	L4	Fence	9/19	11/24	66	12/10	82
	L5	Drift	9/27	11/18	52	12/14	78

[1] Initially the freezing front ($FF_{-0.25}$) was considered to have passed at depth when T_{50} fell below −0.25 °C and declined steadily afterwards. However, the definition was revised so that the freezing front ($FF_{-1.0}$) was considered to have passed at depth when T_{50} fell below −1.0 °C and declined steadily afterwards. As a result, the duration of freezeback (FBD) was also revised. See Section 3.5.3 for details.

relatively warm average ground temperatures (Table 4.18). However, there were exceptions, such as P0L2, which had a freezeback duration of 94 days, but an average winter temperature of −6.0 °C (Table 4.18).

4.4.2 Freezing Degree Days

Average FDD_{10} for the natural tundra differed by less than 10 °C days between km 452 and km 456, and average FDD_{10} values for the drift-affected tundra differed by less than 50 °C days (Table 4.19). Compared to natural tundra, FDD_{10} of snow fence drifts were 504 °C days less at km 452, and 459 °C days less at km 456. The response at 50 cm depth was similar, with the average FDD_{50} beneath snow fence drifts 391 °C days less than natural tundra at km 452, and 340 °C days less at km 456 (Table 4.20).

The annual ground temperature was estimated (see section 3.5.5) to be 1.3 °C and 1.0 °C higher beneath snow fence drifts than natural tundra at depths of 10 cm and 50 cm, respectively. The estimated effect of snow fence drifts on mean annual temperature at 10 cm depth was comparable between the two sites, being an increase of 1.4 °C at km 452 and 1.3 °C at km 456. At 50 cm depth, the estimated mean annual temperature effect was an increase of 1.1 °C at km 452 and 1.0 °C at km 456.

4.5 Ground temperature relations

Table 4.21 summarizes the correlation coefficients between minimum ground and surface temperatures, active-layer depths, vegetation height, snow conditions, freezeback duration (FBD) and freezing degree days (FDD). As expected, the strongest positive correlations at both sites were among the various measures of the ground thermal regime,

Table 4.19. Average freezing degree days of the ground surface at 10 cm depth (FDD_{10}), over winter 2018/19 at various locations including the wROW (L1), protected tundra (L2), drift and natural tundra (L3–L5). The number of measurements (n) is given in parentheses.

Location	FDD_{10} (°C days)		$\bar{F}_{10}$ (°C)[2]	
	km 452	km 456	km 452	km 456
wROW	121[1] (3)	1205 (3)	−0.33	−3.30
Protected Tundra	578[1] (3)	1573 (2)	−1.58	−4.31
Drift Affected	864 (5)	912 (5)	−2.37	−2.50
Natural Tundra	1368 (2)	1371 (3)	−3.75	−3.76
Drift - Tundra	504	459	1.38	1.26

[1] At km 452 extremely short freezing seasons corresponds to areas of deep snow accumulation alongside the road.
[2] $\bar{F}_{10}$ is the approximate winter warming on mean annual ground surface temperature and is the division of FDD_{10} by the number of days in the year, see section 3.5.5 for further explanation of this calculation.

Table 4.20. Average freezing degree days of the ground at 50 cm depth (FDD_{50}), over winter 2018/19 at various locations including the wROW (L1), protected tundra (L2), drift and natural tundra (L3–L5). The number of measurements (n) is given in parentheses.

Location	FDD_{50} (°C days)[3]		$\bar{F}_{50}$ (°C)[2]	
	km 452	km 456	km 452	km 456
wROW[1]	16 (3)	920 (3)	−0.04	−2.52
Protected Tundra	327 (3)	1210 (2)	−0.90	−3.32
Drift Affected	652 (5)	737 (5)	−1.79	−2.02
Natural Tundra	1043 (2)	1077 (3)	−2.86	−2.95
Drift - Tundra	391	340	1.07	0.93

[1] At km 452 extremely short freezing seasons corresponds to areas of deep snow accumulation alongside the road.
[2] $\bar{F}_{50}$ is the approximate annual ground temperature and is the division of FDD_{50} by the number of days in the year, see section 3.5.5 for further explanation of this calculation.
[3] At 50 cm depth, temperatures at 10 of the 27 loggers were already below 0 °C by the beginning of the sampling period, 27 August 2018, and the temperature only rose above 0 °C at one logger by the time the loggers were removed on 4 June 2019. For those 10 loggers, FDD_{50} were calculated by summing the daily mean temperature below 0 °C over the sampling period.

Table 4.21. Spearman's correlation coefficients for a) km 452 and b) km 456 for all measurement locations along the transects with and without snow fences. Variables include active layer thickness (AL) in cm, vegetation height (VegH) in cm, October, December and March snow depths (L) in cm, March snow density (Marρ) in g cm^{-3}, March thermal resistance (MarR) in m^2 K W^{-1}, freezeback duration (FBD) in days, freezing degree days at the ground (FDD_{50}) and surface (FDD_{10}) in °C days, on minimum (min) and average winter (win) ground (T_{50}) and surface (T_{10}) temperatures in °C. Correlations were only colored if significant ($p<0.05$).

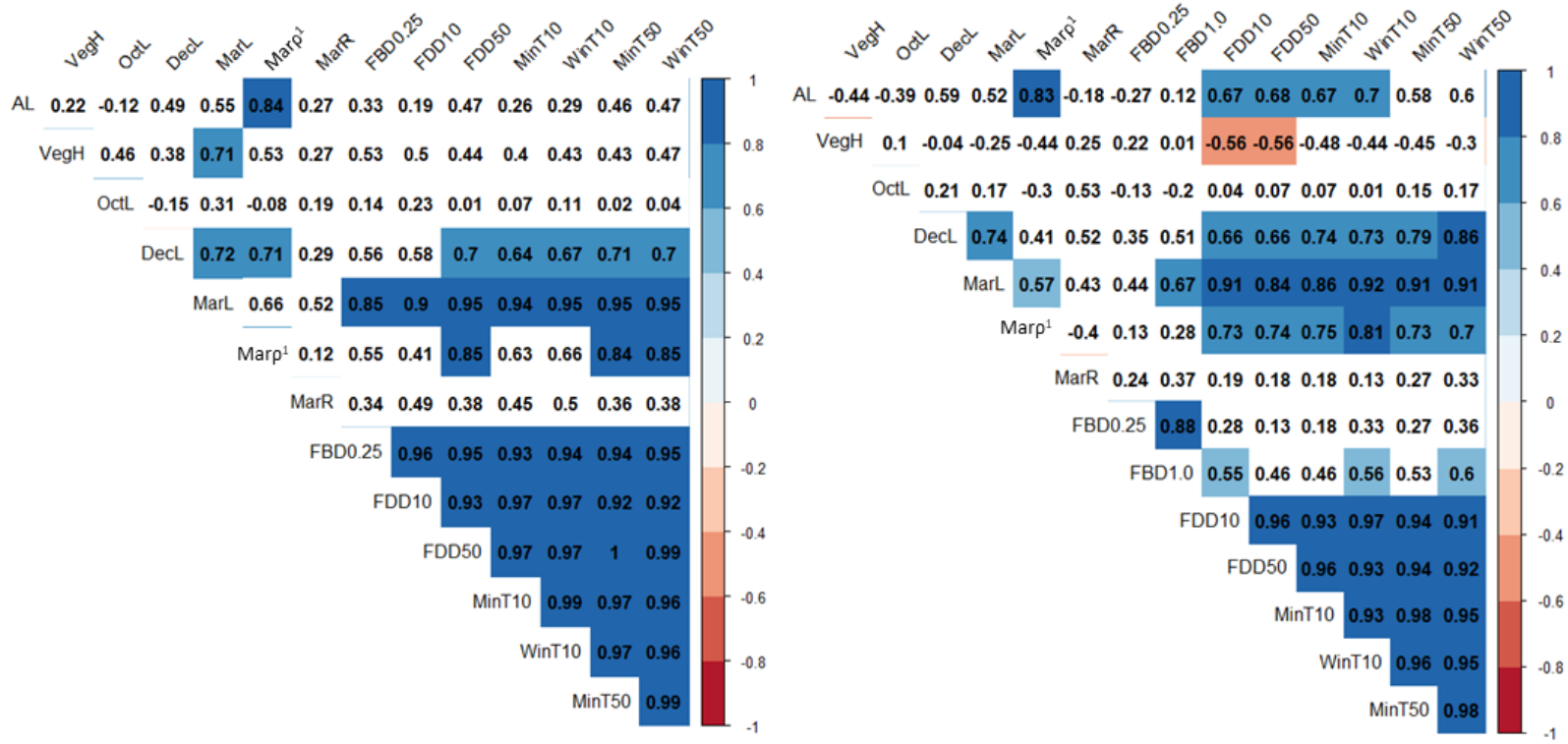

[1] March λ was excluded as it was calculated from March ρ.

T_{10}, T_{50}, FDD and FBD (Table 4.21). The relation between snow depth and ground temperature was similar between the sites, and became more dependent over time, with insignificant correlation between any measures of ground temperatures and snow depth in October, increasing strength of correlations in December, and the greatest correlations in March.

March snow depth typically correlated more strongly with measures of the ground thermal regime than March snow density at both sites (Figs 4.14 and 4.15). For example, there was a similar relationship between T_{50} and March snow depth at the two sites despite deeper snow at km 452 (Fig. 4.14). The relation between March snow density on ground and surface temperatures were similar between sites when plotted (Fig. 4.15), but the relation was often weak or insignificant at km 452, unlike at km 456 (Table 4.21). The relation between March snow density and ground temperature (Fig. 4.15) is counter intuitive, with the expected relation being that high density snow covers would allow for more efficient heat evacuation and would be associated with lower ground temperature. This suggests that the relation in Figure 4.15 shows the effect of snow depth dominates the influence of snow density on ground temperature, and that deep snow covers of high density are associated with relatively warm ground. Despite thermal resistance values being derived from snow depth and density, thermal resistance in March was not correlated with any measures of ground temperature at either site (Table 4.21).

An interesting difference between km 452 and 456 was the lack of correlation between $FBD_{0.25}$ and March snow depth or any of the other ground thermal characteristics at km 456. Even according to the revised definition, FBD was only weakly correlated with minimum and average temperatures and was not related to snow depth in October or

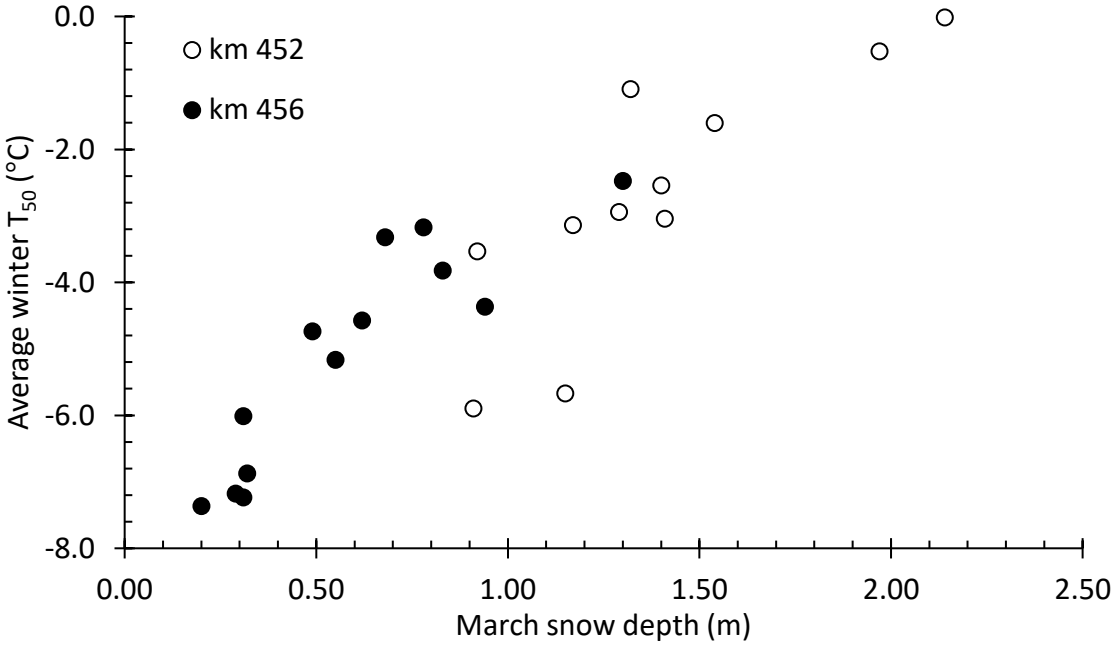

Figure 4.14. Late winter snow depth and average winter temperature (1 December to February 28) at 50 cm (T_{50}) depth.

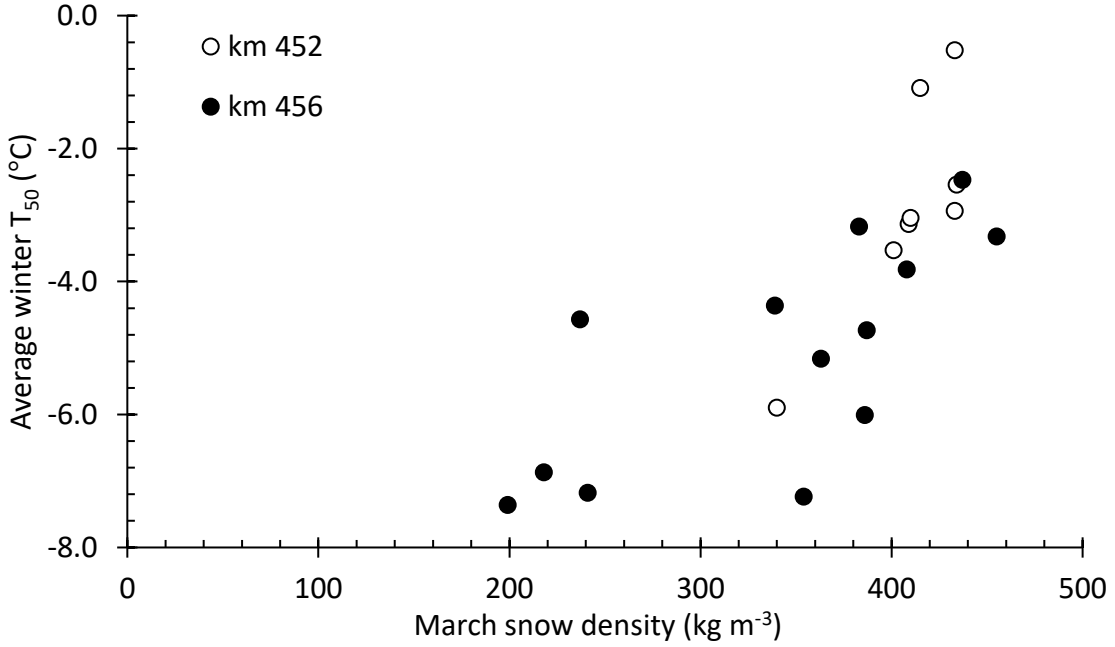

Figure 4.15. March snow density and average winter ground temperature (1 December to 28 February) at 50 cm (T50) depth.

December.

Despite the presence of snow fences as the tallest structures on the tundra, vegetation height significantly correlated with March snow depth at km 452 but not at km 456, likely because of little variation in vegetation height at km 456, with only 12 cm between the shortest and tallest vegetation.

Chapter 5: ANALYSIS AND DISCUSSION

5.1 Introduction

The effect of snow fencing on snowpack conditions and ground temperatures was examined in Chapter 4. This chapter discusses the field observations by (1) outlining key observations; (2) discussing fence efficacy; (3) exploring factors controlling the fences' impact on ground temperature; and (4) placing this study's observations within the context of research in northern Yukon.

5.2 Key field observations

Km 452 of the Dempster Highway is a raised gravel bed embankment on the lee side of a large hill at the southern end of Hurricane Alley. The natural tundra developed a deep snow cover, averaging 90 cm, with enhanced depths at the sides of the embankment and near fencing (Fig. 4.5). Deep snow accumulation (>2 m) along the wROW by December coincided with ground temperatures that remained near 0 °C and freezeback that did not complete. Freezeback in the eROW where snow depths can reach 2 m occurs about 1.5 months later than in natural tundra at this site. Scouring of tundra at km 456 led to a shallower, patchy snow cover. The snow cover was not elevated alongside the wROW as it was flush with the road. While snow depth in the ROW beside the embankment and in tundra at km 452 continued to increase from December to March, snow depth at km 456 did not increase noticeably over the same period.

Fences promoted snow accumulation throughout the winter and approached capacity by December at both sites. By March a deep snow cover across the tundra

visually obscured the difference between drifts and tundra at km 452 (Fig. 4.4b), but the depth of the drift was still substantially higher than of the tundra snowpack. At km 456 the tundra snow depth was shallower, and the effect of the snow fences on snow depth was more apparent, with drifts 175% deeper than the tundra snow cover on average in March.

Freezeback of the natural tundra at km 452 occurred on average 18 days earlier than ground beneath the snow fence drifts and was correlated to ground temperatures. In contrast, freezeback of the natural tundra at km 456 occurred an average of 5 days later than ground beneath fence drifts and was not correlated to ground temperatures; this is discussed further below in section 5.5.2.

The thickest depth hoar layer in both December and March at both sites was found at P0 where snow depth was thinnest. The tundra also had a lower average snow density, and therefore thermal conductivity, than the drifts at both sites. The average thermal resistance at km 456 was not different between the tundra and drift using the arithmetic mean. Unexpectedly, the estimated average thermal resistance of the tundra snowpack was higher than the fence snowdrift in March at km 452. The thermal conductivity and resistance estimates indicate the competing roles of increased snow depth and density. However, the competing role of density was not clearly seen in the correlation analysis. Overall, the natural accumulation regime at km 452 favoured the development of a deep snow cover, and the installation of fencing led to deeper drifts than in the tundra but, nevertheless, a snow cover that was estimated to be *less* effective as an insulator (Table 4.12). Despite a naturally shallow snow cover and deep snow accumulation within drifts at km 456, the insulative effect was the same. While March

snow density and snow depth individually correlated with T_{10} and T_{50} at both sites, thermal resistance did not.

Ground (T_{50}) and ground surface (T_{10}) temperatures were closely related to local snow depths in December and March, but not October. The effects of fencing on snow depth and ground temperature were only apparent directly beneath snowdrifts. The addition of fences to natural tundra led to greater average winter surface temperatures (T_{10}) of 3.3 °C and 3.6 °C, and average winter ground temperatures (T_{50}) of 2.5 °C and 2.8 °C, at km 452 and km 456, respectively (Table 5.1). The differences in ground and surface temperature were well represented by FDD_{10}.

5.3 Research hypotheses revisited

The hypotheses tested in this thesis were: (1) installation of snow fences may redistribute snow, producing a zone of accumulation and a zone of snow protection, with greater reductions in the zone of snow protection at multi-row plots, (2) fence efficacy would be site-specific, with steeper slopes at km 452 increasing snow fence drift height and depth, and (3) increased snow deposition in drifts would raise ground and surface temperatures beneath the drifts and reduce them in the zone of snow protection.

Snow fences produced zones of accumulation with snow depositing in large up- and downwind drifts, however snow accumulation was not reduced in the zone of snow protection at either km 452 or km 456 regardless of the number of fence rows. Snow depth in the potential zone of protection mirrored the snow depth profiles of the natural accumulation regimes (Fig. 4.5, 4.7). Therefore, fences were not found to redistribute snow from the ROW to the tundra in this study. This could be a result of the fences being.

Table 5.1. Summary of effects on ground thermal regime of snow fence drifts within tundra of Hurricane Alley.

Site	FBD (days)[1]			Min T_{10} (°C)			Min T_{50} (°C)			Win T_{10} (°C)			Win T_{50} (°C)			FDD_{10} (°C days)		
	Drift	Tundra	Δ	Drift	Tundra	Δ	Drift	Tundra	Δ	Drift	Tundra	Δ	Drift	Tundra	Δ	Drift	Tundra	Δ
km 452	91	73	18	−6.8	−10.6	3.8	−5.4	−7.7	2.4	−5.0	−8.7	3.7	−3.4	−5.9	2.5	−864	−1368	504
km 456	89	98	−5	−8.1	−15.7	7.7	−6.3	−10.0	3.7	−4.7	−8.0	3.3	−3.0	−5.8	2.8	−912	−1371	459
Avg				−7.4	−13.7	6.2	−5.8	−9.1	3.2	−4.9	−8.4	3.5	−3.2	−5.9	2.7	−888	−1370	482

[1] Freezeback defined as $FBD_{0.25}$ for km 452 and as $FBD_{1.0}$ for km 456.

too short, as the fencing may have reduced snow accumulation along the road, but wind-blown snow from the periphery could have masked the reduction in snow accumulation.

Snow fences are typically setup so that the fence is significantly longer than the area to be protected to account for the variability in wind direction, and for the reduction in snow trapping efficiency towards the ends of the fences (Tabler 1991). For example, Tabler (1980) observed the end-effects for six horizontal slat snow fences extended up to 12H from the end of the fence. Alternatively, the volume of wind-transported snow could be unlimited, and the fences are an insufficient catchment. Fences had reached capacity by mid-December, with maximum drift heights and overall length changing little after this time. The maximum height and length of the drift did not increase from mid-December to mid-March at km 452, although the total volume of snow did increase as noted by an increase in the average snow depth and steady snow density. This increase in average snowdrift height does not suggest the fences reached capacity later as it occurred simultaneously with increases in overall snow depth.

Snow fences have been said to be sensitive to slope with fencing placed on a windward slope leading to a decrease in storage capacity and a leeward slope leading to an increase (Tabler 1991). Naaim-Bouvet *et al.* (2002) observed the steeper the windward slope, the lower the efficacy, and for a slope of 10° snow catch was reduced by half. Table 5.2 presents empirical expressions developed by Tabler (1980) for standard vertical slat snow fences, such as those used in this thesis, which predict various snow fence drift characteristics. These expressions were used to produce estimates and compare to results obtained from this field research.

Higher maximum snow depths were observed at km 452, where the slope is

Table 5.2. Summary of estimated values describing downwind drifts at equilibrium, compared to values obtained from the field.

Variable	Estimate[3]	Actual			
		km 452		km 456	
		P1	P2	P1	P3
Mean snow density, ρ (g cm^{-3})	0.37	0.42[1]	0.42[1]	0.41[1]	0.41[1]
Length, L (m)	32.33	30	18, 22	35	21, 21
Maximum depth, y_{max} (m)	1.29	1.41	1.42–1.50	1.36	1.27–1.36
Location of y_{max}, L_{max} (m)[2]	6.95	4.1	0, 7.3	4.1	3.9, 5.6, 8.4

[1] mean snow density from 5 m up wind to 20 m downwind
[2] location of maximum depth in March 2019
[3] Estimates calculated from the expressions provided for a 1.22 m high vertical slat fence with a 50% porosity in Tabler (1980): $\rho = 352H^{0.18}$, $L = 26.5H$, $y_{max}=1.06H$, $L_{max} = 5.7H$

steeper than km 456, with maximum depths of 1.50 and 1.36 m, respectively. The average slope of km 452 is 5.6° and 4.7° at km 456. The maximum depths at the two sites are slightly higher than the estimated maximum drift height of 1.29 m for a single fence on a flat surface (Table 5.2), but there is generally good agreement between estimated values and field observations for single fence rows (Table 5.2). While drift height corresponded to the steepness of the leeward slope, a steeper slope was not categorically found to increase the overall size of the fence drifts. Drift lengths were longer at km 456, despite a steeper leeward slope at km 452. Single row fences in March had downwind drift lengths of 30 and 35 m at km 452 and km 456, respectively, and the multi-row fences had primary downwind drift lengths of 18 and 21 m at km 452 and km 456, respectively. The estimated downwind drift length for a single row of vertical wood slat fencing on flat terrain is 32.3 m (Table 5.2), slightly higher than the drift lengths at km 452, and slightly lower than those at km 456. Therefore, slope was not observed to alter fence efficacy in terms of maximum drift height or length.

Ground temperature is influenced by multiple environmental factors, but in the northern Yukon, snow depth is a major control (Roy-Léveillée *et al.* 2014). December and March snow depth had a strong effect on T_{10} and T_{50}. Effects on ground temperature due to snow were highly localized with increases in ground temperature restricted to ground directly beneath fence drifts. While snow fences were categorically found to enhance snow accumulation in up- and down-wind drifts, they did not reduce accumulation in the zone of snow protection relative to natural tundra. The lack of change in the snow protection zone is reflected in ground temperatures with no observed difference in T_{10} and T_{50} seen at L2 between the potential snow protected zone and the

natural tundra. Therefore, fences increased snow deposition in drifts and raised ground and surface temperatures locally but they had no effect on ground and surface temperatures in the potential zone of snow protection, or in the wROW in the first winter.

5.4 Snow conditions

5.4.1 Snow accumulation

The differences in general snow accumulation characteristics between km 452 and km 456 are due to the interdependency of wind and topography and their role in snow distribution. This has been studied extensively elsewhere (e.g. Essery and Pomeroy 2004; Föhn and Meister 1983; Liston *et al.* 2007; Ménard *et al.* 2014), leading to conclusions that depend heavily on site- and event-specific information.

The natural snow accumulation regime at km 456 consists of a low-density shallow snow cover. The road at this site runs along the toe slope in the lee of Richardson Mountains. Figure 3.5 illustrates the configuration of Hurricane Alley: the mountain slope descends steeply from mountain ridge to base, where it transitions from exposed rock to a vegetated valley sidewall that slopes gently westward. Despite the position of the road and site on the lee of a steep slope, suggesting the area would experience flow separation and deposition of wind-blown snow (Gray 1978; Tabler 1994), the road and site experience scouring, with the tundra snow depth reaching just 32 cm by the end of winter.

Average windspeed at Rock River weather station at km 457 was 17.6 km h^{-1}, and 9% of hourly observations exceeded 49.7 km h^{-1} (Humphries *et al.* 2019). Nearby, but outside of Hurricane Alley, average wind speed was 11.5 km h^{-1} at km 421, and no storm

force winds, i.e., ≥ 89 km h^{-1}, were recorded in 2015–18. The dominant winds were easterly at both locations and blew downhill from Richardson Mountains. However, in Hurricane Alley, the mountain range is a steep *single* ridge with an elevation of ~1100 m ASL, while at km 421 the mountain is further away from the road and is over 25 km wide with numerous ridges and valleys. The topographic configuration in Hurricane Alley, where wind flow is perpendicular to a thin ridge with steep slopes, produces downslope winds (Durran 1990) and is an example of terrain-forced flow (Whiteman 2000). Simulations have confirmed the high winds are downslope Foehn winds caused by cold air damming (Ribberink *et al.* 2020). The Rocky Mountain chinook or the Santa Ana, for example, are also surface winds resulting from a layer of air being forced over topography (Durran 2015). The acceleration of the atmosphere downslope from the ridge is comparable to accelerating flow of water over a rock that acts as a dam in a stream. Further evidence of scouring is visible in satellite imagery (Fig. 5.1). The road and surrounding tundra in Hurricane Alley, including km 456, were subject to erosion and snow transport by downslope winds.

Four kilometers away at km 452, the natural accumulation regime is quite different. Similar to km 456 snow cover was patchy in October, however by December tundra snow cover was continuous and averaged 52 cm, increasing to 90 cm by March. Km 452 is positioned on a large hill that protrudes from the gently sloping valley profile. The hill's shoulder is upwind of the road, and the road cuts across the foot slope of the hill. Deep snow accumulation over km 452 occurs where the large hill causes deposition on the lee slope. The lee slope is typically an area of accumulation, however the specific snow profiles depend heavily on the shape and sharpness of the hill apex

Figure 5.1. Scouring up to 3 km downslope of the Richardson Mountain ridge near km 457 of the Dempster Highway within Hurricane Alley, on 23 February 2016. Satellite imagery from Digital Globe, Inc., 2016.

(Föhn and Meister 1983; Benson and Sturm 1993). As ridge height and apex angle decrease, the snow depth maximum moves downslope (Föhn and Meister 1983). Ridges with low heights and apex angles lead to accumulation that increases with distance from the apex, cresting in the foot of the slope. This is consistent with observations at km 452, where a large hill with a low apex angle produced a snow profile that increases with distance from the crest.

5.4.2 Snow density

Snow undergoes a period of rapid densification after initial deposition, followed by a much more gradual densification rate over the remainder of the season (Sturm and Benson 1997). Densification can occur by wind erosion, melt-refreeze events, compaction, and metamorphism in response to temperature and vapour gradients within the pack (Colbeck 1982). Melting and refreezing generally requires air temperatures above 0 °C, and the earliest thawing events occurred on 17 March, after snow depth and density measurements were taken. Daily air temperatures rarely exceeded −5 °C (Fig. 4.1), which suggests minimal densification by melt-freeze events. However, wind erosion, compaction and metamorphism are all likely to play a role in the densification of snow covers in Hurricane Alley.

Tabler (1980) suggests that prior to snowmelt in large drifts, densification is primarily a result of the compressive loading by overlying snow. However, regional studies have been able to reliably predict snow density from air temperature and wind speed (Bilello 1957, 1969), without load or snow depth information, because compaction is due to climatically controlled differences in snow characteristics such as grain size,

bonds, temperature and wetness (Sturm and Holmgren 1998). In other words, climatic variables such as wind speed and air temperature generate snow characteristics, which play a larger role in determining the compaction behavior of a snowpack than depth or load. As both sites will exhibit a similar snow type determined by climate, and did not experience thawing events throughout the winter, differences in density between the sites are likely due to localized differences in compaction or metamorphism from variable snow accumulation leading to differences in stratigraphy. Density trends that exist across Hurricane Alley are likely to indicate the influence of climatic factors.

Tundra snow consists of layers of slabs, with high initial density, interspersed with coarse-grained hoar, both of which have a high effective compactive viscosity and resist densification (Sturm *et al*. 1995). Tundra snow cover tends to be dense from shortly after snow fall because drifted snow has already been pulverized into small rounded grains (Sturm and Holmgren 1998). Sturm and Holmgren (1998) suggest that for tundra snow, the higher the wind speed, the higher the initial density of the snow at the beginning of the winter season. As discussed in section 5.4.1, winter wind speed is elevated in Hurricane Alley (Humphries *et al*. 2019), which is the first indication that the snow cover undergoes low rates of densification.

Field results in Hurricane Alley also indicate that the snow cover has a high initial density and experienced minimal densification over the winter. The overall snow pit density from December to March changed little at P1 or P2 at km 452 (Table 4.9), or at P1 and P3 at km 456 (Table 4.11), and ranged from 0.3 to 0.4 g cm^{-3} in the snow fence drifts. The highest snow pit density was obtained at P0 in March, due the presence of a thick wind slab. In contrast, P0 at km 456 had the lowest snow pit densities, a result of

low snow depths (<25 cm), leading to complete metamorphism of the snowpack (94%) by December (Table 4.11). The density at P0 was 0.24 g cm^{-3} in December, which is towards the upper end of the range for depth hoar, and 0.15 g cm^{-3} in March, which is closer to the median value (Table 2.2). The major difference between P0 at km 452 and P0 at km 456 is the snow depth in early winter. At km 452, snow depth of the tundra (P0), while less than the drifts, was still 50 and 82 cm in December and March, respectively. At km 456, the snow depth of the tundra was 9 and 20 cm in December and March, respectively. The shallower snow depth would produce a greater temperature gradient and allow for quicker metamorphism. Differences in the early winter snow depth lead to unique metamorphic trajectories despite a similar initial snow type.

Taken together the field results suggest that high winter winds in Hurricane Alley lay down a snow cover of high initial density which is modified depending on the snow accumulation early in the winter. At locations prone to accumulation, which included all of the km 452 site on the lee of a large hill, as well as snow fence drifts at km 456, a deep snow cover accumulated early in the winter, greatly slowing the constructive metamorphic progression, and leading to low rates of densification over the winter. At locations prone to scouring, such as the tundra at km 456, the snow cover remained very shallow (>20 cm), and allowed for efficient vapour transport and metamorphism of the snow pack, with all but a thin layer of ice at the uppermost surface developing faceting by December. In this case, snow density *decreased* over the winter.

5.4.3 Estimating thermal conductivity

When estimating snowpack thermal conductivity two factors must be considered. First,

the relation between density and thermal conductivity, and second the averaging technique for a layered snowpack. Several functions have been developed to estimate thermal conductivity from density (e.g., Abel 1893; Sturm *et al.* 1997; Calonne *et al.* 2011). In this thesis the method used by Morse and Burn (2014) was employed. In Figure 5.2, estimates for the thermal conductivity of the snowpack using this technique are presented in comparison with the methods of Calonne *et al.* (2011, eq. 12). Additionally, in the case of a layered snowpack, its thermal conductivity can be estimated from the thermal conductivity of the individual layers, using either a weighted arithmetic mean or a weighted harmonic mean.

Using limited data from 12 snow pits, both weighted arithmetic and harmonic mean estimates of thermal conductivity were calculated using data from individual layers within the snowpack, and compared to estimates of thermal conductivity derived from the bulk sample in a nearby snow tube (Fig. 5.2). In Figure 5.2, estimates obtained from bulk measurements of density in the snow tubes are the highest at each site. Comparison of the estimates obtained from the relation in Morse and Burn (2014; purple dots in Fig. 5.2) are higher than those obtained using Calonne *et al.* (2011, eq. 12; red dots in Fig. 5.2). Finally, the estimates obtained using arithmetic and harmonic means indicate that most commonly the arithmetic mean (red dots in Fig. 5.2) yields a higher estimate of snowpack thermal conductivity than the harmonic mean (green dots in Fig. 5.2). As a result, the arithmetic mean provides a relatively low estimate of snowpack thermal resistance compared to use of the harmonic mean (Fig. 5.2).

For extensive field surveys, it is impractical to obtain data on snowpack density and stratigraphy from snow pits. It is necessary under field conditions of limited light and

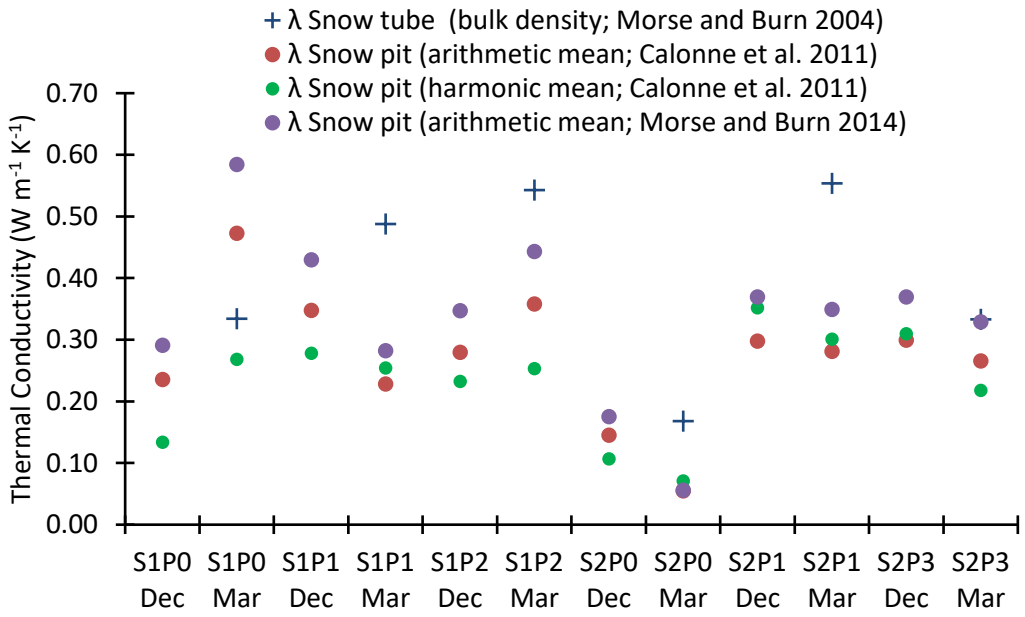

Figure 5.2. Differences in thermal conductivity (λ) derived from different methods at the 12 snow pits examined in this study.

time to survey snowpacks using a snow tube. Therefore, in such surveys only data on bulk characteristics of the snowpack will be obtained. From the discussion presented above and inspection of Figure 5.2, it becomes clear that estimates of thermal conductivity obtained by this method will be relatively high. Of the six points where estimates from snow tubes could be compared with data from a snow pit, in all but one case the snow tube yielded the highest thermal conductivity estimate. The snow tube estimates therefore may be biased. The data do not display a constant ratio or difference between snow tube and snow pit estimates.

5.5 Ground temperature response

5.5.1 Snow cover

The depth and density of snow depends on several factors, many of which have been addressed above. Thermal conductivity of snow ranges from less than 0.10 W m^{-1} K^{-1} for low density fresh snow to greater than 0.50 W m^{-1} K^{-1} for dense, ripened snow. For any given depth the thermal conductivity may vary by more than an order of magnitude (Fig. 5.3) (Sturm *et al.* 1997). This may be due to the differences in temperature under which the data were obtained, differences in snow conditions such as age or grain size distribution, and the effects of vapour diffusion (Yen 1981).

Changes to snow thickness may significantly influence the ground temperature. March snow depth was strongly correlated with minimum and average ground and surface temperatures at both sites (Table 4.21, 4.22). Average snow depth was 37 cm greater in fence drifts than tundra at km 452, while winter ground and surface temperatures were greater by 2.8 °C and 3.3 °C, respectively. Fences at km 456 raised the

average snow depth by 56 cm, and winter ground and surface temperatures by 2.5 °C and 3.6 °C, respectively.

Average snow depth varied with the site and accumulation regime, i.e., natural tundra or drift affected (Fig. 5.3a). Average snow density was higher in the drift than the tundra and did not vary between sites (Fig. 5.3b). While the fences increased average snow depth, insulation effects may have been partially mitigated by increased density within the fence drifts (Fig. 5.3c). Thermal resistance values calculated using the arithmetic mean for the snow cover in Peel Plateau by O'Neill and Burn (2017a) were 9.6 m^2 K W^{-1} near the road where the snow depth was elevated, and 4.5 m^2 K W^{-1} at control sites. While the highest thermal resistance values were also obtained alongside the road in Hurricane Alley in the eROW at km 452 where snow accumulates along the road shoulder, the thermal resistance values are much lower than those in Peel Plateau, with a maximum value of 4.6 m^2 K W^{-1}. The relatively high average snow density (0.38 g cm^{-3}) in Hurricane Alley contributed to the low thermal resistances, which averaged 2.1 m^2 K W^{-1} (n=23) in March.

In addition, the high variation in heat loss potential seen in the tundra is consistent with results of Kershaw and McCulloch (2007). Kershaw and McCulloch (2007) attributed a high variation in snow density in tundra to frequent wind redistribution. Tundra in Hurricane Alley did have slightly higher variation in snow density than drifts, however the variation in thermal resistance observed in this study is due to the sensitivity of the low tundra snow depth to changes in density. This is likely why thermal resistance in March was not significantly correlated with any measures of ground temperature despite both snow depth and density in March commonly being well correlated with

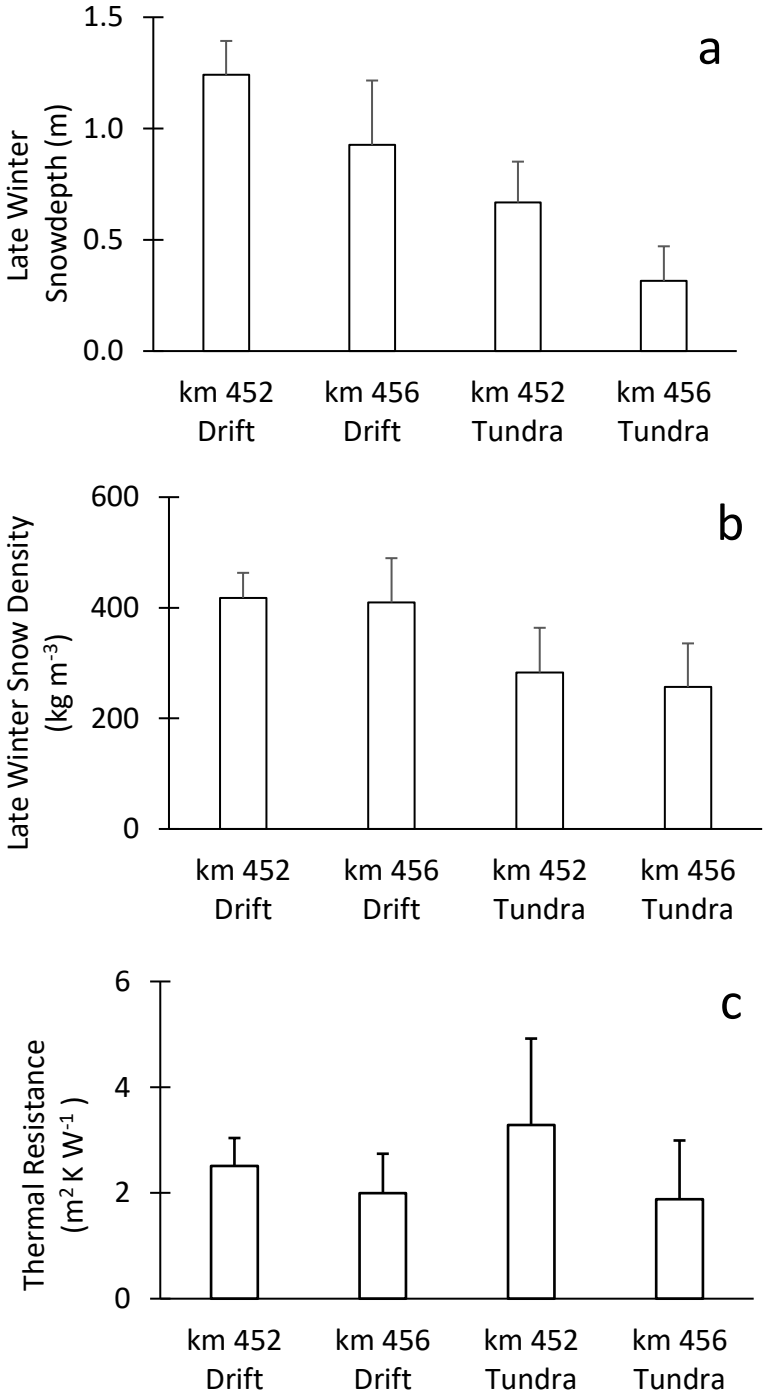

Figure 5.3. Late winter mean with error bar cap at one standard deviation for (a) snow depth, (b) snow density, and (c) thermal resistance. Late winter snow depth varied considerably between snow fence drifts and tundra at the sites, however snow density was nearly identical at fence drifts and tundra between sites, with the end result being high variance, suggested by the standard deviation, in the tundra and minimal difference in thermal resistance between fence drifts and tundra.

measures of ground temperature (Table 4.21).

5.5.2 Freezeback

The timing and duration of freezeback is important as it involves freezing of the active layer. Variability in freezeback has implications for thermal conductivity. Release of latent heat associated with pore water results in the maintenance of isothermal temperatures at or just below 0 °C within the freezing active layer. This period, the zero-curtain, is both a length of time, and a thermal boundary that prevents cooling of the underlying permafrost (Outcalt *et al.* 1990). The decline in temperature at the top of permafrost signifies the closure of the zero curtain, and the completion of active-layer freezeback. The rate of cooling is governed by the thermal resistance of the snowpack and the frozen active layer, and the prevailing thermal gradient between the atmosphere and permafrost (Burn and Zhang 2009). In addition to climatic variables, active-layer thickness, soil water content, and the snow cover regime all influence freezeback dates (Romanovsky and Osterkamp 1995).

At km 452 closure of the zero-curtain and end of freezeback was clearly visible as a decline in ground temperatures (Fig. 5.4a), and the effect of the snow depth on freezeback duration was clear. The first temperature sensors to register freezeback were beneath natural tundra, followed by the ground at the fence line (L4) and those beneath snow fence drifts (L3), and finally the eROW (L2). The deepest snowpack developed by early December in the wROW, where the thick, early snow cover reduced the loss of heat and freezeback did not occur at all. Increased snow cover prolonged active-layer freezeback and limited ground heat loss leading to warmer ground. Delayed active-layer

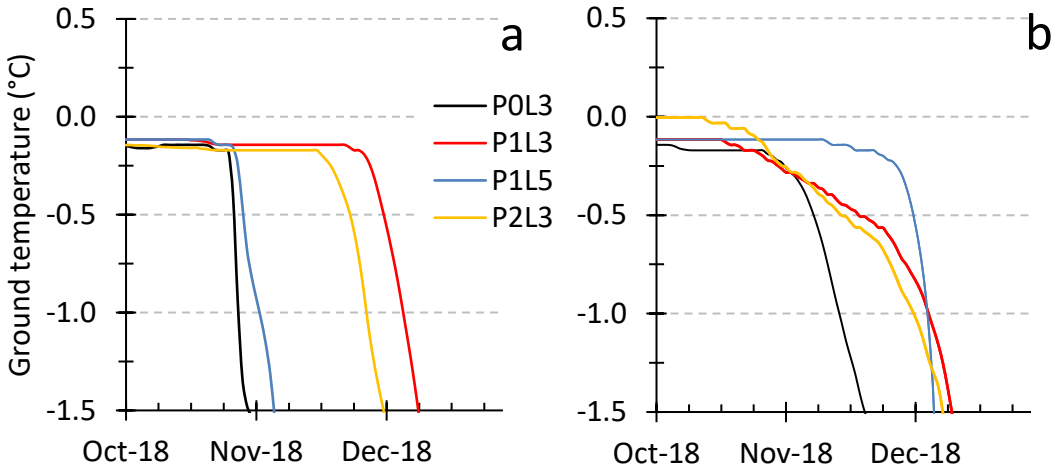

Figure 5.4. Completion of freezeback at 50 cm depth, at: a) km 452, and b) km 456. Where sensor P0L3 is beneath natural tundra, P1L5 is beneath unaffected tundra, and P1L3 and P2L3 are beneath snow fence drifts.

freezeback in response to increasing snow depth was observed by Zhang (1993) using a numerical model.

While freezeback duration was well correlated with ground temperatures at km 452, it was not at km 456 (Table 4.21). Scouring at km 456 produced a thin patchy snow cover (<25 cm), that persisted into December. This thin cover allowed efficient heat evacuation, and rapid freezeback. Freezeback duration at km 456 was not well correlated with winter ground temperatures, nor was it representative of the surface conditions. The closure of the zero-curtain and end of freezeback was not obvious at km 456 as ground freezing occurred at a gradual rate (Fig. 5.4b) and is likely due to the influence of soil characteristics on freezeback. The terrain at km 452 consists of a uniform cover of tussock-sedge on a sloping hill underlain by organic silt and clay, while at km 456, the vegetation cover consists of both tussock-sedge and sedge tundra, with exposed frost boils in the tundra. Frost boils, 'upwellings of mud that occur from cryoturbation activity and differential heave of frost susceptible soils' (ACGR 1988), indicate fine-grained, frost-susceptible material (Calmels *et al.* 2018) and fine-grained mineral soils (Kokelj *et al.* 2014) at km 456.

Once ground at km 452 had frozen, the rate of temperature decline at the top of permafrost exceeded the rates at km 456 (Fig. 5.4). This is consistent with results from Kokelj *et al.* (2014) who demonstrated lower winter temperatures at the top of permafrost in organic soils than mineral soils due to the high thermal conductivity of icy peat (Table 2.3) and a shallower permafrost table. In organic soils most water freezes near or just below 0 °C, so latent heat effects are only seen at temperatures just below 0 °C. Once freezing has occurred any further ground heat loss results in a rapid decline in

temperature. During freezing of fine-grained soils, a higher proportion of the water remains unfrozen (Williams and Smith 1989) and latent heat effects are seen over −2 to −5 °C (Kokelj and Burn 2003), so the same ground heat loss results in a reduced decrease in temperature (Williams and Smith 1989). The higher unfrozen water content in fine-grained soils means it is difficult to define the freezing-front as there is often a zone that is partially frozen and any specific temperature used to separate the partially frozen and fully frozen zones is arbitrary (Burn 1998b). Overall, km 456 demonstrates the influence of soil characteristics on freezeback (Kokelj *et al.* 2014) and the difficulty in defining the bottom of the active layer as described in Burn (1998b).

5.6 Regional context of snow cover and ground thermal response

The eight-month field study presented an opportunity to extend the work on snow conditions including depth, density and thermal properties, and their role in the ground temperature regime conducted in Peel Plateau, NT, by O'Neill and Burn (2017b). O'Neill and Burn (2017b) discussed the development of a talik beneath a snow fence installed in the 1980's adjacent to the Dempster Highway, approximately 60 km from the current study area. The fence effects were comparable, with maximum snow depths approximately the height of the fence ranging from 1 to 1.8 m between years, and snow depths ranging from 0.3 to 0.7 m in tundra on either side of the transect. The snow depths at the site (O'Neill and Burn 2015) are similar to those obtained in this study.

O'Neill and Burn (2017b) determined that over the 2012 to 2014 winter seasons minimum ground surface temperatures (5 cm depth) at the fence line ranged from −1.1 to −2.4 °C, and from −2.9 to −8.9 °C 25 m upwind of the fence. Minimum ground

temperatures (1.0 m depth) varied from −0.2 to −0.6 °C at the fence line and −0.6 to −3.4 °C 25 m upwind. The localized ground temperature effects observed by O'Neill and Burn (2017b), were also noted in this study. Numerical simulations supported the development of a talik beneath the fence, with an increase in thaw depth from 0.5 to 1.75 m, and ground subsidence of 0.50 m occurring from time of installation in the 1980s (O'Neill and Burn 2017a). However, in Peel Plateau permafrost is sensitive to disturbance, with relatively high (> −2.5 °C) permafrost temperatures and ice-rich ground. In addition, the fence was in a poorly drained peatland, and the ground substrate profile in the simulations was a 0.8 m thick layer of saturated peat above saturated silty clay. In contrast, in Hurricane Alley, ground and surface temperatures were lower, the ground ice content was unknown, and fences were in sloped tundra with an organic layer of 30 cm. While active-layer thickness increased significantly near fences in flat ground in Peel Plateau, it did not increase near fences on sloping ground, likely due to drainage preventing increases in latent heat content of the active layer (O'Neill and Burn 2015).

5.7 Recommendations

Based on the results of this field work a NNE-SSW fence orientation works well to accumulate blowing snow. However, one to three rows of traditional fencing offered insufficient protection against large volumes of blowing snow. Adequate protection from blowing snow would require fences of greater height or a higher number of rows, both of which are problematic. A higher number of rows are not feasible to construct and maintain, and preliminary field results indicate that the maximum snow depth should not exceed far beyond the snow depths achieved from a traditional snow fence. The

traditional snow fences used in this field study increased snow depth and density. Snow depth was also found to be significantly correlated with ground temperatures. Winter ground temperatures, while warmer beneath snow drifts, remained well below 0 °C, suggesting that the use of low height snow fences does not present an immediate risk to permafrost stability. However, winter ground temperatures near 0 °C in the wROW of km 452 highlight that high snow accumulation (> 2 m) over a prolonged period may contribute to thawing permafrost in the study area.

Future snow management options along the highway will need to balance redistributing snow with maintaining sufficiently low ground temperatures. For example, an option to protect the road at km 452 where the road cuts across a depositional area in the lee of a hill slope would be the installation of a greater number of snow fences, of slightly greater height (e.g. ≤ 2 m). An alternative solution would allow for snow accumulation alongside the road, with winter snow clearing working to equalize the profile across the road thus allowing drifting snow to pass by unimpeded. At km 456 the gravel cut acts as a catchment. Fencing placed further upwind of the catchment size would increase the size, however, would once again need to balance fence height and increasing ground temperatures. Alternatively, markers indicating the extent of the flat gravel area east of the road could be installed to clear a greater area throughout the winter, alleviating the need to increase the catchment size and reducing the risk of permafrost thaw upwind of the gravel bank.

Chapter 6: SUMMARY AND CONCLUSIONS

6.1 Summary

This thesis reports a field investigation on the modification of snow cover by installation of fences at the north end of Dempster Highway in Yukon. Ground and surface temperatures were monitored at 26 points in order to examine the effects of changes in snow cover wrought by the fences on ground temperatures. The field study was conducted over winter 2018-19 and involved the collection of detailed snow depth and density measurements. Fence efficacy was evaluated in terms of the reduction in snow depth in the zone of snow protection. The snow cover thermal properties were calculated as well. Ground temperature data were used to determine the consequence of fence drifts on average winter and minimum temperatures and on freezing degree days, and to estimate the impact on annual ground temperature.

6.2 Conclusions

The following five conclusions can be drawn from examination of the snow regime and snow fences near the Dempster Highway in Hurricane Alley:

1) Natural snow accumulation regimes ranged from a shallow snowpack (32 cm) composed of faceted snow protected by a surface crust with an average density of 0.26 g cm^{-3} in wind scoured upland plateau at km 456, to a deep snowpack of 90 cm with a density of 0.28 g cm^{-3} in the lee slope of a large hill, and depended largely on topographic factors.
2) The installation of vertical slat wooden snow fences accumulated wind-blown

snow in large drifts of high density (0.41 to 0.42 g cm^{-3}) with fencing at both km 452 and km 456 nearing capacity by December. However, snow fences were not observed to produce a zone of snow protection directly after the zone of accumulation.

3) Fence efficacy was not site-specific; slope was not categorically observed to alter fence efficacy in terms of maximum drift characteristics.
4) Increased snow deposition in drifts raised ground and surface temperatures locally but did not affect ground and surface temperatures in the expected zone of snow protection, or in the wROW regardless of the number of fences. Snow fences performed similarly however differences in the natural accumulation regime led to site-specific ground temperature responses. The installation of fencing increased winter ground temperatures beneath drifts at 10 cm and 50 cm depths by 3.6 °C and 2.5 °C, respectively, at km 456, and 3.3 °C, and 2.8 °C, respectively at km 452.
5) Ground temperature was found to be highly dependent on snow depth, with density of lesser importance. Thermal resistance was not well correlated to measures of ground temperature.

6.3 Research implications and future work

The results of this study have implications for infrastructure planning and operation and future permafrost research. Infrastructure planners and operators in the western Arctic should understand the importance of approaching snow management on a case-by-case basis. For example, in the case of km 456 regularly clearing the natural snow trap

produced by the gravel bank may be more efficacious than further snow fence installation or road clearing. The significance of topography and its role in determining the natural accumulation regime at a local scale, as well as the role of wind conditions moderating the efficacy of the fences, make generalized predictions on snow fence efficacy problematic. Snow management recommendations emphasize the importance of limiting deep snow accumulation in order to maintain sufficiently low ground temperatures.

Future research in this study area may advance the understanding of snow management effects on ground temperature in tundra of the western Arctic. Understanding the influence of topography and wind conditions on natural and artificial snow accumulation regimes may contribute to better understanding the potential of snow fences for snow management. Evidence of high winds near the road provides further reason to research the wind regime in Hurricane Alley and the role of downslope winds as a hazard for traffic. Further examination of the influence of snow conditions and thermal characteristics on ground temperatures would also be useful to understand the competing roles between density and depth. At the local scale, modelling could refine recommendations of the maximum allowable snow depths, and subsequently fence heights, to maintain stable ground temperatures given the density obtained from snow fences in Hurricane Alley.

References

Abel, G. 1893. Daily variation of temperature in snow and the relation between the thermal conductivity of snow and its density. *Meteorol. Vestnik*, vol. 3.

Andersland, O., and Ladanyi, B. 2004. Frozen ground engineering, 2nd Edition. John Wiley & Sons, Inc., Hoboken, New Jersey.

Associate Committee on Geotechnical Research (ACGR). 1988. *Glossary of permafrost and related ground-ice terms.* National Research Council of Canada, Ottawa, ON. doi:10.2307/1551636.

Albert, M.R., and Shultz, E.F. 2002. Snow and firn properties and air–snow transport processes at Summit, Greenland. *Atmospheric Environment*, **36**: 2789–2797. doi:10.1016/S1352-2310(02)00119-X.

Basnet, K., Constantinescu, G., Muste, M., and Ho, H. 2015. Method to assess efficiency and improve design of snow fences. *Journal of Engineering Mechanics,* **141**: 04014136. doi:10.1061/(ASCE)EM.1943-7889.0000871.

Beltrami, H., and Kellman, L. 2003. An examination of short- and long-term air-ground temperature coupling. *Global and Planetary Change,* **38**: 291–303. doi:10.1016/S0921-8181(03)00112-7.

Benson, C.S., and Sturm, M. 1993. Structure and wind transport of seasonal snow on the Arctic slope of Alaska. *Annals of Glaciology*, **18**: 261–267. doi:10.3189/s0260305500011629.

Bilello, M.A. 1957. *A survey of Arctic snow-cover properties as related to climatic conditions.* U.S. Army Snow Ice and Permafrost Research Establishment (SIPRE), Wilmette, IL, Research Report 39.

Bilello, M.A. 1969. *Relationships between climate and regional variations in snow-cover density in North America.* U.S. Army Cold Regions Research and Engineering Laboratory (CRREL), Hanover, NH, Research Report 267.

Blanken, P.D. 2009. Designing a living snow fence for snow drift control. *Arctic, Antarctic, and Alpine Research,* **41**: 418–425. doi:10.1657/1938-4246-41.4.418.

Bostock, H.S. 1948a. *Physiography of the Canadian Cordillera, with special reference to the area north of the fifty-fifth parallel.* Geological Survey of Canada, Ottawa, ON, Memoir 247. doi:10.4095/103300.

Bostock, H. S. 1948b. *Physiographic subdivisions of the Canadian Cordillera, north of fifty-fifth Parallel*. Geological Survey of Canada, Ottawa, ON, "A" Series Map no

922A.

Bureau of Land Management. 1999. *Sampling vegetation attributes: Interagency technical reference.* Bureau of Land Management, National Applied Resource Sciences Center, Denver, CO, Report no BLM/RS/ST-96/002+1730. http://www.blm.gov/nstc/library/pdf/samplveg.pdf.

Burn, C.R. 1998a. The response (1958-1997) of permafrost and near-surface ground temperatures to forest fire, Takhini River valley, southern Yukon Territory. *Canadian Journal of Earth Sciences,* **35**: 184–199. doi:10.1139/e97-105.

Burn, C.R. 1998b. The active layer: two contrasting definitions. *Permafrost and Periglacial Processes,* **9**: 411-416.

Burn C.R. 2004. The Thermal Regime of Cryosols. In *Cryosols*. Edited by J. M. Kimble. Springer, Berlin, Heidelberg.

Burn, C.R. 2011. Permafrost Distribution and Stability. In *Changing Cold Environments: A Canadian Perspective*, First Edition. Edited by H. French and O. Slaymaker. John Wiley & Sons, Ltd. doi:10.1002/9781119950172.

Burn, C.R., and Kokelj, S. V. 2009. The environment and permafrost of the Mackenzie Delta area. *Permafrost and Periglacial Processes*, **20**: 83–105. doi:10.1002/ppp.665.

Burn, C.R., Mackay, J.R., and Kokelj, S. V. 2009. The thermal regime of permafrost and its susceptibility to degradation in upland terrain near Inuvik, N.W.T. *Permafrost and Periglacial Processes,* **20***:* 221–227. doi:10.1002/ppp.649.

Burn, C.R., Moore, J.J.L., O'Neill, H.B.B., Hayley, D.W., Trimble, J.R., Calmels, F., Orban, S.N., and Idrees, M. 2015. Permafrost characterization of the Dempster Highway, Yukon and Northwest Territories. In *Proceedings of the 68th Canadian Geotechnical Conference and 7th Canadian Permafrost Conference,* 21-23 September 2015, Québec City, QC. Canadian Geotechnical Society, Richmond, BC, Paper 705.

Burn, C.R., and Zhang, Y. 2009. Permafrost and climate change at Herschel Island (Qikiqtaruq), Yukon Territory, Canada. *Journal of Geophysical Research: Earth Surface*, **114**: F02001. doi:10.1029/2008JF001087.1087.

Burt, T.P., and Williams, P.J. 1976. Hydraulic conductivity in frozen soils. *Earth Surface Processes*, **1**(4): 349-360. doi:10.1002/esp.3290010404.

Calmels, F., Roy, L. P., Grandmont, K., and Pugh, R. 2018. *A summary of climate- and geohazard-related vulnerabilities for the Dempster Highway corridor.* Yukon Research Centre, Yukon College, Whitehorse, YT.

Calonne, N., Flin, F., Morin, S., Lesaffre, B., Du Roscoat, S.R., and Geindreau, C. 2011. Numerical and experimental investigations of the effective thermal conductivity of snow. *Geophysical Research Letters,* **38**(3): 1–6. doi:10.1029/2011GL049234.

Catto, N.R. 1996. Richardson Mountains, Yukon-Northwest Territories: The northern portal of the postulated "ice-free corridor." *Quaternary International,* **32:** 3–19. doi:10.1016/1040-6182(95)00062-3.

Colbeck, S.C. 1982. An overview of seasonal snow metamorphism. *Reviews of Geophysics and Space Physics,* **20**: 45–61. doi:10.1029/RG020i001p00045.

Colbeck, S.C. 1983. Theory of metamorphism of dry snow. *Journal of Geophysical Research,* **88:** 5475–5482. doi: 10.1029/JC088iC09p05475.

Colbeck, S.C. 1989. Air movement in snow due to windpumping. *Journal of Glaciology,* **35:** 209–213. doi:10.3189/S0022143000004524.

Colbeck, S.C. 1991. The layered character of snow covers. *Reviews of Geophysics,* **29**: 81–96. doi:10.1029/90RG02351.

Colbeck, S.C., Akitaya, E., Armstrong, R.L., Gubler, H., Lafeuille, J., Lied, K., McClung, D.M., and Morris, E.M. 1991. *The international classification for seasonal snow on the ground.* The International Commission on Snow and Ice (ICSI), International Association of Scientific Hydrology, Wallingford, UK.

Davenport, A.G. 1960. Rationale for determining design wind velocities. *ASCE Journal of the Structural Division*, **86** (ST 5): 39–68.

DigitalGlobe, Inc. 2016. *Image ID: 1030010052D7DA00*. WorldView-2. February 23, 2016. Available from: https://discover.digitalglobe.com/ [accessed January 2019].

Dominé, F., Albert, M., Huthwelker, T., Jacobi, H.W., Kokhanovsky, A.A., Lehning, M., Picard, G., and Simpson, W.R. 2008. Snow physics as relevant to snow photochemistry. *Atmospheric Chemistry and Physics*, **8**: 171–208. doi:10.5194/acp-8-171-2008.

Dominé, F., Cabanes, A., and Legagneux, L. 2002. Structure, microphysics, and surface area of the Arctic snowpack near Alert during the ALERT 2000 campaign. *Atmospheric Environment,* **36**: 2753–2765. doi:10.1016/S1352-2310(02)00108-5.

Dominé, F., Lauzier, T., Cabanes, A., Legagneux, L., Kuhs, W.F., Techmer, K., and Heinrichs, T. 2003. Snow metamorphism as revealed by scanning electron microscopy. *Microscopy Research and Technique*, **62**: 33–48. doi:10.1002/jemt.10384.

Donald, W., and Entine, L. 2002. *Basic surveying manual.* Wisconsin Transportation

Information Center, Madison, WI. doi:10.4324/9780080499895.

Durran, D.R. 1990. Mountain Waves and Downslope Winds. In: *Atmospheric Processes over Complex Terrain*. Edited by W. Blumen. Meteorological Monographs, vol 23, no 45. American Meteorological Society, Boston, MA.

Durran, D.R. 2015. Downslope Winds. In: *Encyclopedia of Atmospheric Sciences*, Second Edition. Edited by G. R. North, J. Pyle, and F. Zhang. Elsevier Science Ltd. pp. 69–74. ISBN 9780123822253.

Eaton, A.K., Rouse, W.N., Lafleur, P.M., Marsh, P., and Blanken, P.D. 2001. Surface energy balance of the western and central Canadian subarctic: Variations in the energy balance among five major terrain types. *Journal of Climate*, **14**: 3692–3703. doi:10.1175/1520-0442(2001)014<3692:SEBOTW>2.0.CO;2.

Ecological Stratification Working Group. 1995. *A national ecological framework for Canada.* Agriculture and Agri-Food Canada, Research Branch, Centre for Land and Biological Resources Research and Environment Canada, State of the Environment Directorate, Ecozone Analysis Branch, Ottawa/Hull.

Expert Committee on Soil Survey (ECSS). 1983. *The Canada Soil Information System (CanSIS): Manual for describing soils in the field, 1982 revised.* Land Resource Research Institute (LRRI), Research Branch, Agriculture Canada, Ottawa, ON, LRRI Contribution no 82-52.

Environment Canada. 2018a. *Historical data*. Available from: http://climate.weather.gc.ca/historical_data/search_historic_data_e.html [accessed 1 September 2018].

Environment Canada. 2018b. *Canadian climate normals 1981-2010 station data.* Available from: http://climate.weather.gc.ca/climate_normals/index_e.html [accessed 1 September 2018].

Essery, R., Li, L., and Pomeroy, J.W. 1999. A distributed model of blowing snow over complex terrain. *Hydrological Processes,* **13**: 2423–2438. doi:10.1002/(SICI)1099-1085.

Essery, R., and Pomeroy, J.W. 2004. Vegetation and topographic control of wind-blown snow distributions in distributed and aggregated simulations for an Arctic tundra basin. *Journal of Hydrometeorology,* **5**: 735–744. doi:10.1175/1525-7541.

Fierz, C., Armstrong, R.L.L., Durand, Y., Etchevers, P., Greene, E., McClung, D.M.M., Nishimura, K., Satyawali, P.K.K., and Sokratov, S. a. A. 2009. *The international classification for seasonal snow on the ground.* IHP-VII Technical Documents in Hydrology N°83, IACS Contribution N°1, UNESCO-IHP, Paris.

Föhn, P.M.B., and Meister, R. 1983. Distribution of snow drifts on ridge slopes:

Measurements and theoretical approximations. *Annals of Glaciology*, **4**: 52–57. doi: 10.1017/S0260305500005231.

French, H.M. 2007. Permafrost. In *The periglacial environment*, Third Edition. Wiley, Chichester. pp. 83–115.

Geiger, R. 1980. *The Climate Near the Ground,* Sixth print. Harvard University Press, Cambridge. p. 209.

Gold, L.W., and Williams, G.P. 1957. *Some results of the snow survey of Canada*. National Research Council of Canada, Division of Building Research, Ottawa, ON, Research Paper no 38.

Goodrich, L.E. 1982. The influence of snow cover on the ground thermal regime. *Canadian Geotechnical Journal,* **19**: 421–432. doi:10.1139/t82-047.

Google Earth. 2014. Landsat/Copernicus. Northern Yukon, Canada. 66.96° N, 136.21° W, Eye alt 4.06 km. December 30, 2014. Available from: http://www.earth.google.com [accessed March 2020].

Google Earth. 2015. Landsat/Copernicus. Northern Yukon, Canada. 66.95° N, 136.26° W, Eye alt 14.45 km. December 30, 2015. Available from: http://www.earth.google.com [accessed March 2020].

Gray, D.M. 1978. *Snow accumulation and distribution*. Paper presented to the workshop/meeting on "Modeling Snow Cover Runoff" U.S. Army Cold Regions Research and Engineering Laboratory (CRREL), Hanover, NH, September 26-29, 1978.

Heavy, J.P. 2013. Structure and function of living snow fences in New York State. MSc Thesis, Department of Forest and Natural Resources Management, State University of New York, Syracuse, NY. https://www.esf.edu/willow/lsf/Litterature/Heavey%202013%20-%20Structure%20and%20Function%20of%20LSF.pdf

Heginbottom, J.A., Dubreuil, M.A., and Harker, P.T. 1995. Canada: Permafrost. In *National Atlas of Canada,* Fifth Edition. Natural Resources Canada, Ottawa, ON, Plate 2.1, MCR 4177. http://ftp.geogratis.gc.ca/pub/nrcan_rncan/raster/atlas_5_ed/eng/environment/land/mcr4177.jpg

Hiemstra, C.A., Liston, G.E., and Reiners, W.A. 2006. Observing, modelling, and validating snow redistribution by wind in a Wyoming upper treeline landscape. *Ecological Modelling,* **197**: 35–51. doi:10.1016/j.ecolmodel.2006.03.005.

Hinkel, K.M., Bockheim, J.G., Peterson, K.M., and Norton, D.W. 2003. Impact of snow fence construction on tundra soil temperatures at Barrow, Alaska. In *Proceedings of*

the 8th International Conference on Permafrost, 21-25 July 2003, Zurich, Switzerland. Edited by M. Phillips, S.M. Springman, and L.U. Arenson. Swets & Zeitlinger Publishers. pp. 401–405.

Hinkel, K.M., and Hurd, J.K. 2006. Permafrost Destabilization and Thermokarst following Snow Fence Installation, Barrow, Alaska, U.S.A. *Arctic, Antarctic, and Alpine Research*, **38**: 530–539. doi:10.1657/1523-0430.

Hughes, O.L. 1972. *Surficial geology of northern Yukon Territory and northwestern District of Mackenzie, Northwest Territories*. Geological Survey of Canada, Paper 69-36. doi:10.4095/102354.

Humphries, J.K., Burn, C.R., MacDougall, S., and Brais, C. 2019. Storm Wind Frequency and Direction, Dempster Highway, Richardson Mountains, Yukon and Northwest Territories. In *Proceedings of the 18th International Conference on Cold Regions Engineering and 8th Canadian Permafrost Conference*, 18-22 August 2019, Québec City, QC. American Society of Civil Engineers, Reston, VA. pp. 137–145.

Idrees, M., Burn, C.R., Moore, J., and Calmels, F. 2015. Monitoring permafrost conditions along the Dempster Highway. In *Proceedings of the 68th Canadian Geotechnical Conference and 7th Canadian Permafrost Conference,* 21-23 September 2015, Québec City, QC. Canadian Geotechnical Society, Richmond, BC. Paper 703.

Judge, A. 1973. The prediction of permafrost thicknesses. *Canadian Geotechnical Journal*, **10** (1): 313–321.

Karunaratne, K.C., and Burn, C.R. 2004. Relations between air and surface temperature in discontinuous permafrost terrain near Mayo, Yukon Territory. *Canadian Journal of Earth Sciences*, **41**: 1437–1451. doi:10.1139/e04-082.

Kershaw, P.G., and McCulloch, J. 2007. Midwinter snowpack variation across the arctic treeline, Churchill, Manitoba, Canada. *Arctic, Antarctic, and Alpine Research,* **39**: 9–15. doi:10.1657/1523-0430(2007)39.

Kinsley, D.B. 1963. *Influence of snow cover on frost penetration*. U.S. Geological Survey, Professional Paper 475-B. doi:10.1038/312192a0.

Klock, R., Hudson, E., Aihoshi, D., and Mullock, J. 2001. *The weather of the Yukon, Northwest Territories and Western Nunavut: Graphic area forecast 35*. NAV CANADA. http://www.navcanada.ca/EN/media/Pages/publications-operational-weather-manuals.aspx.

Kok, J.F., Parteli, E.J.R., Michaels, T.I., and Karam, D.B. 2012. The physics of wind-blown sand and dust. *Reports on Progress in Physics*, **75**: 106901.

doi:10.1088/0034-4885/75/10/106901.

Kokelj, S.V, Lantz, T.C., Wolfe, S.A., Kanigan, J.C., Morse, P.D., Coutts, R., Molina-Giraldo, N., and Burn, C.R. 2014. Distribution and activity of ice wedges across the forest-tundra transition, western Arctic Canada. *Journal of Geophysical Research: Earth Surface,* **119**. doi:10.1002/2014JF003085.

Kokelj, S. V., and Burn, C.R. 2003. Ground ice and soluble cations in near-surface permafrost, Inuvik, Northwest Territories, Canada. *Permafrost and Periglacial Processes*, **14** (3): 275–289. doi:10.1002/ppp.458.

Lacelle, D., Lauriol, B., Zazula, G., Ghaleb, B., Utting, N., and Clark, I.D. 2013. Timing of advance and basal condition of the Laurentide Ice Sheet during the last glacial maximum in the Richardson Mountains, NWT. *Quaternary Research,* **80**: 274–283. doi:10.1016/j.yqres.2013.06.001.

Lachenbruch, A.H., Cladouhos, T.T., and Saltus, R.W. 1988. Permafrost temperature and the changing climate. In *Proceedings of the 5th International Conference on Permafrost,* 2–5 August 1988, Trondheim, Norway. Edited by K. Senneset. Tapir Publishers, Trondeim, Norway. pp. 9–17.

Lantz, T.C., Kokelj, S. V., Gergel, S.E., and Henry, G.H.R. 2009. Relative impacts of disturbance and temperature: Persistent changes in microenvironment and vegetation in retrogressive thaw slumps. *Global Change Biology*, **15**: 1664–1675. doi:10.1111/j.1365-2486.2009.01917.x.

Lauriol, B. 1990. Cryoplanation terraces. *The Canadian Geographer*, **34**: 347–351. doi:10.1111/j.1541-0064.2000.tb00712.x.

Legagneux, L., Cabanes, A., and Dominé, F. 2002. Measurement of the specific surface area of 176 snow samples using methane adsorption at 77 K. *Journal of Geophysical Research Atmospheres,* **107**: 4335–4350. doi:10.1029/2001JD001016.

Li, L., and Pomeroy, J.W. 1997. Estimates of threshold wind speeds for snow transport using meteorological data. *Journal of Applied Meteorology*, **36**: 205–213. doi:10.1175/1520-0450(1997)036<0205:EOTWSF>2.0.CO;2.

Ling, F., and Zhang, T. 2007. Modeled impacts of changes in tundra snow thickness on ground thermal regime and heat flow to the atmosphere in Northernmost Alaska. *Global and Planetary Change,* **57**: 235–246. doi:10.1016/j.gloplacha.2006.11.009.

Liston, G.E., Haehnel, R.B., Sturm, M., Hiemstra, C.A., Berezovskaya, S., and Tabler, R.D. 2007. Simulating complex snow distributions in windy environments using SnowTran-3D. *Journal of Glaciology*, **53**: 241–256. doi:10.3189/172756507782202865.

Liston, G.E., and Sturm, M. 2004. The role of winter sublimation in the Arctic moisture

budget. *Nordic Hydrology*, **35**: 325–334. doi:10.2166/nh.2004.0024.

Mackay, J.R. 1978. The use of snow fences to reduce ice-wedge cracking, Garry Island, Northwest Territories. In *Current Research*, *Part A*, Geological Survey of Canada, Paper **78-1A**, pp. 523-24.

Mackay, J.R. 1983. Downward water movement into frozen ground, western arctic coast, Canada. *Canadian Journal of Earth Sciences*, **20**: 120–134. doi:10.1139/e83-012.

Mackay, J.R., and MacKay, D.K. 1974. Snow cover and ground temperatures, Garry Island, N.W.T. *Arctic*, **27**: 287-296. doi:10.14430/arctic2885.

Male, D.H., and Gray, D.M. (eds). 1981. *Handbook of snow: Principles, processes, management & use*. Pergamon Press, Toronto.

Malenfant-Lepage, J., Doré, G., and Fortier, D. 2012. Thermal effectiveness of the mitigation techniques tested at Beaver Creek experimental road site based on a heat balance analysis: Yukon, Canada. In *Proceedings of the 15th International Conference on Cold Regions Engineering*, 19-22 August 2012, Québec City, QC. pp. 42–51. doi:10.1061/9780784412473.005.

McConnell, R.G. 1891. *Report on an exploration in the Yukon and Mackenzie Basins, N.W.T.* Geological Survey of Canada, Annual Report Vol. 4, (1888-1889), Part D. doi:10.4095/225895.

McKay, G.A., and Gray, D.M. 1981. The distribution of snowcover. In *Handbook of snow: Principles, processes, management & use*. Edited by D.H. Male and D.M. Gray. Pergamon Press, Toronto. pp. 153–187.

Mellor, M. 1965. *Blowing snow*. U.S. Army Cold Regions Research and Engineering Laboratory (CRREL), Hanover, NH, CRREL monograph, Part III, Section A3c.

Ménard, C.B., Essery, R., and Pomeroy, J.W. 2014. Modelled sensitivity of the snow regime to topography, shrub fraction and shrub height. *Hydrology and Earth System Sciences*, **18**: 2375–2392. doi:10.5194/hess-18-2375-2014.

Morse, P.D., and Burn, C.R. 2014. Perennial frost blisters of the Mackenzie Delta, Western Arctic Coast, Canada. *Earth Surface Processes and Landforms*, **39**: 200–213. doi:10.1002/esp.3439.

Morse, P.D., Burn, C.R., and Kokelj, S. V. 2012. Influence of snow on near-surface ground temperatures in upland and alluvial environments of the outer Mackenzie Delta, Northwest Territories. *Canadian Journal of Earth Sciences,* **49**: 895–913. doi:10.1139/E2012-012.

Naaim-Bouvet, F., and Mullenbach, P. 1998. Field experiments on “living” snow fences.

Annals of Glaciology, **26**: 217–220. doi:10.1017/S0260305500014841.

Naaim-Bouvet, F., Naaim, M., and Michaux, J.L. 2002. Snow fences on slopes at high wind speed: Physical modelling in the CSTB cold wind tunnel. *Natural Hazards and Earth System Science*s, **2**: 137–145. doi:10.5194/nhess-2-137-2002.

Norris, D. 1985. *Geology of the Northern Yukon and Northwestern District of Mackenzie.* Geological Survey of Canada, Ottawa, ON, "A" Series Map no 1581A. doi:10.4095/120537.

O'Neill, H.B., and Burn, C.R. 2015. Permafrost degradation adjacent to snow fences along the Dempster Highway, Peel Plateau, NWT. In *Proceedings of the 68th Canadian Geotechnical Conference and 7th Canadian Permafrost Conference,* 21-23 September 2015, Québec City, QC. Canadian Geotechnical Society, Richmond, BC. Paper 219.

O'Neill, H.B., and Burn, C.R. 2017b. Talik Formation at a Snow Fence in Continuous Permafrost, Western Arctic Canada. *Permafrost and Periglacial Processes*, **28**: 558–565. doi:10.1002/ppp.1905.

O'Neill, H.B., Burn, C.R. 2017a. Impacts of variations in snow cover on permafrost stability, including simulated snow management, Dempster Highway, Peel Plateau, Northwest Territories. *Arctic Science*, **3**: 150–178. doi:10.1139/as-2016-0036.

O'Neill, H.B., Burn, C.R., and Kokelj, S. V. 2015b. Field measurements of permafrost conditions beside the Dempster Highway embankment, Peel Plateau, NWT. In *Proceedings of the 68th Canadian Geotechnical Conference and 7th Canadian Permafrost Conference,* 21-23 September 2015, Québec City, QC. Canadian Geotechnical Society, Richmond, BC. carleton.ca/permafrost/wp-content/uploads/380.pdf

O'Neill, H.B., Burn, C.R., Kokelj, S. V., and Lantz, T.C. 2015a. "Warm" tundra: Atmospheric and near-surface ground temperature inversions across an alpine treeline in continuous permafrost, Western Arctic, Canada. *Permafrost and Periglacial Processes*, **26**: 103–118. doi:10.1002/ppp.1838.

Ogilvie, W. 1890. *Exploratory survey of part of the Lewes, Tat-on- Duc, Porcupine, Bell, Trout, Peel, and Mackenzie Rivers, 1887-1888*. Canada Department of the Interior, Annual Report 1889, 1890. Brown Chamberlain, Ottawa. https://archive.org/download/exploratorysurve00ogil/exploratorysurve00ogil.pdf

Oke. T.R. 1987. *Boundary Layer Climates*, Second Edition. Routledge, London. 435 pp. Master e-book ISBN 0-203-40721-0.

Onuchin, A.A., and Burenina, T.A. 1996. Climatic and geographic patterns in snow density dynamics, Northern Eurasia. *Arctic and Alpine Research,* **28**: 99–103.

doi:10.2307/1552091.

Osterkamp, T.E., and Romanovsky, V.E. 1997. Freezing of the active layer on the Coastal Plain of the Alaskan Arctic. *Permafrost and Periglacial Processes,* **8**: 23–44. doi:10.1002/(sici)1099-1530(199701)8:1<23::aid-ppp239>3.3.co;2-u.

Outcalt, S.I., and Hinkel, K.M. 1996. The response of near-surface permafrost to seasonal regime transitions in tundra terrain. *Arctic and Alpine Research,* **28**: 274–283. doi:10.2307/1552106.

Outcalt, S.I., Nelson, F.E., and Hinkel, K.M. 1990. The zero-curtain effect: heat and mass transfer across an isothermal region in freezing soil. *Water Resources Research*, **26**: 1509–1516. doi:10.1029/WR026i007p01509.

Peterson, T.C., and Schmidt, R.A. 1984. Outdoor scale modeling of shrub barriers in drifting snow. *Agricultural and Forest Meteorology,* **31**: 167–181. doi:10.1016/0168-1923(84)90018-2.

Pomeroy, J.W. 1991. Transport and sublimation of snow in wind-scoured alpine terrain. In *Snow, Hydrology and Forests in High Alpine Areas – Proceedings of the Vienna Symposium,* August 1991. International Association of Hydrological Sciences (IAHS) Publication no 205. pp. 131–140.

Pomeroy, J.W., Bewley, D.S., Essery, R.L.H., Hedstrom, N.R., Link, T., Granger, R.J., Sicart, J.E., Ellis, C.R., and Janowicz, J.R. 2006. Shrub tundra snowmelt. *Hydrological Processes*, **20**: 923–941. doi:10.1002/hyp.6124.

Pomeroy, J.W., and Brun, E. 2001. Physical properties of snow. In *Snow ecology: An interdisciplinary examination of snow-covered ecosystems*. Edited by H.G. Jones, J.W. Pomeroy, D.A. Walker, R. Hoham. Cambridge University Press, Cambridge. pp. 45–126. doi:10.1017/CBO9781107415324.004.

Pomeroy, J.W., and Gray, D.M. 1994. Sensitivity of snow relocation and sublimation to climate and surface vegetation. In *Snow and ice covers: Interactions with the atmosphere and ecosystems – Proceedings of Yokohama Symposia,* 2-5 July 1993. International Association of Hydrological Sciences (IAHS) Publication no 423. pp. 213–225.

Pomeroy, J.W., and Gray, D.M. 1995. *Snowcover: Accumulation, relocation and management.* National Hydrology Research Institute (NHRI), Saskatoon, SK, NHRI Science Report No. 7. Environment Canada, Saskatoon – Saskatchewan.

Pomeroy, J.W., Gray, D.M., and Landine, P.G. 1993. The prairie blowing snow model: Characteristics, validation, operation. *Journal of Hydrology*, **144**: 165–192. doi:10.1016/0022-1694(93)90171-5.

Pomeroy, J.W., and Male, D.H. 1992. Steady-state suspension of snow. *Journal of*

Hydrology, **136**: 275–301. doi:10.1016/0022-1694(92)90015-N.

Pomeroy, J.W., Marsh, P., and Gray, D.M. 1997. Application of a distributed blowing snow model to the Arctic. *Hydrological Processes,* **11**: 1451–1464. doi:10.1002/(SICI)1099-1085(199709)11:11<1451::AID-HYP449>3.0.CO;2-Q.

Presley, D., and Tatarko, J. 2009. Principles of wind erosion and its control. Kansas State University, Manhattan, KS, Research and Extension Publication MF-2860. https://infosys.ars.usda.gov/WindErosion/publications/publications.shtml

Rampton, V.N. 1982. *Quaternary Geology Yukon Coastal Plain, Yukon Territory-Northwest Territory*. Geological Survey of Canada, Bulletin 317. doi:10.4095/111347.

Rampton, V.N. 1988. *Quaternary geology of the Tuktoyaktuk Coastlands, Northwest Territories.* Geological Survey of Canada, Memoir 423. doi:10.4095/126937.

Ribberink, M., Chui, T., Steinhart, R., Modzelewski, H., Howard, R., and Stull, R. 2020. An Analysis of Dempster Highway Strong-Wind Events for Winter 2019-2020 Through Numerical Simulations. University of British Columbia, Vancouver, BC, Weather Forecast Research Team, Department of Earth, Ocean and Atmospheric Sciences. 80 pp.

Riseborough, D.W. 2002. The mean annual temperature at the top of permafrost, the TTOP model, and the effect of unfrozen water. *Permafrost and Periglacial Processes,* **13**: 137–143. doi:10.1002/ppp.418.

Romanovsky, V.E., and Osterkamp, T.E. 1995. Interannual variations of the thermal regime of the active layer and near-surface permafrost in Northern Alaska. *Permafrost and Periglacial Processes,* **8**: 1–22. doi:10.1002/ppp.3430060404.

Roy-Léveillée, P., Burn, C.R., and McDonald, I.D. 2014. Vegetation-Permafrost Relations within the Forest-Tundra Ecotone near Old Crow, Northern Yukon, Canada. *Permafrost and Periglacial Processes*, **25**: 127–125. doi:10.1002/ppp.1805.ppp.1805.

Sañudo-Fontaneda, L.A., Castro-Fresno, D., del Coz-Diaz, J.., Rodriguez-Hernandez, J. 2011. Classification and comparison of snow fences for the protection of transport infrastructures. *Journal of Cold Regions Engineering,* **25**: 162–181. doi:10.1061/(ASCE)CR.1943-5495.

Schmidt, R.A. 1980. Threshold windspeeds and elastic impact in snow transport. *Journal of Glaciology,* **26** (94): 453–467. doi:10.1017/S0022143000010972.

Scudder, G.G.E. 1997. Environment of the Yukon. In *Insects of the Yukon*. Edited by H. V. Danks and J.A. Downes. Biological Survey of Canada, Ottawa, ON. pp. 13–57.

https://biologicalsurvey.ca/monographs/read/3

Sladen, W.E. 2017. *Icings near the Tibbitt to Contwoyto winter road, Great Slave Uplands, Northwest Territories.* MSc Thesis, Department of Geography. Carleton University, Ottawa, ON. 154 pp.

Smith, M.W., and Riseborough, D.W. 2002. Climate and the limits of permafrost: A zonal analysis. *Permafrost and Periglacial Processes*, **13**: 1-15. doi:10.1002/ppp.410.

Soil Classification Working Group. 1998. *The Canadian system of soil classification, 3rd Edition*. Agriculture and Agri-Food Canada, Publication 1646, 187 pp. http://sis.agr.gc.ca/cansis/publications/manuals/1998-cssc-ed3/index.html.

Stockton, E.J., Burn, C.R., Idrees, M., Calmels, F., and Elmer, K. 2019. Monitoring ground temperatures in permafrost along the Dempster Highway, Yukon and NWT. In *Proceedings of the 18th International Conference on Cold Regions Engineering and the 8th Canadian Permafrost Conference*, 18-22 August 2019, Québec City, QC. pp. 92–101.

Sturm, M., and Benson, C.S. 1997. Vapor transport, grain growth and depth-hoar development in the subarctic snow. *Journal of Glaciology,* **43**: 42–58. doi:10.3189/s0022143000002793.

Sturm, M., and Holmgren, J. 1998. Differences in compaction behaviour of three climate classes of snow. *Annals of Glaciology*, **26**: 125–130. doi:10.1017/S0260305500014683.

Sturm, M., Holmgren, J., Koenig, M., and Morris, K. 1997. The thermal conductivity of seasonal snow. *Journal of Glaciology*, **43**: 26–41. doi:10.3198/1997JoG43-143-26-41.

Sturm, M., Holmgren, J., and Liston, G.E. 1995. A seasonal snow cover classification system for local to global applications. *Journal of Climate*, **8**: 1261–1283. doi:10.1175/1520-0442(1995)008%3C1261:ASSCCS%3E2.0.CO;2.

Tabler, R.D. 1968. Physical and economic design criteria for induced snow accumulation projects. *Water Resources Research*, **4**: 513–519. doi:10.1029/WR004i003p00513.

Tabler, R.D. 1973. New snow fence design controls drifts, improves visibility, reduces road ice. In *Proceedings of the 46th Annual Transportation Engineering Conference*, 22-23 February 1973, Denver, CO. pp. 16–27.

Tabler, R.D. 1980. Geometry and density of drifts formed by snow fences. *Journal of*

Glaciology, **26**: 405–419. doi:10.1017/S0022143000010935.

Tabler, R.D. 1986. *Snow fence handbook* (Release 1.0). Laramie, WY. 169 pp.

Tabler, R.D. 1991. *Snow fence guide.* Strategic Highway Research Program, National Research Council, Washington, DC, SHRP-W/FR-91-106. 76 pp.

Tabler, R.D. 1994. *Design guidelines for the control of blowing and drifting snow*. Strategic Highway Research Program, National Research Council, Washington, DC, SHRP-H-381. 364 pp.

Tabler, R.D. 2003. *Controlling blowing and drifting snow with snow fences and road design*. National Cooperative Highway Research Program, NCHRP Project 20-7(147).

Tabler, R.D. 2004. Effect of blowing snow and snow fences on pavement temperature and ice formation. In *Proceedings of the Sixth International Symposium on Snow Removal and Ice Control Technology*, 7–9 June 2004, Spokane, WA. Transportation Research Circular, No. E-C063. pp. 401–413. http://trb.org/publications/circulars/ec063.pdf

Tabler, R.D., Pomeroy, J.W., and Santana, B.W. 1990. Drifting snow. In *Cold regions hydrology and hydraulics*: *A state of practice report.* Technical Council on Cold Regions Engineering Monograph. Edited by W.L. Ryan, and R.D. Crissman. American Society of Civil Engineers, New York, NY. pp. 95–145.

The Canadian Avalanche Association. 2014. *Observation guidelines and recording standards for weather, snowpack and avalanches*. https://www.avalancheassociation.ca/resource/resmgr/standards_docs/OGRS2016web.pdf

Vyalov, S.S. 1979. *Engineering geocryology abroad – Proceedings of the Third International Conference on Engineering Geocryology.* Soil Mechanics and Foundations Engineering, **16**: 212–126. doi:10.1007/BF01704135.

Wahl, H.E., Fraser, D.B., Harvey, R.C., and Maxwell, J.B. 1987. *Climate of Yukon*. Environment Canada, Atmospheric Environment Service, Downsville, ON, Climatological Studies No. 40.

Whiteman, C.D. 2000. Terrain-Forced Flows. In *Mountain Meteorology: Fundamentals and applications.* pp. 141–169. Oxford University Press, Inc., New York.

Williams, P., and Smith, M. 1989. *The Frozen Earth: Fundamentals of geocryology*. Cambridge University Press, Cambridge.

Yen, Y.C. 1981. *Review of thermal properties of snow, ice and sea ice.* U.S. Army Cold Regions Research and Engineering Laboratory (CRREL), Hanover, NH, CRREL

Report 81-10.

Yukon Ecoregions Working Group. 2004. *Ecoregions of the Yukon Territory: Biophysical properties of Yukon landscapes*. Edited by C.A.S. Smith, J.C. Meikle, and C.F. Roots. Summerland, BC.

Yukon Government. 2014a. *file name: Dempster_464.* Dempster Highway, Yukon, Canada. July 23, 2014. Available from: ftp://ftp.geomaticsyukon.ca/GeoYukon/Imagery/Aerials/DempsterHighway/7-23-2014/ [accessed September 2019].

Yukon Government. 2014b. *file name: Dempster_472.* Dempster Highway, Yukon, Canada. July 23, 2014. Available from: ftp://ftp.geomaticsyukon.ca/GeoYukon/Imagery/Aerials/DempsterHighway/7-23-2014/ [accessed September 2019].

Zhang, T. 2005. Influence of seasonal snow cover on the ground thermal regime: An overview. *Reviews in Geophysics*, **43**: RG4002. doi:10.1029/2004RG000157.

Zhang, T. 1993. Climate, seasonal snow cover and permafrost temperatures in Alaska north of the Brooks Range. PhD dissertation, University of Alaska Fairbanks, 232 pp.

Zhang, T., Osterkamp, T.E., and Stamnes, K. 1996. Influence of the depth hoar layer of the seasonal snow cover on the ground thermal regime. *Water Resources Research*, **32**: 2075–2086. doi:10.1029/96WR00996.

Zoltai, S., and Pettapiece, W.W. 1973. *Studies of vegetation, landform and permafrost in the Mackenzie Valley: Terrain, vegetation and permafrost relationships in the northern part of the Mackenzie Valley and Northern Yukon.* Environmental-Social Committee, Northern Pipelines, Task Force on Northern Oil Development, Report No 73-4.

Appendices

Appendix A

A.1 Snow depth profiles at km 452

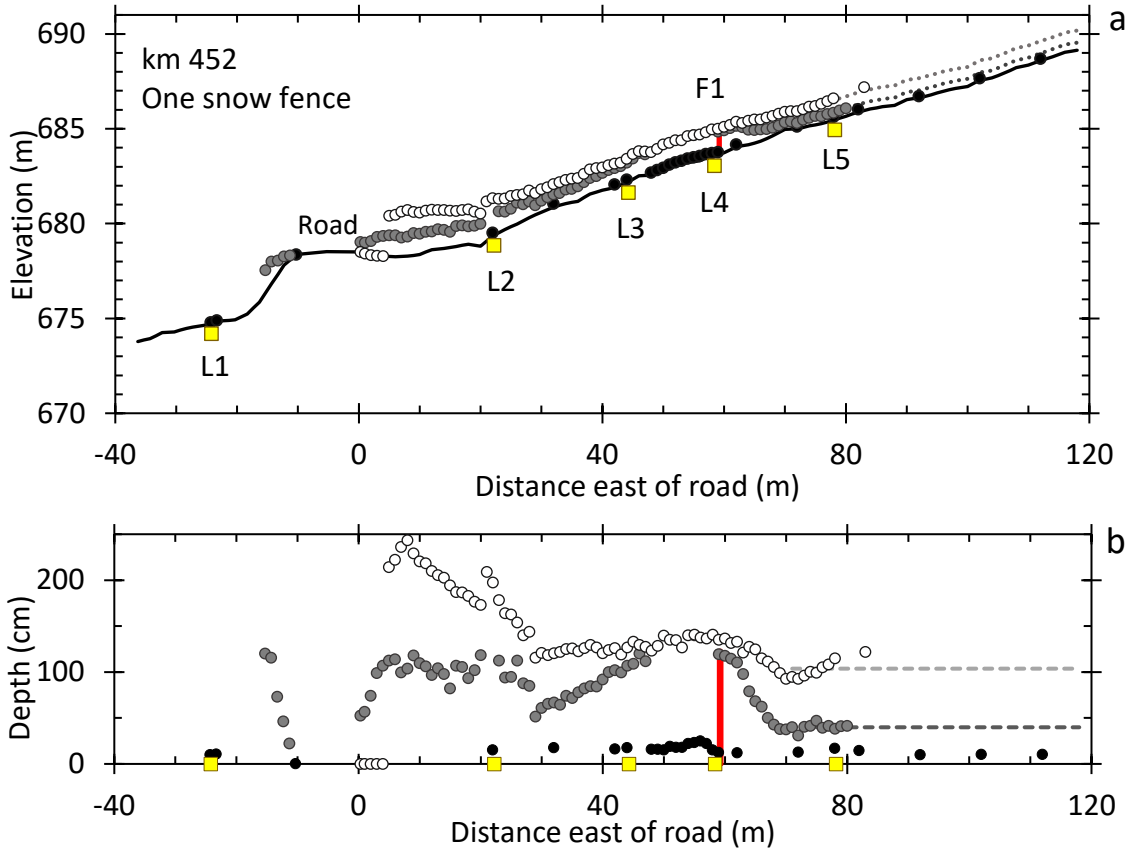

Figure A.1. Snow depth profiles at km 452 with one snow fence row (P1), (a) with elevation, and (b) normalized for elevation. Filled circles represent measured snow depths while dashed lines represent inferred snow depths based on field observations. Circles are black, grey, or open, to indicate measurements in October, December, and March 2018–19, respectively. Yellow squares mark the position of ground temperature loggers along the transect, and red vertical lines mark the position and height (1.22 m) of the fence. The primary (F1) fence was located 59 m from the eastern road edge (0 m), and loggers were located −24.2, 22.2, 44.3, 58.4, and 78.2 m from the eastern road edge.

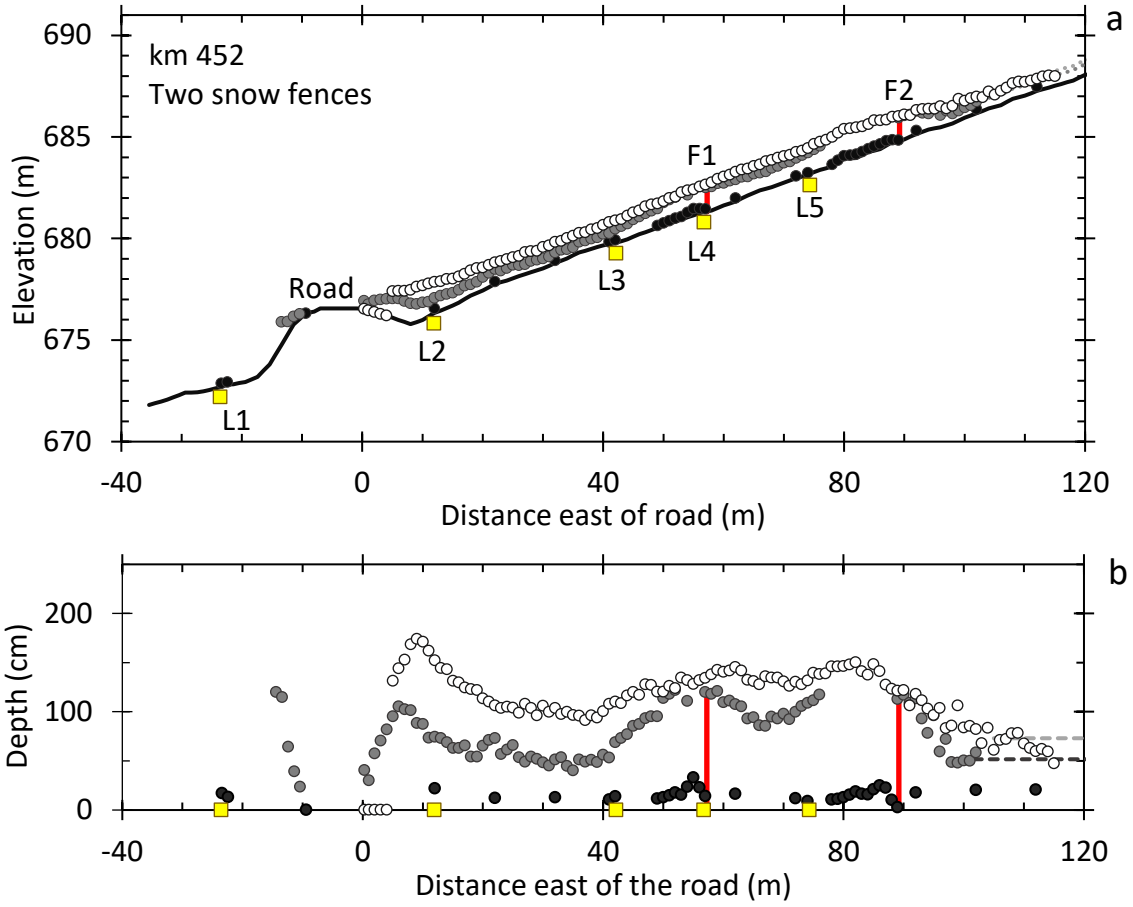

Figure A.2. Snow depth profiles at km 452 with two snow fence rows (P2), (a) with elevation, and (b) normalized for elevation. Filled circles represent measured snow depths while dashed lines represent inferred snow depths based on field observations. Circles are either black, grey, or open, to indicate measurements in October, December, and March 2018–19, respectively. Yellow squares mark the position of ground temperature loggers along the transect, and red vertical lines mark the position and height (1.22 m) of the fence rows. The primary (F1) fence was positioned closest to the road, 57 m from the eastern road edge (0 m), while the secondary (F2) fence was positioned further back at 89 m. Loggers were located −23.6, 11.9, 42.1, 56.7, and 74.3 m from the eastern road edge.

A.2 Snow depth profiles at km 456

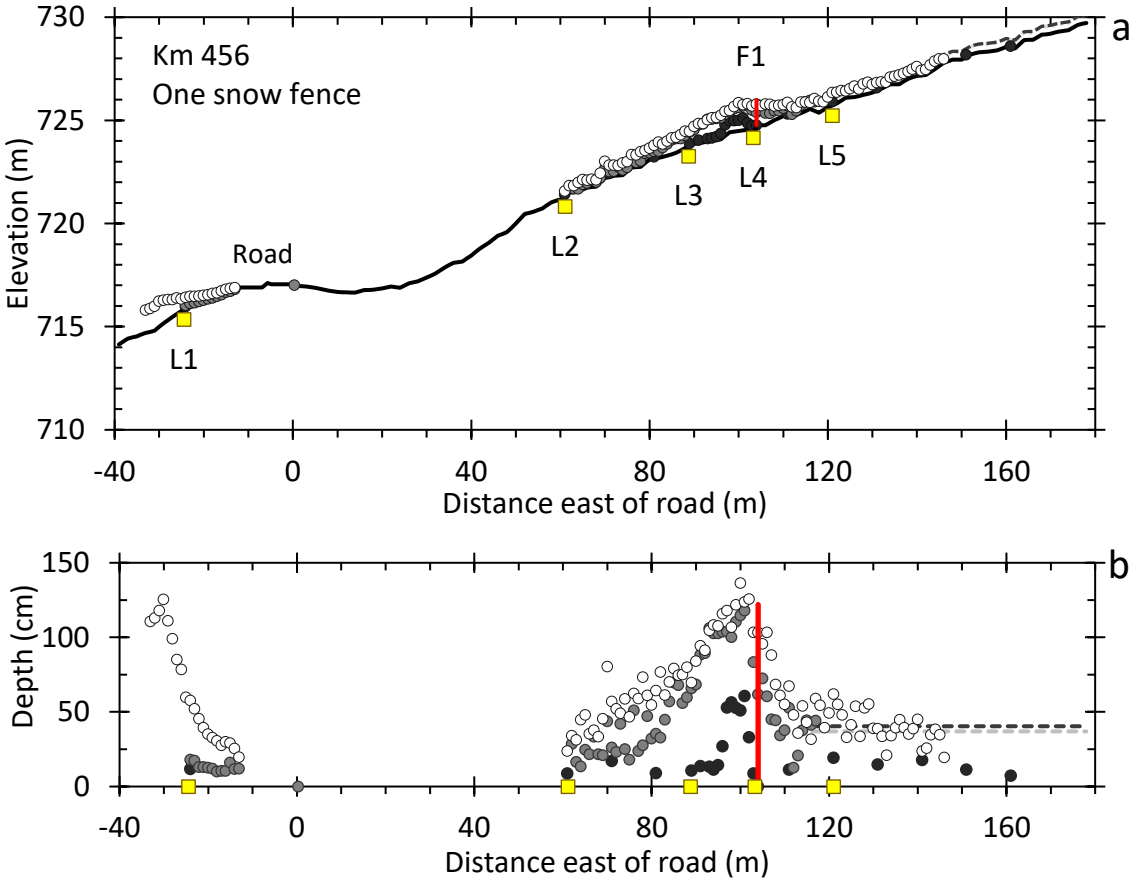

Figure A.3. Snow depth profiles at km 456 with one snow fence row (P1), (a) with elevation, and (b) normalized for elevation. Filled circles are measured snow depths while dashed lines represent inferred snow depths based on field observations. Circles are black, grey, or open, to indicate measurements in October, December, and March 2018–19, respectively. Yellow squares mark the position of ground temperature loggers along the transect. Red vertical lines mark the position and height (1.22 m) of the fencing. Snow depths on the road surface were near 0 cm, and snow depths were not measured from 0–49 m east of the road. The primary (F1) fence was placed 104 m from the eastern road edge (0 m). Loggers were placed at −24.5, 61.1, 88.8, 103.3, and 121 m from the eastern road edge.

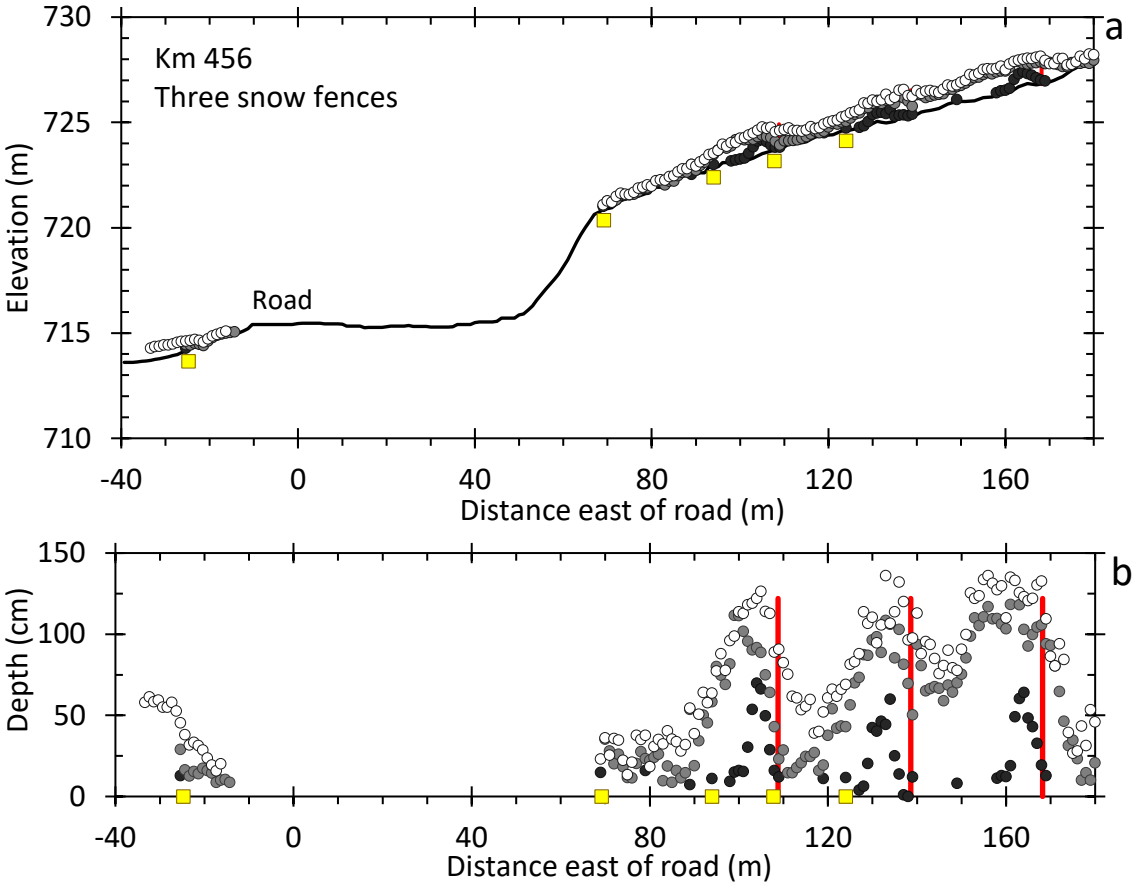

Figure A.4. Snow depth profiles at km 456 with three snow fence rows (P3), (a) with elevation, and (b) normalized for elevation. Filled circles are measured snow depths while dashed lines represent inferred snow depths based on field observations. Circles are black, grey, or open, to indicate measurements in October, December, and March 2018–19, respectively. Yellow squares mark the position of ground temperature loggers along the transect. Red vertical lines mark the position and height (1.22 m) of the snow fence rows. Snow depths on the road surface were near 0 cm, and snow depths were not measured from 0–49 m east of the road. The primary (F1) row was placed 109 m from the eastern road edge (0 m), while secondary (F2) and tertiary (F3) rows were positioned further back at 139 m, and 168 m, respectively. Loggers were placed at −24.8, 69.2, 94, 107.8, and 124 m from the eastern road edge.